Probing viral replication of HCV and XMRV:

Biochemical characterization, inhibition kinetics and role of

host proteins in viral replication

A Dissertation

Presented to

The Faculty of the Graduate School

At the University of Missouri

In Partial Fulfillment

Of the Requirements for the Degree

Doctor of Philosophy

By

TANYARADZWA P. NDONGWE

Dr. Stefan G. Sarafianos, Dissertation Supervisor

MAY 2015

The undersigned, appointed by the dean of the Graduate School,

have examined the dissertation entitled

Probing viral replication of HCV and XMRV:

Biochemical characterization, inhibition kinetics and role of

host proteins in viral replication

Presented by Tanyaradzwa P. Ndongwe

A candidate for the degree of

DOCTOR OF PHILOSOPHY

And hereby certify that, in their opinion, it is worthy of acceptance

---

Dr. Stefan Sarafianos

Dr. Donald Burke

Dr. Bumsuk Hahm

Dr. Shan-Lu Liu

Dr. Michael Parniak

ACKNOWLEDGEMENTS

I thank God for leading me to graduate school and for the strength to complete it. Every step in my life has led me to this point, and I know it has all been according to his plan. I would also like to thank my mother. From the very beginning she has gone above and beyond, and sacrificed everything she had to make sure I went to the best schools. She has always believed in me and pushed me to be the best I could be. I also wouldn't be writing this thesis without my father; who taught me to love learning and to always pursue knowledge. My parents got me to graduate school, but I would not have made it through without my best friend and husband; Yemi. From my very first day you challenged and encouraged me, you were my lifeline and oasis through the challenges of research. You've taught me so much about research, life, and myself.

I would like to thank my mentor; Dr. Sarafianos for affording me the opportunity to work with and learn from very talented and diverse colleagues. Thank you for allowing me to work independently and providing the resources to learn skills that will continue to guide me in my career. Thank you for the opportunity to teach and train others.

I would like to thank Dr. Kamal Singh for being a patient and very resourceful teacher during my first years in the lab. Thank you for training me in biochemical assays and painstakingly helping me to understand protein expression and expression and enzyme kinetics. For my virology work, I would like to thank Dr. Robert Ralston for teaching me cell culture techniques, and working with infectious viruses. Thank you for your patience, productive discussions, and fostering my love for virology. My appreciation goes to my committee members Dr. Donald Burke, Dr. Bumsuk Hahm, Dr. Shan-Lu Liu, and Dr. Michael Parniak for their guidance and support over the years.

To the amazing friends I have made here: Richard, Femi, Angela, Lefteris, Yee, Obi, and Mary; thank you for always being there. From babysitting Michael, or visiting me in the hospital, or giving me a ride when I needed it to just hanging out; you kept me sane and encouraged. I am

forever grateful. To all the former and current lab members; Karen, Jennifer, Bruno, Emily, Daniel S., Dandan, Andrew, Jen, Maritza, Anna, Jackie, Juan, and Grace; thank you for all your help, advice and fostering a collaborative working environment.

Lastly, but definitely not least; I am grateful to my son Ademide Michael. Having you instantly made me more responsible, independent, patient, and efficient. In the two years I have had you, you have forever changed my life.

TABLE OF CONTENTS

LIST OF TABLES

TABLE Page

LIST OF FIGURES

FIGURE Page

Probing the viral replication of HCV and XMRV:

Biochemical characterization, inhibition kinetics and role of

host proteins in viral replication

Tanyaradzwa P. Ndongwe

Dr. Stefan G. Sarafianos, Dissertation advisor

ABSTRACT

The studies described in this thesis focus on RNA viruses XMRV and HCV. In Chapter II we focused on Xenotropic Murine leukemia-Related Virus (XMRV), which was discovered as a novel gammaretrovirus with possible roles in prostate cancer (PC) and chronic fatigue syndrome (CFS). However, further studies showed XMRV was not associated with neither PC nor CFS. We characterized the biochemical activity and kinetics of the XMRV reverse transcriptase and discovered key mechanistic differences between XMRV, Moloney murine leukemia virus (MoMLV), and human immunodeficiency virus (HIV-1) reverse transcriptase (RT) enzymes. Using steady and pre-steady state kinetics we demonstrated that XMRV RT is significantly less efficient in DNA synthesis and in unblocking chain-terminated primers. By surface plasmon resonance experiments we observed that XMRV's decreased DNA binding ability was due to a remarkably higher rate of dissociating from DNA. Consistent with these data, XMRV RT has lower processivity when compared to HIV-1 RT, likely the result of XMRV RT's faster dissociation from bound DNA. Transient kinetics of incorporation of a mismatched nucleotide substrate revealed that XMRV RT has higher fidelity than HIV-1 RT.

In addition to characterizing XMRV RT we determined whether agents known to inhibit MoMLV and HIV-1 RT are effective against XMRV. Hence, we identified RNA aptamers that potently inhibit XMRV, but not HIV-1 RT. XMRV RT is highly susceptible to some nucleoside RT inhibitors, including Translocation Defective RT inhibitors, but not to nonnucleoside RT inhibitors, that are potent against HIV-1 RT. We demonstrated that XMRV RT mutants K103R and Q190M, which are equivalent to HIV-1 mutants that are resistant to tenofovir (K65R) and AZT (Q151M), are also resistant to the respective drugs, suggesting that XMRV can acquire resistance to these compounds through the decreased incorporation mechanism reported in HIV-1.

In Chapter III we focused on Hepatitis C Virus (HCV), the causative agent of hepatitis C infection. We studied the role of the Mov10 host factor in the viral replication of HCV. Mov10 is an antiviral host factor that has been reported to restrict replication of retroviruses, including HIV-1. It has also been reported to inhibit HCV. However, the mechanism of this inhibition has yet to be studied. We investigated the effect of Mov10 on HCV infection to determine which steps of the viral life-cycle are affected by overexpression of Mov10. We demonstrate that Mov10 overexpression in human hepatoma cells restricts HCV RNA production from a sub-genomic replicon (genotype 1a) and in a fully infectious virus (genotype 2a) HCV cell culture system. Inhibition of RNA replication in the infectious virus system leads to decreased virus production over time as measured by HCV RNA levels in cell culture media by RT-qPCR, and the viral titer ($TCID_{50}$/ml) of released virus. In addition to decreasing virus production, overexpression of Mov10 in producer cells decreases the infectivity of the produced

virus. In contrast, overexpression of a control P-body protein Dcp1a has no effect on HCV RNA production, virus production, or infectivity of progeny virus.

Confocal imaging of uninfected cells shows endogenous Mov10 to be localized at P-bodies. However, HCV infection results in redistribution of Mov10 to circular structures surrounding lipid droplets where it co-localizes with HCV NS5A and the core protein. Finally, we demonstrate that the RNA-binding function of Mov10 is responsible for its antiviral effect, as Mov10 mutants that affect its helicase or ATP-binding functions have no effect on its antiviral effect, whereas mutations that disrupt the RNA binding ability of Mov10 seem to abrogate its anti-HCV effect. We also show that localization to P-bodies is not required for the antiviral activity of Mov10. Decreasing Mov10 protein expression levels using CRISPR-Cas9 genome editing technology decreased HCV replication and infection levels, consistent with disruption of Mov10-Ago2/miR122 binding, which would destabilize the HCV genome. Our data reveal a complex balance between Mov10 and HCV, with Mov10 knockdown data suggesting optimum levels of Mov10 are required for HCV infection, whereas Mov10 overexpression is detrimental to the virus.

In Chapter IV we studied several aspects of HCV. (i) We discovered two novel small molecule inhibitors of the HCV helicase that have antiviral function. (ii) We discovered that Dcp2 is a novel HCV host restriction factor that can block HCV replication, and (iii) we provide insights into the mechanism(s) of action of approved and clinically advanced direct-acting antiviral agents (DAAs). Specifically: (i) we screened a chemical library of compounds for inhibitors of NS3's helicase domain (NS3h) and identified two compounds that inhibited NS3h *in vitro* (~12 μM IC_{50}s). Both compounds

were validated as anti-HCV antivirals in cell-based assays. These preliminary hits will be optimized in future structure activity relationship studies.

(ii) Host proteins can restrict viral replication by directly interacting with the affected viruses. However, they may also act indirectly by affecting the interferon (IFN) response pathway. We discovered one such factor, Dcp2. Overexpression of Dcp2 restricts HCV replication (up to 50% decrease) by causing a profound (30-fold) increase in transcription of IFNβ. This inhibition of HCV replication leads to a decrease in virus production, but unlike Mov10 it does not affect the infectivity of the virus produced.

(iii) Several DAAs have advanced in clinical trials and have been approved as drugs for the treatment of HCV infection. Among them, NS5A-targeting drugs have been reported to rapidly eliminate HCV RNA. However, their exact mechanism of action is not clear. We and others demonstrate that daclatasvir (DCV) treatment redistributes NS5A in HCV infected cells. Similarly, we show that ledipasvir (LDV) (the recently approved and most potent anti-HCV NS5A DAA), and cyclosporine A (CsA) (that targets the host factor cyclophilin A) also redistribute NS5A into circular structures. We determined that these circular structures were NS5A redistributed at lipid droplets where it co-localized with the core protein. However, the three drugs had distinctly different effects on the size and number of circular structures and lipid droplets per cell. Additionally, LDV treatment disrupted the localization of HCV dsRNA to lipid droplets and its association with NS5A. We provide insights into the mechanism of action of DCV, CsA, and LDV and their effects on viral complexes and processes.

This work provides insights into the replication processes of XMRV and HCV, strategies to restrict them, the mechanisms of action of drugs that inhibit them, and for HCV; its interaction with host restriction factors.

I.A GENERAL INFORMATION: XMRV

A.1. DISCOVERY OF XMRV

XMRV and prostate cancer

Beginning in 2006 several studies reported on the isolation of a potential human virus in prostate cancer patient samples from studies of familial prostate cancer (*1-3*). One familial form of prostate cancer had been genetically mapped to defects in the ribonuclease L (RNAse L) gene. RNase L is an interferon stimulated gene and patients homozygous for a polymorphic RNAse L allele that expressed RNAse L protein (R462Q) with lower enzymatic activity had an increased susceptibility to inherited prostate cancer (*4*), reviewed in (*5*). RNAse L being involved in the innate immune system suggested that individuals with a defective protein would be more susceptible to virus infections and more specifically a virus that induces prostate cancer. Based on this hypothesis cDNA sequences from familial and non-familial prostate cancer patients were prepared and hybridized to a virochip containing the DNA sequences from the genes of all known viruses (*1*).

A positive hit; xenotropic murine leukemia virus was found in familial prostate cancer patient samples. The hybridized cDNAs were recovered from the chip, cloned and the resulting virus was called Xenotropic Murine Leukemia Virus-Related Virus (XMRV), and reported as a novel human retrovirus potentially linked or associated with prostate cancer. The same investigators later described an infectious XMRV clone (VP62) that was reconstituted from the XMRV cDNAs from a prostate cancer patient (*1*). The infectious XMRV clone VP62 could replicate in human prostate cancer cells and also in hamster cell engineered to express the XMRV receptor XPR-1; showing it was xenotropic with a range of hosts. More significantly, the authors were able to determine XMRV integration sites within the patients'

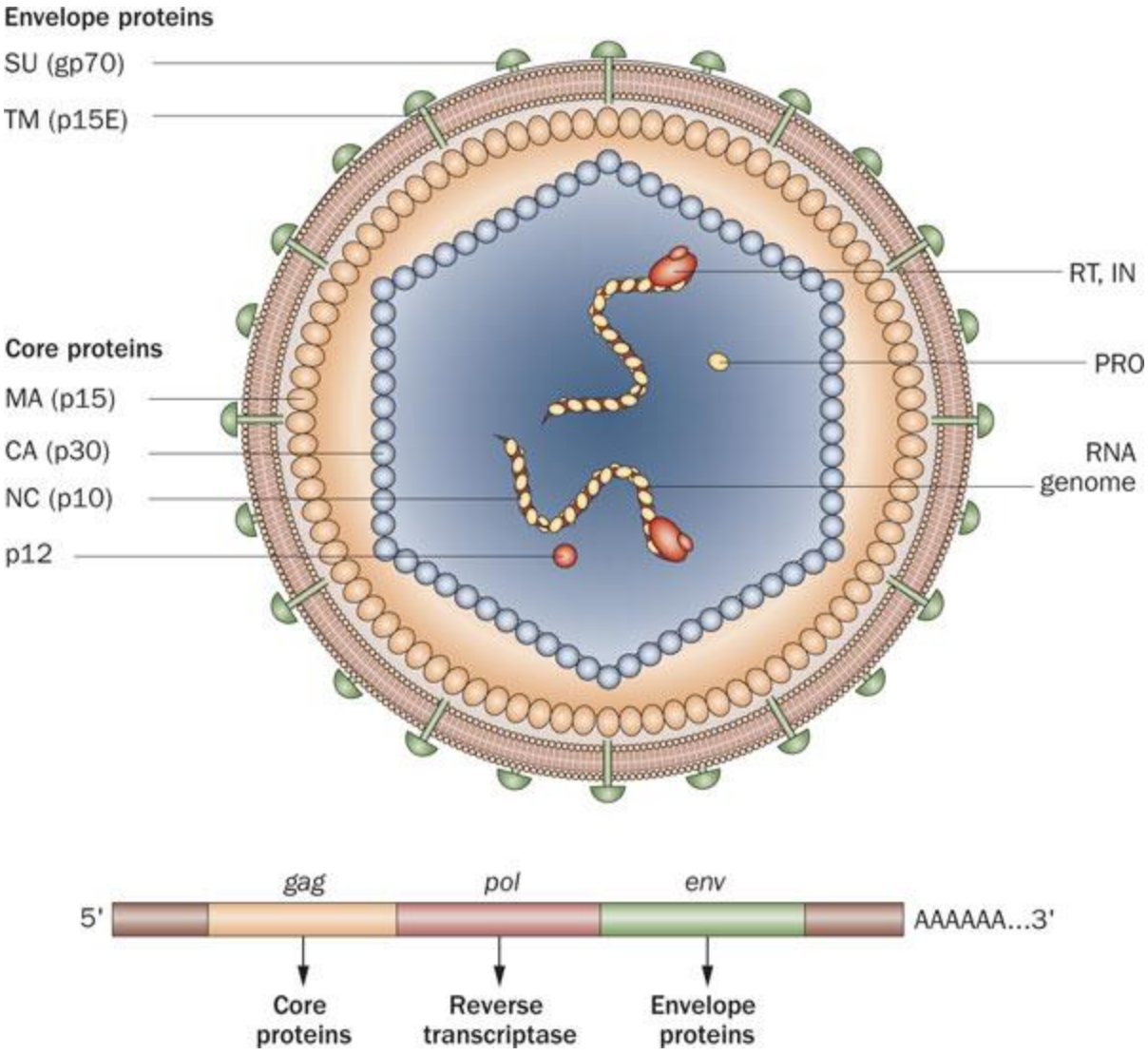
Envelope proteins
SU (gp70)
TM (p15E)
Core proteins
MA (p15)
CA (p30)
NC (p10)
p12
RT, IN
PRO
RNA genome
5'
gag
pol
env
AAAAAA...3'
Core proteins
Reverse transcriptase
Envelope proteins

Figure I.A-1: Schematic of the structure of a retrovirus, viral genome and proteins. The diagram shows the viral envelope proteins (surface subunit (SU) and transmembrane subunit (TM)), the core proteins from the *gag* gene (matrix (MA), capsid (CA), nucloecapsid (NC), and p12), and from the *pol* gene (protease (PRO), reverse transcriptase (RT), and integrase (IN)). Virions contain a lipid bilayer, carry two RNA genomes, and some co-packaged non-structural viral and cellular proteins. Figure adapted from (*6*)

cellular DNA. This suggested that XMRV was a retrovirus that could indeed infect and replicate in human cells and integrate into the host genome.

Despite the promising initial reports, subsequent studies were inconsistent in determining XMRV's association or role in prostate cancer. In one report, a study of US prostate cancer high-grade tumors. However, in this study they found no correlation of XMRV with RNAse L allele status, suggesting XMRV infection was more diffusely distributed in all prostate cancer samples detected XMRV gag protein in a significant fraction of tumors tested (*7*), and detection correlated with patients. XMRV LTR activity was reportedly higher in primary stromal fibroblasts isolated from the prostate cancer cell line LNCaP, when compared to other cell lines.

The prostate cancer cell line 22Rv1 was derived from a human prostate cancer patient. A very important finding in 2009 was that this cell line contained multiple copies and highly expressed XMRV DNA (*8*). On the other hand a study on European prostate cancer samples reported very low overall detection levels of XMRV(about 1%) (*9*). They also found that XMRV detection qwas not associated with homozygosity for the RNAse L allele R462Q. Several subsequent studies also failed to detect XMRV in prostate tissue, serum, or peripheral blood mononuclear cells (PBMCs) of patients with prostate cancer in Europe or the United States (*10-14*).

XMRV and chronic fatigue syndrome

XMRV was in the publication limelight once again in 2009 when Lombardi *et al.* (*15*) reported XMRV in 67% of PBMCs isolated form patients with chronic fatigue syndrome (CFS, also called myalgic encephalomyelitis or ME). The cause of CFS/ME is unknown. Lombardi *et al.* detected XMRV using several different methods including PCR for XMRV DNA, the presence of anti-XMRV antibodies, and isolation of infectious virus from patient CD4+ T-cells. In 2010 Lo *et al. (16)* reported detection of polytropic MLV-related sequences, but not XMRV, in CFS patient samples. Although they did not detect XMRV, this suggested gammaretrovirus

infection in CFS patients. Despite the excitement and interest generated by these reports, especially in the CFS community, the association of XMRV with CFS has since been disproven. Several studies around the world have failed to detect XMRV in CFS patient samples, individuals at high risk for infections, or in the general human population (including (*11, 17-25*)).

A.2. RETROVIRUSES, THEIR REPLICATION, AND REVERSE TRANSCRIPTION

Murine leukemia viruses (MLVs) are retroviruses, belonging to the genus gammaretrovirus. MLVs cause cancers and other diseases in mice, and they are classified under ecotropic, amphotropic, polytropic, and xenotropic, depending on their receptor usage. Xenotropic MLVs cannot infect inbred mice, but can infect cells from other species, including humans. Extensively studied members of the gammaretrovirus genus include murine leukemia virus and the feline leukemia virus. Compared to other retroviruses, XMRV has a relatively simple genome expressing three major viral proteins from an 8kb single-stranded RNA genome. Similar to other retroviruses after entry of the virus into the host cell, the released ssRNA genome must be converted to DNA for replication. For this purpose XMRV encodes the pol gene, which after translation is processed into the protease, reverse transcriptase, and integrase enzymes. The reverse transcriptase enzyme (RT) has three functionalities as i) a DNA dependent DNA polymerase, ii) an RNA dependent DNA polymerase, and iii) RNAse H activity, which cleaves RNA from DNA/RNA hybrids.

Reverse transcription

The most studied reverse transcriptase enzymes are from the human immunodeficiency virus (HIV) and murine leukemia virus (MLV). Mainly from studies with HIV-1 RT, it is known that RT uses a cellular tRNA as a primer and copies the 5’ end of the ssRNA viral genome. This results in a DNA/RNA hybrid, from which the RNAse H function of RT cleaves off the RNA.

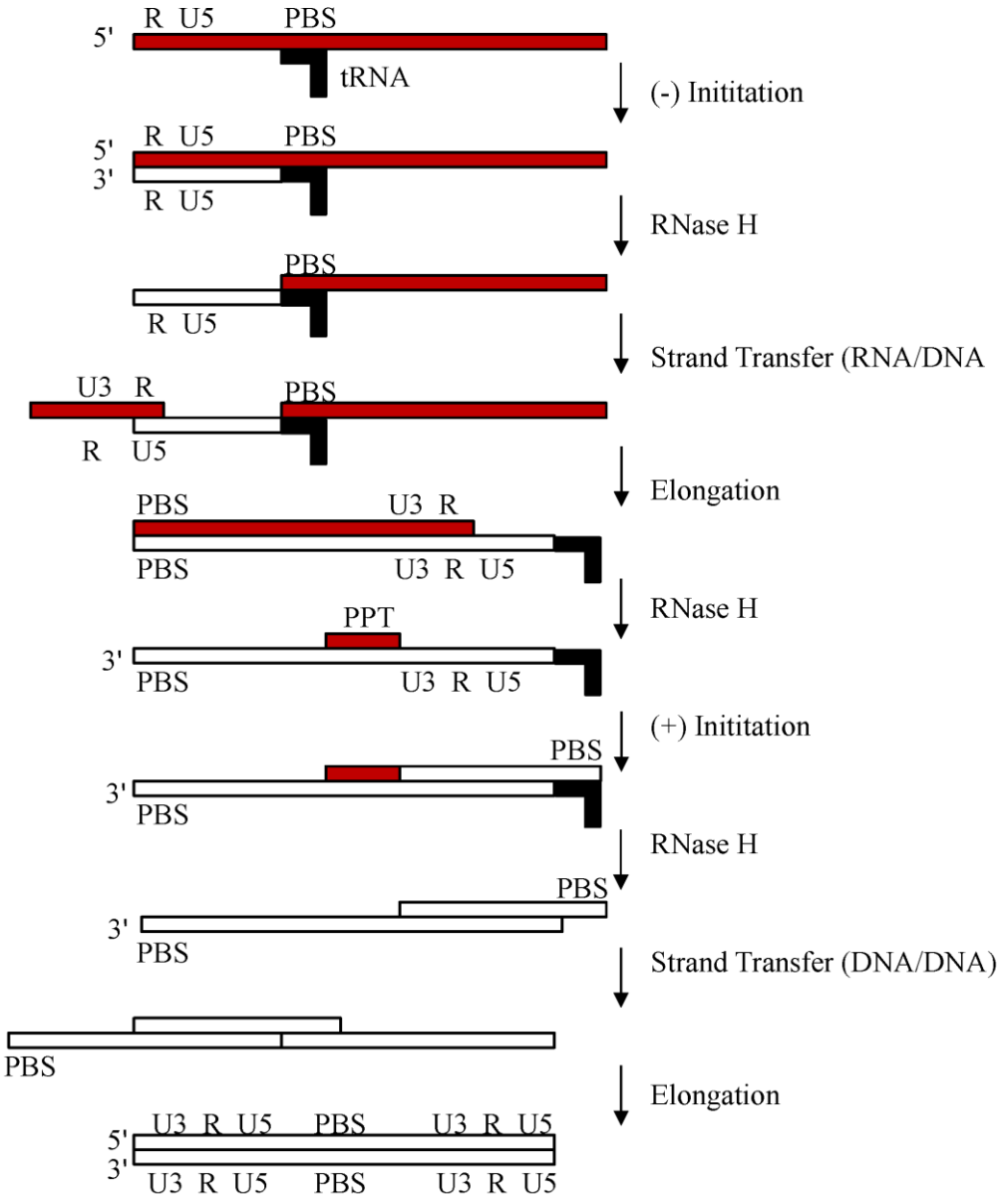
5'
R U5
PBS
tRNA
(-) Inititation
3'
RNase H
Strand Transfer (RNA/DNA
U3 R
Elongation
PPT
(+) Inititation
Strand Transfer (DNA/DNA)

Figure I.A-2: Diagram summarizes the reverse transcription process for HIV-1 RT. Figure adapted from (*26*).

The remaining negative-sensed DNA strand is used as a template for synthesis of the second DNA strand. The genomes of retroviruses have identical sequences at the 5'- and 3'-ends. This allows the first minus strand transfer, where the single-stranded DNA hybridizes to the complementary repeat sequence at the 3' end of the RNA genome. RT continues extension of the DNA sequence, using the viral RNA strand as a template (using RT's RNA-dependent DNA polymerase capability). The RNAse H then degrades the RNA strand. A purine rich sequence near the 3' end of the RNA genome (called the polypurine tract) is not degraded efficiently by the RNAse H. This sequence remains and RT uses it as a primer for synthesis of the second DNA strand (using RT's DNA-dependent DNA polymerase capability). The tRNA used as an initial primer is cleaved off by the RNAse H, leading to a second strand transfer event. The resulting double stranded DNA has identical sequences at both ends, called long terminal repeats (LTRs).

A.3. INHIBITION OF REVERSE TRANSCRIPTION

In depth understanding of reverse transcription has led to the discovery of compounds that inhibit specific steps in the reverse transcription process. These compounds are classified into two groups. The first group, nucleoside reverse transcriptase inhibitors (NRTIs), are analogs of natural nucleosides that mimic the natural substrate. The incorporation of the compound into DNA blocks the addition of further nucleotides, effectively blocking reverse transcription and ultimately virus replication. The second class of inhibitors, non-nucleoside reverse transcriptase inhibitors (NNRTIs), bind at a site away from the RT active site and allosterically inhibit incorporation by affecting the enzyme's flexibility. Several drugs in each of these classes are used for the treatment of HIV infection. One significant drawback of NRTIs and NNRTIs is the development of drug resistant variants of RT.

A.4. XMRV, MoMLV, AND HIV-1 REVERSE TRANSCRIPTASES

XMRV RT is similar to the Moloney murine leukemia virus (MoMLV) RT, which has been the subject of structural and biochemical studies (*27-32*). Most of the differences between these gammaretroviral enzymes are at the RNase H domain (Figure 1.A-3(b)). Comparisons of human immunodeficiency virus type-1 (HIV) RT with MoMLV RT have revealed structural and sequence differences (*29*). For example, HIV-1 RT is a heterodimer composed of two related subunits (*33, 34*) (reviewed in (*35, 36*)). Its larger p66 subunit (~66 kDa) contains both the polymerase and RNase H domains; the smaller p51 subunit, (~51 kDa), is derived from the p66 subunit by proteolytic cleavage and its role is to provide structural support and optimize RT's biochemical functions (*37*). In contrast, structural studies have demonstrated that MoMLV RT is a monomer of about 74 kDa, although one study reported that it may form a homodimer during DNA synthesis (*38*). The present study on XMRV RT and its comparison to related enzymes provides an excellent opportunity to advance our biochemical understanding of the mechanism of reverse transcription, its inhibition and drug resistance.

A.5. THE ORIGINS OF XMRV

Due to the discrepancies in the detection and relevance of XMRV, studies were initiated to understand the origins of this virus. In order to investigate whether XMRV could have arisen from *in vivo* passaging, Paprotka *et al. (39)* studied human prostate cancer cell lines CWR22R*v1* and CWR-R1, which produce large amounts of XMRV that is almost genetically identical to the XMRV clones isolated and sequenced from prostate cancer patient samples. These cell lines were generated from multiple xenograft passages of a prostate cancer patient tumor (CW22) in nude mice. They performed PCR analysis to detect XMRV cDNA sequences in the cell lines, and also in the early and late passage tumor xenografts. XMRV infection was not detected in the earlier passage xenografts, suggesting that the original tumor donor was not infected with XMRV. The late passage xenografts and the two cell lines, however, were positive for XMRV infection. This

suggested that XMRV arose from the *in vivo* passaging in nude mice, possibly from activated endogenous murine leukemia proviruses in the mice.

Analysis of the nude mice strain identified endogenous MLVs with two stretches over 3.2 kilobases almost identical (99.2% identity) to regions in XMRV. These long stretches were each named PreXMRV-1 and PreXMRV-2, and their schematics shown in Figure I.A-4. PreXMRV-2 contained all three retroviral open reading frames intact. PreXMRV-1, however, had mutations that rendered it incapable of producing functional proteins; a 16-nt deletion in the *gag* gene, and a frame-shift mutation in the *pol* gene.

It was possible to generate the XMRV genome by six recombination events between the two endogenous viruses. The generated XMRV was identical to sections of the PreXMRVs save for four mutations; three single nucleotide substitutions and one nucleotide insertion, also shown in Figure I.A-4. This concluded that XMRV was not present in the original prostate cancer tumor, but was generated by recombination of two endogenous MLV proviruses during tumor passaging in mice, with ~10^{12} probability that an identical recombinant occurred independently. Follow-up cell-culture studies have confirmed that the recombination between the two PreXMRVs can produce replication-competent viruses, although the exact recombination sites were different from the ones initially predicted (*40*). Taken together, these new findings demonstrated that the association of XMRV with human disease was due to contamination of samples with the XMRV originating from this recombination event.

(a)

```
XMRV     22 ..TWLSDFLQAWAETGGMGLAVRQAPLIIPLKATSTPVSIKQYPMSQEARLGIKPH
MoMLV    22 ..TWLSDFPQAWAETGGMGLAVRQAPLIIPLKATSTPVSIKQYPMSQEARLGIKPH
HIV-1     1 ...................PISPIETVPVKLKPGMDGPKVKQWPLTEEKIKALVEI

XMRV     76 IQRLLDQGIL..VPCQSPWNTPLLPVKKPGTNDYRPVQDLREVNKRVED...IHPT
MoMLV    76 IQRLLDQGIL..VPCQSPWNTPLLPVKKPGTNDYRPVQDLREVNKRVED...IHPT
HIV-1    37 CTEMEKEGKISKIGPENPYNTPVFAIKKKDSTKWRKLVDFRELNKRTQDFWEVQLG
                                          Motif F

XMRV    130 VPNPYNLLSGLPPSHQWYTVLDLKDAFFCLRLHPTSQPLFAFEWRDPEMGISG.QL
MoMLV   130 VPNPYNLLSGLPPSHQWYTVLDLKDAFFCLRLHPTSQPLFAFEWRDPEMGISG.QL
HIV-1    94 IPHPAGL.....KKKKSVTVLDVGDAYFSVPLDEDFRKYTAFTIPSINNETPGIRY
                          Motif A

XMRV    184 TWTRLPQGFKNSPTLFDEALHRDLADFRIQHPDLILLQYVDDLLLAATS.EQDCQR
MoMLV   184 TWTRLPQGFKNSPTLFDEALHRDLADFRIQHPDLILLQYVDDLLLAATS.ELDCQQ
HIV-1   145 QYNVLPQGWKGSPAIFQSSMTKILEPFKKQNPDIVIYQYMDDLYVGSDLEIGQHRT
                 Motif B                          Motif C

XMRV    239 GTRALLQTLGNLGYRASAKKAQICQKQVKYLGYLLKEGQRWLTEARKETVMGQ..P
MoMLV   239 GTRALLQTLGNLGYRASAKKAQICQKQVKYLGYLLKEGQRWLTEARKETVMGQ..P
HIV-1   201 KIEELRQHLLRWGLTTPDKKHQK.EPPFLWMGYELH.PDKWTVQPI..VLPEKDSW
               Motif D                  Motif E

XMRV    303 TPKTPRQLREFLGTAGF..CRLWIPGFAEMAAPLYPLTKTGTLFNWGPDQQK.AYQ
MoMLV   303 TPKTPRQLREFLGTAGF..CRLWIPGFAEMAAPLYPLTKTGTLFNWGPDQQK.AYQ
HIV-1   253 TVNDIQKLVGKLNWASQIYPGIKVRQLSKLLRGTKAL......TEVIPLTEEAELE

XMRV    356 EIKQAL.LTAPALGLPDLTKPFELFVDEKQG..YAKGVLTQKLGPWRRPVAYLSKK
MoMLV   356 EIKQAL.LTAPALGLPDLTKPFELFVDEKQG..YAKGVLTQKLGPWRRPVAYLSKK
HIV-1   303 LAENREILKEPVHGVY..YDPSKDLIAEIQKQGQGQWTYQIYQE.PFKNLKTGKYA


XMRV    410 LDPVAAGWPPCLRMVAAIAVLTKNAGKLTMGQPLVIKAPHA..VEALVKQPPDRWL
MoMLV   410 LDPVAAGWPPCLRMVAAIAVLTKDAGKLTMGQPLVILAPHA..VEALVKQPPDRWL
HIV-1   356 RMRG..AHTNDVKQLTEAVQKITTESIVIWGKTPKFKLPIQKETWETWWTEY.WQA

XMRV    464 SNARMTHYQALLLDTDRVQFGP
MoMLV   464 SNARMTHYQAMLLDTDRVQFGP
HIV-1   409 TWIPEW....EFVNTPPLVK..
```

(b)

```
XMRV     496 -GILAEAHGTRPDLTDQPLPDADHTWYTDGSSLLQEGQRKAGAAVTTETEVIWAKALPAG
MoMLV    496 GSILAETHGTRPDLTDQPIPDADYTWYTDGSSFLQEGQRRAGAAVTTETEVIWARALPAG
HIV-1    426 -----------YQLEKEPIVGAET-FYVDGAANRETKLGKAGYVTNKGRQKVVP---LTN

XMRV     556 TSAQRAELIALTQALKMAEGKKLNVYTDSRYAFATAHLTSEGKEIKNKDEILALLKALFL
MoMLV    556 TSAQRAELIALTQALKMAEGKKLNVYTDSRYAFATAHVHSEGREIKNKNEILALLKALFL
HIV-1    471 TTNQKTELQAIYLALQDS-GLEVNIVTDSQYALGIIQAQPDKSESELVN---QIIEQLIK

XMRV     616 PKRLSIIHCPGHQKGHSAEARGNRMADQAARKAAITETPDTSTLL
MoMLV    616 PKRLSIIHCPGHQKGNSAEARGNRMADQAAREAAMKAVLETSTLL
HIV-1    528 KEKVYLAWVPAH-KGIGGNEQVDKLVSAGIRKILFL---------
```

Figure I.A-3(a): Sequence alignment of XMRV, MoMLV, and HIV-1 RT polymerase domains. The polymerase domains of MoMLV and HIV-1 RTs (PBD IDs: 1RW3 and 1DLO respectively) were aligned with XMRV RT's polymerase domain using ClustalW. The aspartate active site residues (XMRV residues D150, D224, and D225) are conserved in all three enzymes and highlighted. Motifs A to F in the three enzymes are color coded and labeled accordingly. Residues that differ between XMRV RT and MoMLV RT are underlined and in bold. **(b): Sequence alignment of XMRV, MoMLV, and HIV-1 RT RNAse H domains.** An alignment of MoMLV, XMRV, and HIV-1 RNase H domains (PDB IDs: 2HB5, 3P1G, and 1HRH respectively) using ClustalW, with the conserved active site residues (XMRV residues E562, D524, and D583) highlighted.

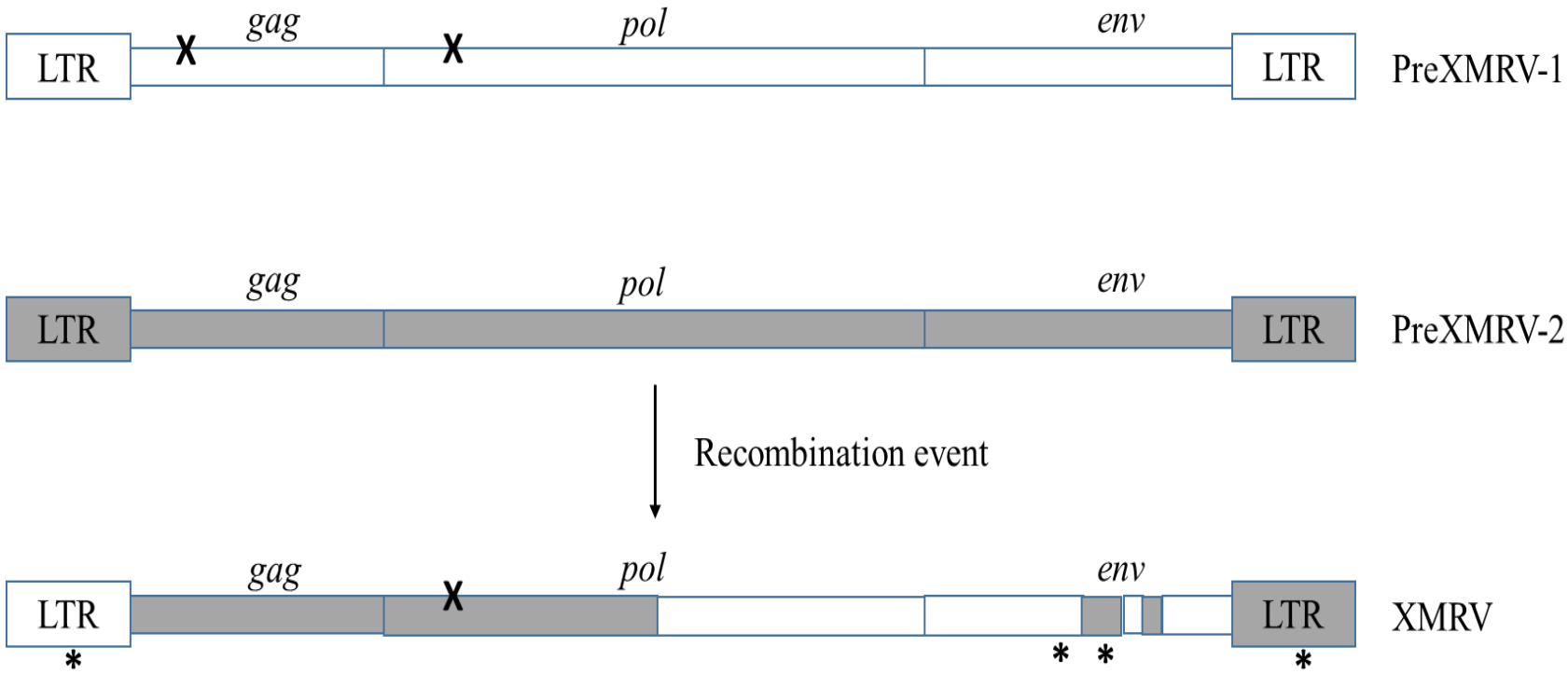
gag
pol
env
LTR
LTR
PreXMRV-1
gag
pol
env
LTR
LTR
PreXMRV-2
Recombination event
gag
pol
env
LTR
LTR
XMRV

Figure I.A-4: Generation of the XMRV genome by recombination. Two endogenous MLV proviruses, PreXMRV-1 and PreXMRV-2, were found present in nude mice. The larger boxes represent the long terminal repeats at the ends of the genome. PreXMRV-1 has mutations (labeled 'X') in the *gag* and *pol* genes; a 16-nt deletion and a one nucleotide frame-shift mutation respectively. These mutations render PreXMRV-1 incapable of encoding functional proteins. The *env* gene is intact. All reading frames in PreXMRV-2 are intact. XMRV generated from recombinations between PreXMRV-1 and PreXMRV-2 is shown at the bottom of the figure. Four mutations, three single nucleotide substitutions and one insertion (labeled *) resulted during the development of infectious XMRV. One of the substitutions is in the LTRs on both ends of the genome.

I.B. GENERAL INTRODUCTION: HEPATITIS C VIRUS

B.1 HCV PATHOLOGY AND EPIDEMIOLOGY ‘

An estimated 2-3% of the world’s population is infected with hepatitis c virus (HCV) with 3-4 million people becoming newly infected every year (*41-43*). More than 80% of HCV infections become chronic and in 20% of persons with untreated chronic HCV, infection leads to liver cirrhosis (*42*). In the last three years the incidence of hepatocellular carcinoma has tripled in the USA and HCV infection is the leading cause of liver transplants in developed countries (*43-45*).

Blood tests to detect and identify hepatitis A and B viruses were developed between 1960 and 1970. However, routinely patients samples were found that were negative for both viruses. Scientists and doctors classified these as non-A, non-B hepatitis (NANBH). Experts now believe that up to 95% of these samples were in fact hepatitis C. In 1989 scientists at the Center for Disease Control and Chiron Pharmaceuticals isolated a cDNA clone of NANBH (*46*) (reviewed in (*47*)). By 1992 a blood test had been developed to screen for and eliminate NANBH from the United States blood transfusion supply.

Over 200 years HCV has mutated to have very diverse genetic variability. The virus is classified into six subtypes (numbered 1 through 6), and several genotypes under each subtype (labeled a through e). The distribution of these genotypes is greatly varied worldwide, as shown in Figure I.A-1. The major genotype in the United States is genotype 1a; with a lesser percentage of genotype 1b, 2, and 3. Genotype 1b is the most prevalent in the United Kingdom, Europe and Japan. Genotype 4 is the predominant genotype in most of the African continent and the Middle East, whereas genotype 3 is responsible for most HCV infections in South America and Australia.

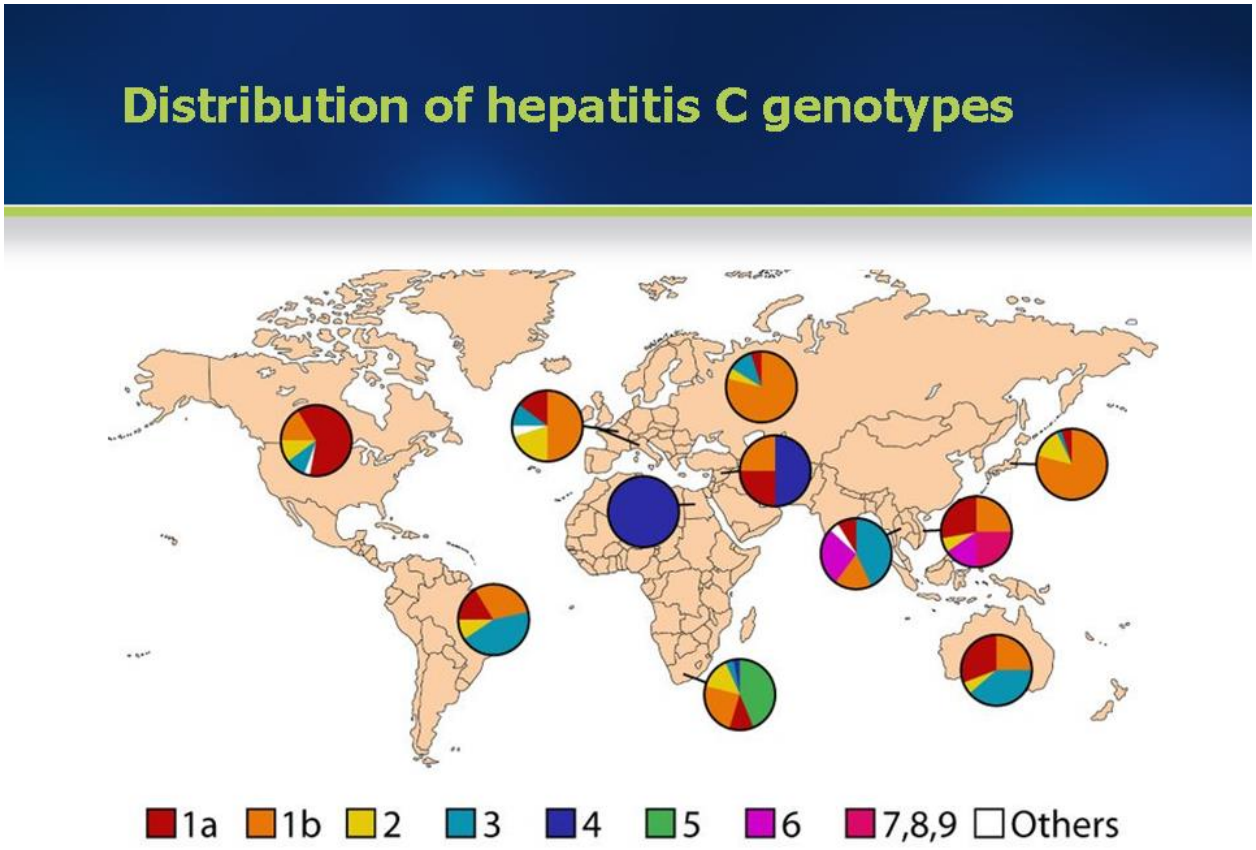
Distribution of hepatitis C genotypes
1a
1b
2
3
4
5
6
7,8,9
Others

“

`.

Figure I.B-1: Worldwide distribution of hepatitis C virus infection by genotype. Hepatitis C virus is classified under nine genotypes (1 to 9), and subtypes under each (a to f). The most prevalent genotype and subtypes with their global distribution are shown. Map copyright: John Hopkins Bloomberg School for Public Health, available at http://ocw.jhsph.edu.

Unraveling the details of the HCV lifecycle was greatly hindered by the lack of *in vitro* cell culture systems to study the virus. The first cell culture techniques involved portions of the virus, termed replicons that lacked the structural proteins (*48*). These were instrumental in studying HCV translation and RNA replication. However, lacking the structural regions, entry and the later stages of the lifecycle (packaging, assembly, and release) could not be studied. In addition, most of the sub-genomic replicons were from genotypes 1a and 1b. Recently, breakthroughs were made by the discovery of cell-culture replicating fully infectious HCV (*49, 50*). This in turn allowed a better understanding of all parts of the virus life cycle and also contributed immensely in drug discovery.

B.2 HCV LIFECYCLE: STRUCTURAL AND NON-STRUCTURAL PROTEINS

HCV entry

Hepatitis C virus, a member of the *flaviviridae* family, is an enveloped, positive sensed, single-stranded RNA virus. The 9.6 kb genome encodes a single polyprotein of approximately 3,000 amino acids that is cleaved post translationally by host and viral proteases into three structural proteins (core, E1, and E2), the hydrophobic peptide p7, and six non-structural (NS) proteins (NS2, NS3, NS4A, NS4A, NS5A, and NS5B) (recently reviewed in (*51*)).

HCV entry is a complex and involved process (steps 1 and 2 in Figure I.B-3)(reviewed in(*52, 53*)). The HCV envelope proteins E1 and E2 are exposed on the surface of virions and interact with several different host cell proteins to mediate viral entry. These cell surface receptors include scavenger receptor class B protein 1 (SRB1), heparin sulfate proteoglycans (HSPGs), and low density-lipoprotein receptor (LDLR). Interactions of the virion with SRB1 might delipidate HCV-associated lipoproteins and induce conformational changes to expose the CD81 receptor-binding domain of E2. The interaction of E2 and CD81 activates signal transduction *via* the epidermal growth factor receptor (EGFR), HRAS, and RHO GTPases. HCV-CD81 complexes then move laterally along the cell surface to sites of cell-to-cell contact; where

CD81 interacts with another cell receptor claudin 1 (CLDN1). The last step in the entry cycle is internalization of the HCV virion *via* clathrin-mediated endocytosis. The acidic pH in the endosome triggers fusion of the HCV envelope with the endosomal membrane, leading to release of the HCV RNA genome into the cytoplasm.

HCV translation and protein processing

The HCV genome is encoded in a single-stranded positive sensed RNA. Within hours of infection the released RNA genome is ready for direct translation by the host cell machinery. The HCV genome is uncapped and encodes an internal ribosome entry site within the 5' untranslated genome to recruit translation machinery (Figure I.B-2). The viral proteins are expressed as a 3,000 amino acid polyprotein that is cleaved by the host signal peptidase at the C-E1, E1-E2, E2-p7, and p7-NS2 junctions; releasing the individual proteins E1 to p7. The autoprotease and assembly factor NS2 cleaves the NS2-NS3 junction. HCV encodes a second (serine) protease NS3 that works with the cofactor NS4A to cleave the sites within the rest of the non-structural proteins. HCV protein translation and polyprotein processing occurs on the ER lumen (step 3 in Figure I.B-3). Once cleaved, most of the HCV proteins (structural proteins E1, E2, and p7; non-structural proteins NS2, NS3-NS4A, NS4B, and NS5B) have one or more transmembrane domains anchoring them (for the most part) to the ER. The rest of the proteins (core and NS5A), despite lacking transmembrane domains, are also found on the surface of the ER.

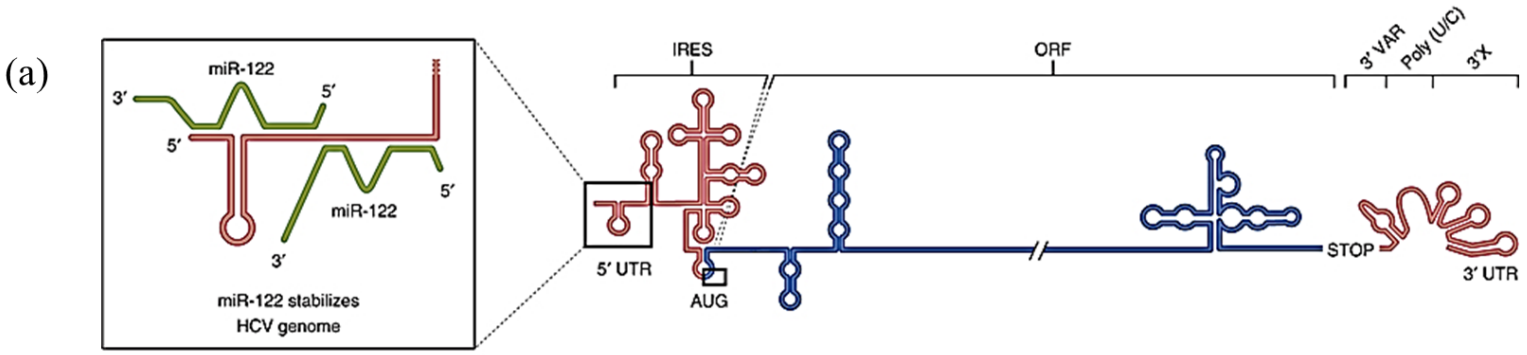
(a)
miR-122
3′
5′
5′
miR-122
5′
3′
miR-122 stabilizes
HCV genome
IRES
ORF
3′ VAR
Poly (U/C)
3′X
5′ UTR
AUG
STOP
3′ UTR

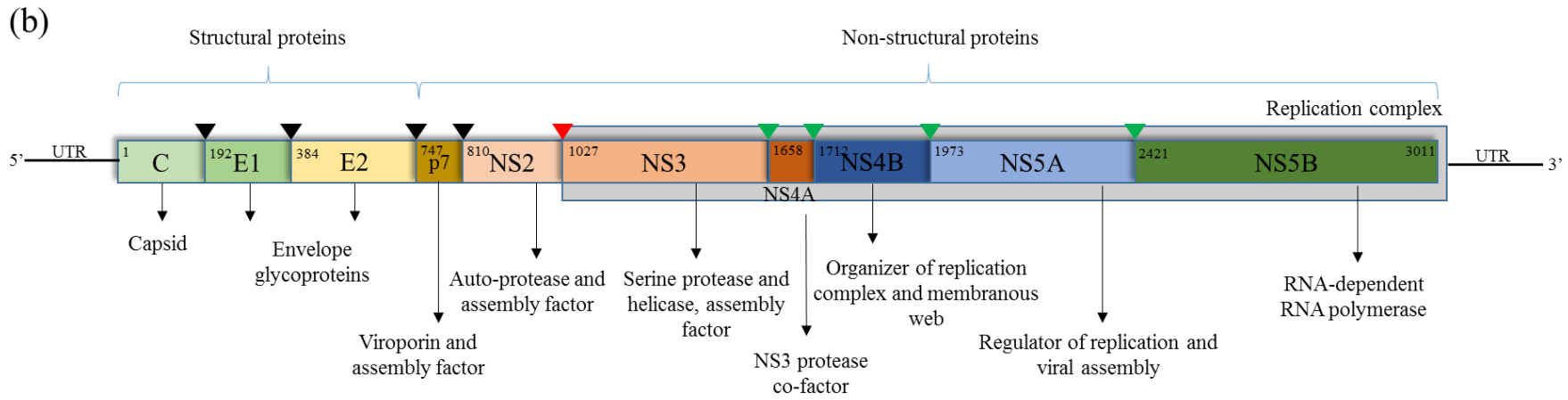
(b)
Structural proteins
Non-structural proteins
Replication complex
5’
UTR
1
C
192
E1
384
E2
747
p7
810
NS2
1027
NS3
1658
NS4A
1712
NS4B
1973
NS5A
2421
NS5B
3011
UTR
3’
Capsid
Envelope glycoproteins
Viroporin and assembly factor
Auto-protease and assembly factor
Serine protease and helicase, assembly factor
NS3 protease co-factor
Organizer of replication complex and membranous web
Regulator of replication and viral assembly
RNA-dependent RNA polymerase

Figure I.B-2: Schematic of the HCV genome. The HCV ssRNA genome (top) contains one long open reading frame (ORF, blue) with untranslated regions (UTRs) at the 5' and 3' ends (red). The 5'UTR contains binding sites for two copies of miR-122 (green), inset. Also within the 5'UTR is an internal ribosome entry site (IRES) from which translation of the ORF into a polyprotein (bottom) begins. The polyprotein is co- and post-translationally cleaved into four structural and six non-structural proteins. A cellular signal peptide peptidase cleaves the core, E1, E2, and p7 from the polyprotein at sites marked by black triangles. The NS2-NS3 protease cleaves itself (red triangle). The protease domain of NS3, with its cofactor NS4A cleaves the remaining proteins NS4A, NS4B, NS5A and NS5B (green triangles). The functions of the proteins are also shown. Panel (a) is adapted from (*54*).

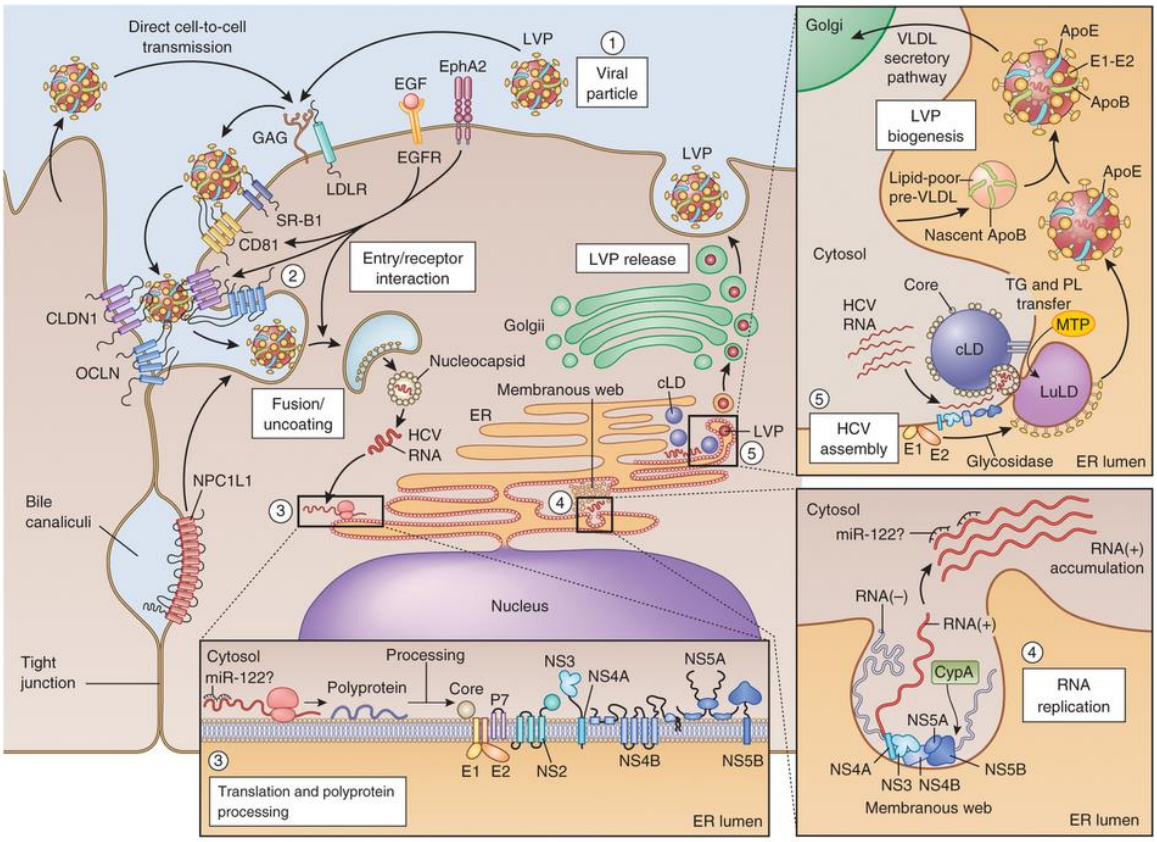
Direct cell-to-cell transmission
LVP
1
Viral particle
EGF
EphA2
GAG
EGFR
LDLR
SR-B1
CD81
LVP
LVP release
Entry/receptor interaction
2
CLDN1
OCLN
Golgii
Nucleocapsid
Fusion/ uncoating
Membranous web
cLD
ER
HCV RNA
LVP
5
NPC1L1
Bile canaliculi
3
4
Nucleus
Tight junction
Cytosol
miR-122?
Processing
Polyprotein
Core
P7
NS3
NS4A
NS5A
E1
E2
NS2
NS4B
NS5B
3
Translation and polyprotein processing
ER lumen
Golgi
VLDL secretory pathway
ApoE
E1-E2
ApoB
LVP biogenesis
Lipid-poor pre-VLDL
Nascent ApoB
ApoE
Cytosol
Core
TG and PL transfer
HCV RNA
MTP
cLD
LuLD
5
HCV assembly
E1
E2
Glycosidase
ER lumen
Cytosol
miR-122?
RNA(+) accumulation
RNA(–)
RNA(+)
4
CypA
RNA replication
NS5A
NS4A
NS3
NS4B
NS5B
Membranous web
ER lumen

Figure I.B-3: The HCV viral life-cycle. Points in the lifecycle are marked with numbered circles. (1) Interaction of HCV lipoviral particles with cellular surface receptors. (2) The entry process can also occur from cell-to cell transmission. (3) After pH-dependent fusion, the released genome is translated and processed into viral proteins (shown in the bottom insert). (4) HCV replication takes place in ER-derived invaginations in membranous webs, bottom left insert. (5) During assembly the core protein is recruited from cLDs to form nucleocapsids that contain viral RNA. The replication complex proteins bind HCV RNA during transfer from replication to packaging. Viral RNA might be transiently present on cLDs. P7, NS2, NS3-NS4A proteins are also involved in assembly. Production of HCV virions is dependent on the VLDL pathway, virions are produced highly modified with lipids (lipoviral particles, LVPs). Cell culture derived virions have less ApoB, as illustrated. LVPs also associate with ApoC (not shown). Figure adapted from (*54*).

HCV RNA replication

The HCV lifecycle is greatly linked to membranes within the host cell. Once viral proteins are expressed and processed the RNA replication begins. During HCV replication an alteration of the cellular membrane structure, called the 'membranous web' can be seen by electron microscopy in infected cells (shown in Figure I.B-4, panel a). The membranous web is the site for HCV RNA replication and is similar to the 'sponge-like inclusions' seen in the livers of HCV-infected chimpanzees. The membranous web is seen in distinct pockets juxtaposed to the nucleus, and there are no other noticeable changes in surrounding cytoplasmic structures (*55, 56*). Although not thoroughly characterized, one of the functions of the NS4B protein is to induce formation of the membranous web (*55, 57*). At higher magnification, the membranous web is made up of numerous small double membrane vesicles (DMVs)(*58, 59*).

Within the membranous web there are invaginations where proteins NS3 (a serine protease-helicase), the NS3 co-factor NS4A, NS4B, NS5A, and NS5B (the pendent RNA polymerase) assemble along with HCV RNA into the replication complex (shown in Figure I.B-3, step 4). Several host proteins have been implicated to associate with the replication complex and help facilitate RNA replication. One of these is cyclophilin-A which interacts with several proteins in the replication complex (*60, 61*). The viral RNA produced is susceptible to degradation by cellular processes in the cytoplasm.

Several studies have shown that RNA produced from non-replicative viral constructs have a very short half-life and are cleared from the cell hours after entry or

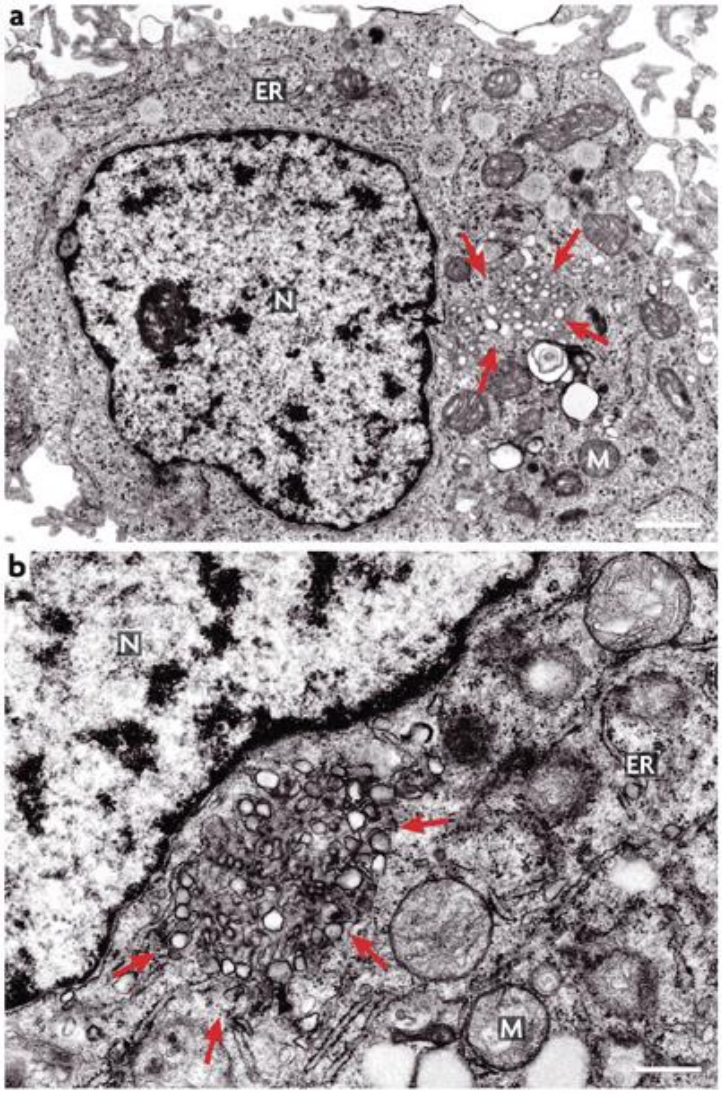

Nature Reviews | Microbiology

Figure I.B-4: Electron micrograph of a Huh-7 cell harboring an HCV replicon. (a) In cells with ongoing HCV infection or replication an alteration of membranes (called the membranous web) is found next to or surrounding the nucleus. The web contains all HCV non-structural proteins and viral RNA, and is the site for HCV RNA replication. Aside from this alteration, the rest of the organelles in the cell are unaffected. Scale bar = 1µm. (b) Higher magnification of a membranous web (arrows). The web is closely associated with the rough ER, and is made up of small vesicles embedded in a membrane matrix. A closer view would show these vesicles as double membraned. Scale bar = 500nm. ER, endoplasmic reticulum; M, mitochondria; N, nucleus. Figure from (*62*).

half-life. Within the HCV 5' untranslated region there is a sequence of RNA that has perfect complementarity to a micro-RNA that is abundant only in the liver; the site for HCV infection (Figure I.B-2) (*63, 64*). MiR-122 binds to a binding site within the 5'-UTR of the virus (*65-67*) and recruits argonaute-2 (Ago2, a component of the RNA-induced silencing complex) (*68, 69*). The exact mechanism is not yet clear, however, this binding protects the HCV RNA from degradation and extends the half-life of the RNA, (*70-72*) reviewed in (*73*). Adding exogenous miR-122 promotes HCV replication (*74*) and in reverse a miR-122 antagonist inhibits HCV replication (*75*).

HCV assembly, viral release, and maturation

Similar to HCV's translation and RNA replication, virion assembly is very dependent on cellular structures and host proteins. Due to the relatively recent development of cell-culture systems with fully infectious virus the exact mechanisms of packaging, assembly, and release are not yet clear. Non-structural protein NS5A is a cryptic protein with several functions attributed to it (*66, 76-81*). One of these functions is binding HCV genomic RNA and bringing it to the sites for viral assembly. Viral packaging and assembly presumably occurs on cytosolic lipid droplet (cLD) structures in the cytoplasm. cLDs are made up of a phospholipid monolayer that is derived from outer endoplasmic reticulum, around a hydrophobic core of neutral lipids and cholesterol esters (*82, 83*).

After synthesis in the ER the core protein forms a homodimer and is trafficked to cLDs (*84-86*). This trafficking is supported by diacylglycerol O-acetyltransferase (DGAT1), one of the DGAT enzymes that are required to synthesize triglycerides stored in cLDs

(*87*). One of the key steps in HCV assembly is the recruitment of NS5A to interact with the core protein at cLDs, which is enhanced by DGAT1 (*88-90*) . The NS5A protein also forms a homodimer, can be phosphorylated, and binds RNA (*77, 91*). It contains an N-terminal helix, which anchors it to membranes followed by a zinc-binding domain (*92*) that mediates NS5A homodimerization and two long unfolded flexible domains. The C-terminal unfolded domains contain determinants that are required for virus assembly (*93*). It is possible that NS5A's role in the assembly process is to bring genomic RNA for packaging from replication complexes to cLDs (*88-90*).

The next key step is the interaction of the p7-NS2 complex with NS3-NS4A, which is required to sequester the core protein from cLDs to the ER (*94-96*). The recruitment of the core protein may be simply due to protein interactions, but it might also involve the helicase and protease activity of the NS3-NS4A complex. At the ER viral particles bud of the ER, with the E1 and E2 proteins that were anchored there after translation and processing. This process is highlighted in Figure I.B-3 and shown in more detailed in Figure I.B-5.

The endosomal sorting complex required for transport (ESCRT) pathway has been implicated in assisting HCV particle budding and release. This pathway is involved

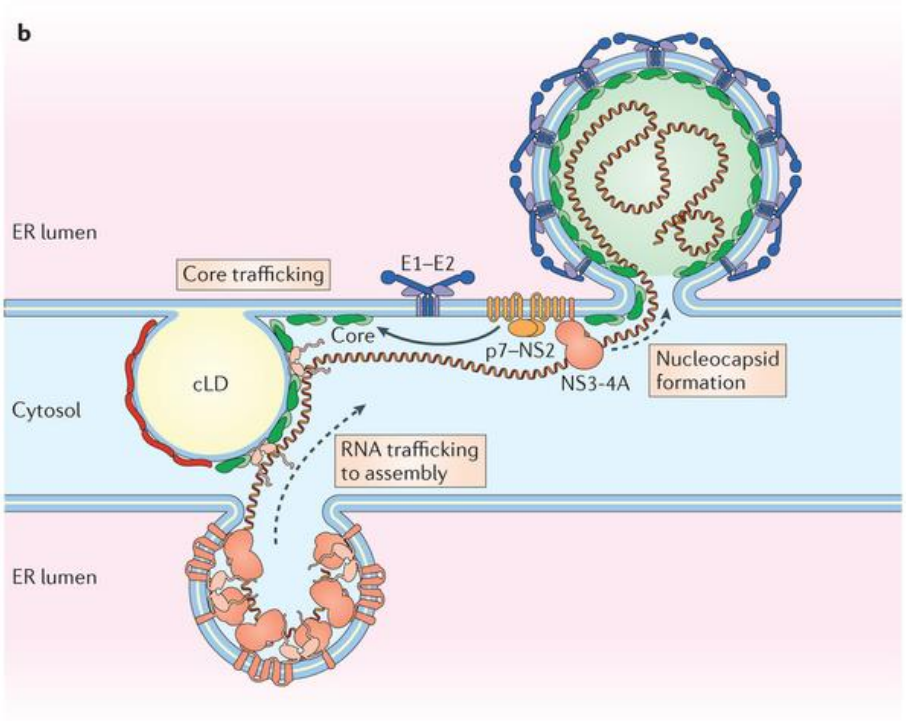
b
ER lumen
Core trafficking
E1–E2
Core
p7–NS2
NS3-4A
Nucleocapsid formation
cLD
Cytosol
RNA trafficking to assembly
ER lumen

Figure I.B-5: Late events in the HCV lifecycle. RNA replication occurs in ER membrane invaginations within the membranous web (bottom). Following this the RNA is shifted towards virus assembly. p7-NS2 interacts with NS3-NS4A, which recruits the viral core protein from the cLD to the site of assembly. Particles assemble by recruitment of E1-E2 complexes and budding into the ER. Figure from (*52*).

in budding and fission of membranous compartments and has been utilized by several different viruses during budding. Several groups have reported that in cell-culture experiments HCV particle release depends on ESCRT pathway components (*97-99*).

After packaging and assembly the HCV particles pass through the secretory pathway. E1 and E2 are post-translationally modified acquiring high mannose and complex *N*-linked glycans (*100, 101*). As particles transit through the secretory pathway they interact with lipoproteins. HCV utilizes the pathway for producing very-low density lipoproteins (VLDLs), which export triglycerides and cholesterol from hepatocytes (*102*).

B.3 HCV TREATMENT: NEW DIRECT ACTING ANTIVIRALS AND HOST TARGETING AGENTS

In 1957, many years before the discovery and isolation of HCV, scientists discovered interferon, a naturally occurring substance in the human body. Three classes of interferon are known: alpha, beta, and gamma, each having antiviral properties. In 1991, soon after the discovery of HCV, interferon alpha was approved for use against HCV (reviewed in (*103*)). In 1998 addition of ribavirin to the treatment regimen provided a major breakthrough in HCV treatment. One major hindrance of interferon treatment was the short half-life of interferon. A pegylated form of interferon increased the half-life of interferon in the bloodstream and was approved for treatment in 2001. These changes provided therapeutic options that couldsuppress the virus to lower levels.

Although the peg-interferon + ribavirin regimen was a significant breakthrough in HCV treatment the combination was not universally effective and many patients experienced severe side-effects. 50% of HCV genotype 1 patients on peg-interferon + ribavirin achieved sustained virological response (SVR). The SVR rate was much lower

for other genotypes. Additionally, patient genetics play a significant role in the regimen's efficiency. Sometimes, patients reported debilitating side-effects including flu-like symptoms, extreme fatigue, and suicidal thoughts.

The first compounds specifically targeting an HCV protein or process were the protease inhibitors boceprevir and telaprevir. These were approved in 2011, for use in combination with the existing peg-interferon + ribavirin regimen, only for the treatment of genotype 1 HCV. The success rate of the new regimen was significantly lower for other genotypes of HCV. The SVR rates for the protease DAA/peg-interferon/ribavirin combination reached ~90%.

New direct-acting antivirals

Since the approval of boceprevir and telaprevir several DAAs have entered and progressed in clinical trials (reviewed in (*104*)). One of the most intriguing class of DAAs are drugs that target the NS5A protein. As detailed earlier in this chapter, NS5A plays several important roles at different stages of the viral lifecycle. HCV is required for the proper assembly and function of the replication complex. HCV is also required for localization of viral RNA from replication complexes to assembly sitesand ultimately proper packaging of the RNA into virions. Interestingly, NS5A reportedly has other functions in modulating the innate immune response during infection (*105*). NS5A does not have an enzymatic activity, but its interaction with cellular membranes, dimerization, and hyperphosphorylation state are all critical parameters for its functionality (*77*).

The first NS5A targeting compound to progress in clinical trials was daclatasvir (DCV) (*106*) (formerly BMS790052, trade name Daklinza). DCV, unlike previously approved

DAAs has broad genotype coverage, with picomolar EC_{50}s against the most common genotypes. In the United States DCV is in Phase II clinical trials and in September 2014 DCV was approved for treatment in Europe. Second generation NS5A targeting drugs are now entering clinical trials. Of these, ledipasvir (LDV) (formerly GS-5885) is most promising being more efficient than DCV against all genotypes.

Sofosbuvir (SOF) (formerly GS-7977, brand name Sovaldi) is a nucleoside analog targeting the polymerase NS5B with broad genotype coverage and efficient SVR rates (*107*). In October 2014 SOF was approved for use in a combined tablet with LDV (brand name Harvoni) (*106, 108*) for the treatment of genotype 1 HCV, in combination with ribavirin. This is the first interferon-free regiment approved for HCV treatment.

Host targeting agents (HTAs)

During its lifecycle, HCV heavily depends on cellular proteins and processes. Taking advantage of this several drugs that target these host co-factors to inhibit the virus are being investigated. As mentioned above, the microRNA miR-122 interacts with the HCV genome and stabilizes it, thus extending the RNA's half-life. Miravirsen (formerly SPC3949) is a locked nucleic acid oligonucleotide with a sequence complementary to miR-122 and it completed phase IIa clinical trials in 2011 (*109*). Miravirsen binds and sequesters miR-122, lowering the amount available to bind and protect the HCV genome. This leads to the rapid degradation of the viral RNA from cellular processes, leading to inhibition of the virus (*110*).

Cyclophilins (Cyps) are cellular proteins that are utilized by multiple viruses, and different points in the viral lifecycle. Cyps are molecular chaperones that catalyze the cis-

trans isomerization of proline residues (*111*). Sixteen Cyp members have been identified, seven of these being the major ones found in humans(*111*). CypA and CypB have been shown to directly interact with HCV's polymerase NS5B. Depleting cyclophilin A (cypA) or inhibiting its isomerase activity decreases HCV replication, and virus production (*112*). It is not yet clear how Cyp A aides in HCV infection, or specifically for which point of the lifecycle it is required (*113, 114*). Nonetheless, several compounds have been discovered that bind to cyclophilins and lead to viral inhibition. One such group are cyclosporine inhibitors. Cyclosporin A (CsA) used in this study is a common immunosuppressive drug during organ transplants. CsA inhibits HCV replication and virus production *via* as yet unclear mechanisms.

Mechanism of action for NS5A targeting drugs

NS5A is a 447-amino acid protein with an N-terminal alpha helix (residues 5 to 25) followed by three structural domains labelled I, II, and III. Domain I spans residues 28 to 213; it contains RNA and zinc binding motifs (*91, 92*). This domain dimerises *in vitro* and is essential for RNA replication. Domain II (residues 250 to 342) is unfolded *in vitro* and also plays a role in replication. Domain III (residues 356 to 447) is also unfolded *in vitro* and is important for virus assembly (*88*). Although several NS5A-targeting drugs have been discovered their exact mechanism(s) of action are not well understood.

Daclatasvir (DCV)

DCV is a potent and specific inhibitor of NS5A. Based on crystal structures of NS5A and the positions of DCV resistance mutations it is expected to bind at the NS5A dimer interface,. DCV causes a rapid and potent decrease in viral replication, assembly,

and virus production (*106*). Intriguingly, the drug also causes a fast and distinct change of NS5A's cytoplasmic distribution (*115, 116*). Studies have proposed that this alteration prevents the formation of RNA replication complexes (*116*). Recent studies have shown that DCV disrupts the formation of replication complexes by somehow inhibiting the formation of the membranous web, the sub-cellular site for viral RNA replication (*117*). After addition of the drug to infected cells, NS5A redistribution can be detected hours before a decrease in viral RNA or virus production. Intriguingly, DCV's effect on the membranous web points to a new role for NS5A in the web's formation.

It is not known exactly how DCV disrupts formation of the membranous web, how it prevents NS5A from localizing to replication complexes, or how the drug diverts NS5A to cLDs. Additionally. it is yet unknown how diverting NS5A to cLDs affects virus assembly and replication.

Ledipasvir (LDV)

The mechanism of action of LDV, the most advanced of the second generation NS5A inhibitors, is just as poorly understood as DCV's. LDV has a broader genotype coverage than DCV. LDV has faster kinetics, leading to a more rapid decrease in viral replication and virus production. Before the initiation of the studies outlined in Chapter II of this thesis the effect of LDV on the localization of NS5A was unknown. Its effect, if any, on the membranous web or replication complex formation had yet to be determined.

B.4 RELATIONSHIP BETWEEN HCV AND THE HOST

Activation and evasion of the innate immune system

The innate immune response is the first line of defense against HCV infection. HCV RNA, either from replication, or genomic RNA released from virions is detected as foreign by cellular pattern recognition receptors. RNA-binding receptors MDA5 and RIG-I are the major receptors that detect the presence of foreign RNA. MDA5 typically detects double-stranded RNA over 2000 nts in length, while RIG-I signals for shorter 5' uncapped RNA and single stranded RNA (*118*). Flaviriruses such as HCV are typically recognized by RIG-I.

Hijacking host proteins and processes

During its replication cycle HCV interacts with and co-opts several host proteins and processes to establish and maintain infection (reviewed in (*119*)). Of these, several proteins facilitate and potentially aid the virus, including processing body components Rck/p54 (DDX6), PatL1, and LSm1 (*120-122*), while others through diverse and as yet understood mechanisms restrict viral replication (some reviewed in (*123*)).

In addition to its own viral proteins and RNA, HCV has been shown to hijack or recruit several host proteins to the lipid droplets. Some of these proteins are found in processing bodies (P-bodies). During infection, at least up to 10 different proteins are prevented from going to P-bodies, and instead localize with viral proteins at lipid droplets (*124-128*). It is not clear what role any of these proteins play in HCV replication or assembly. However, decreasing the levels of some of these proteins hinders HCV infection (*124*, *126*).

Restriction by host factors

Several screens to identify ISGs with antiviral activity against HCV have been performed (*129-132*). ISGs that significantly reduce HCV replicon activity include IFI6,

IRF1, IRF9, ISG20, MX1, OASR1, PKR, and viperin (*129, 130*). ISGs have been identified that restrict almost every step of the HCV viral lifecycle. However, for some of the most recently identified antiviral ISGs it is unknown which stage of HCV infection they restrict, and further the exact mechanism(s) by which this occurs (reviewed in (*123*)).

In a larger screen; 380 ISGs were tested for antiviral activity against six viruses, including HCV (*131*). This screen resulted in the identification of several genes that had either not been characterized as antiviral, or were not known to inhibit the viruses tested. Interestingly, compared to the entire panel of ISGs, genes with antiviral properties were enriched for proteins with helicase, hydrolase, and nucleic acid binding functionalities. Mov10 (Moloney leukemia 10) was one such antiviral factor identified in this screen (*131*).

B.5 RESTRICTION HOST FACTOR MOV10

Mov10 is expressed from an interferon stimulated gene and is a component of mRNA P-bodies and RNA interference signaling complexes (RISC). It interacts with canonical P-body and RISC proteins including APOBEC3G, Argonaute 1 and Argonaute 2 (*133-135*). In addition, Mov10 is an RNA helicase that belongs to the DExD superfamily (*133*) and the Upf1-like group of helicases (*136*). Inhibition of retroviruses by Mov10 has been well documented and in the case of HIV well characterized (*134, 137-140*). However, the specific effects of Mov10 in the life cycle of HCV are unknown.

Here we studied Mov10's restriction of HCV in-depth, identified which stages in the viral lifecycle were affected by this host factor, and whether any or all of the putative

functions of Mov10 were required for antiviral activity. We report that overexpression of Mov10, but not of other P-body component Dcp1a, inhibits HCV. Specifically, Mov10 overexpression inhibited HCV RNA production leading to inhibition of viral production. Additionally, we demonsrated that the infectivity of virions produced in cells overexpressing Mov10 was impaired. Also, we show that the localization of Mov10 to P-bodies is not required for antiviral activity, and that Mov10's putative helicase and ATP-binding domains were similarly not required for inhibition of HCV.

II. Biochemical mechanism and inhibitor resistance studies of xenotropic murine leukemia virus-related virus reverse transcriptase

B. ABSTRACT

We report key mechanistic differences between the Reverse Transcriptases (RT) of Human Immunodeficiency Virus type-1 (HIV-1) and of Xenotropic Murine Leukemia Virus-Related Virus (XMRV), a gammaretrovirus that can infect human cells. Steady and pre-steady state kinetics demonstrated that XMRV RT is significantly less efficient in DNA synthesis and in unblocking chain-terminated primers. Surface plasmon resonance experiments showed that the gammaretroviral enzyme has a remarkably higher dissociation rate (k_{off}) from DNA, which also results in lower processivity than HIV-1 RT. Transient kinetics of mismatch incorporation revealed that XMRV RT has higher fidelity than HIV-1 RT. We identified RNA aptamers that potently inhibit XMRV, but not HIV-1 RT. XMRV RT is highly susceptible to some nucleoside RT inhibitors, including Translocation Deficient RT inhibitors, but not to nonnucleoside RT inhibitors. We demonstrated that XMRV RT mutants K103R and Q190M, which are equivalent to HIV-1 mutants that are resistant to tenofovir (K65R) and AZT (Q151M), are also resistant to the respective drugs, suggesting that XMRV can acquire resistance to these compounds through the decreased incorporation mechanism reported in HIV-1.

B. MATERIALS AND METHODS

Expression and Purification of XMRV, HIV-1, and MoMLV RTs

The plasmid pBSK-XMRV containing the coding sequence of XMRV RT from the VP62 clone (GenBank: DQ399707.1) was chemically synthesized and optimized for bacterial expression by Epoch Biolabs Inc (Missouri City, Texas). The 2013 bp XMRV RT sequence was amplified from pBSK-XMRVRT by PCR, using the forward and reverse primers 1 (all primer sequences are shown in Table II-7), resulting in *NdeI* and *HindIII* restriction sites. Drug resistant XMRV RT mutants Q190M and K103R (equivalent to HIV-1 Q151M RT and K65R) were generated by site-

directed mutagenesis using forward and reverse primers 2 and 3. The digested amplicons were ligated into pET-28a (Novagen), resulting into a construct that expresses an N-terminal hexa-histidine tag. pET-28a-MRT encoding full-length wild-type MoMLV RT was provided by Dr. M. Modak (New Jersey Medical School, Newark NJ).

Expression and purification of MoMLV and XMRV RTs were carried out similarly to our previously published protocols (*31, 32*). Briefly, RTs were expressed in BL21-pLysS *E. coli* (Invitrogen) grown at 37°C and induced with 150 µM IPTG at OD_{600} 0.8, followed by 16 hours growth at 17°C. A cell pellet from a 3 L culture was incubated with 40 ml lysis buffer (50 mM Tris-HCl, pH 7.8, 500 mM NaCl, 1 mM PMSF, 0.1% NP-40, 1% sucrose, and 2 mg/ml lysozyme), then sonicated and centrifuged at 15,000 x g for 30 min. The supernatant was diluted 2-fold in Buffer A (50 mM Tri-HCl pH 7.8, 1 mM PMSF, 4% streptomycin sulfate, and 10% sucrose), stirred on ice for 30 min and centrifuged. The supernatant was loaded on a Ni-NTA column and bound proteins were washed with 20 ml Buffer B (20 mM Tris-HCl pH 7.5, 500 mM NaCl) and 5 mM imidazole, followed by 20 ml Buffer B with 75 mM imidazole. RT was eluted in 2 ml fractions with 20 ml buffer B containing 300 mM imidazole. Fractions with RT were pooled and further purified by size exclusion chromatography (Superdex 75; GE Healthcare). RTs (>95% pure) were stored in 50 mM Tris-HCl pH 7.0, 100 mM NaCl, 1 mM DTT, 0.1% NP-40, and 30% glycerol in 10 µl aliquots at -20°C. Protein concentrations were determined by measuring UV_{280} (molar extinction coefficients of 106 and 103 $M^{-1}cm^{-1}$ for XMRV and MoMLV RT).

HIV-1 RT was cloned in a pETduo vector and purified as described previously (*37, 141, 142*). Oligonucleotide sequences (IDT-Coralville, IA) of DNA/RNA substrates are shown in Table II-7. Nucleotides were purchased from Fermentas (Glen Burnie, MD). They were treated with inorganic pyrophosphatase (Roche Diagnostics, Mannheim, Germany) as described previously (*143*) to remove PPi that might interfere with excision assays.

Steady State Kinetics

Steady state parameters K_m and k_{cat} for dATP incorporation were determined using single nucleotide incorporation gel-based assays. XMRV RT and MoMLV RT reactions were carried out in 50 mM Tris-HCl pH 7.8, 60 mM KCl, 0.1 mM DTT, 0.01% NP-40, and 0.01% bovine serum albumin (BSA) (Reaction Buffer) with 6 mM $MgCl_2$ or 1.5 mM $MnCl_2$, 0.5 mM EDTA, 200 nM or 100 nM T_{d26}/5′-Cy3-P_{d18b}, 20 nM or 5 nM RT for XMRV and MoMLV RTs, respectively and varying concentrations of dNTP in a final volume of 10 µl. The reactions for HIV-1 RT were carried out in Reaction Buffer with 100 nM T_{d26}/5′-Cy3-P_{d18b}, 10 nM HIV-1 RT, and 6 mM $MgCl_2$ in a 20 µl reaction. All the concentrations mentioned here and in subsequent assays reflect final concentration of reactants otherwise mentioned Reactions were stopped after 15 minutes for XMRV, 4 minutes for MoMLV RT, and 2.5 minutes for HIV-1. The products were resolved on 15% polyacrylamide–7M urea gels. The gels were scanned with a Fuji Fla-5000 PhosphorImager (Stamford, CT) and the bands were quantified using MultiGauge. Results were plotted using GraphPad Prism 4. K_m and k_{cat} were determined graphically using Michaelis-Menten equation.

Active Site Titration and Determination of $K_{D.DNA}$

Active site concentrations and kinetic constants of DNA binding for XMRV, HIV-1 and MoMLV RTs were determined using pre-steady state experiments. Reactions with XMRV and MoMLV RTs were carried out in the reaction buffers listed above. For XMRV RT 100 nM protein was pre-incubated with increasing concentrations of T_{d31}/5′-Cy3-P_{d18a}, followed by rapid mixing with a reaction mixture containing 5 mM $MgCl_2$ and 100 µM next incoming nucleotide (dATP). The reactions were quenched at various times (5 ms to 4 s) by adding EDTA to a final concentration of 50 mM. The amounts of 19-mer product were quantified and plotted against time. The data were fit to the following burst equation:

$$P = A\left(1 - e^{-k_{obs}t}\right) + k_{ss}t \qquad \text{(Eq.1)}$$

where *A* is the amplitude of the burst phase that represents the RT-DNA complex at the start of the reaction, k_{obs} is the observed burst rate constant for the dNTP incorporation used, k_{ss} is the steady state rate constant, and *t* is the reaction time. The rate constant of the linear phase (k_{cat}) was estimated by dividing the slope of the linear phase by the enzyme concentration. The active site concentration and T/P binding affinity ($K_{D.DNA}$) were determined by plotting the amplitude (*A*) against the concentration of T/P. Data were fit to the quadratic equation (Eq. 2) using non-linear regression:

$$A = 0.5(K_D + [RT] + [DNA]) - \sqrt{0.25(K_D + [RT] + [DNA])^2 - ([RT][DNA])}$$

(Eq. 2)

where K_D is the dissociation constant for the RT-DNA complex, and [RT] is the concentration of active polymerase. HIV-1 RT's DNA binding affinity was determined as previously described (*37*).

Surface Plasmon Resonance Assay

We used surface plasmon resonance (SPR) to measure the binding constants of XMRV and HIV-1 RTs to double-stranded DNA. Experiments were carried out by Dr. Bruno Marchand using a Biacore T100 (GE Healthcare). To prepare the sensor chip surface we used the 5′-biotin-T_{d37}/P_{d25} oligonucleotide (Table II-7). 120 RUs of this DNA duplex were bound in channel 2 of a streptavidin-coated sensor chip (Series S Sensor Chip SA (certified)) by flowing a solution of 0.1 µM DNA at a flow rate of 10 µl/min in a buffer containing 50 mM Tris pH 7.8, 50 mM NaCl. The binding constants were determined as follows: RT binding was observed by flowing

solutions containing increasing concentrations of the enzyme (0.2, 0.5, 1, 2, 5, 10, 20, 50, 100 and 200 nM) in 50 mM Tris pH 7.8, 60 mM KCl, 1 mM DTT, 0.01% NP40 and 10 mM $MgCl_2$ in channels 1 (background) and 2 (test sample) at 30 µl/min. The trace obtained in channel 1 was subtracted from the trace in channel 2 to obtain the binding signal of RT. This signal was analyzed using the Biacore T100 Evaluation software to determine K_D, k_{on}, and k_{off}.

Pre-steady State Kinetics of dNTP Incorporation

The optimal nucleotide incorporation rates (k_{pol}) were obtained by pre-steady state kinetics analysis using single nucleotide incorporation assays. A solution containing XMRV RT (150 nM final concentration) and T_{d31}/5′-Cy3-P_{d18a} (40 nM) was rapidly mixed with a solution of $MgCl_2$ (5 mM) and varying dATP (5-200 µM) for 0.1 to 6 s before quenching with EDTA (50 mM) (all concentrations in parentheses are final, unless otherwise stated). Products were resolved and quantified as described above. Burst phase incorporation rates and substrate affinities were obtained from fitting the data to Eq.1. Turnover rates (k_{pol}), dNTP binding to the RT-DNA complex ($K_{d.dATP}$), and observed burst rates (k_{obs}) were fit to the hyperbolic equation:

$$k_{obs} = \left(k_{pol}\left[dNTP\right]\right)/\left(K_{d.dNTP} + \left[dNTP\right]\right) \quad \text{(Eq. 3)}$$

HIV-1 RT's DNA binding affinity was determined as previously described (*37*).

Fidelity of DNA Synthesis

The fidelity (error-proneness) of XMRV RT was determined and compared to that of MoMLV RT and HIV-1 RT by primer extension assays using 10 nM heteropolymeric T_{d100}/5′-Cy3-P_{d18a}. Reactions (10 µl) were carried out in Reaction Buffer containing all four dNTPs (100 µM each) or only 3 dNTPs (missing either dATP, dGTP, or dTTP) at 100 µM each. Incubations of the XMRV and MoMLV (50 nM) reactions were at 37 °C for 45 min and 30 min for HIV-1 RT (20

nM). Reactions were initiated by adding dNTPs, stopped with equal volume of formamide-bromophenol blue, and an aliquot was run on a 16% polyacrylamide–7M urea gel.

Kinetics of Mismatch Incorporation

For these experiments, instead of including the next correct nucleotide (dATP) in the polymerase reactions, we used dTTP as the mismatched incoming nucleotide. Hence, 50 nM XMRV RT was pre-incubated with 35 nM T_{d31}/5′-Cy3-P_{d18a} in reaction mixture. Reactions were initiated by adding dTTP (5–750 μM) and 5 mM $MgCl_2$, followed by incubation (37 °C) for 5 min, due to the decreased mismatch incorporation rate of XMRV. For MoMLV RT, 30 nM RT and 20 nM DNA used and the reactions were carried out for 2.5 minutes. For HIV-1, 30 nM RT, 20 nM DNA, and 0–200 μM nucleotide were used and the reactions were carried out for 2.5 min. The amount of extended primer was quantified and plotted against the concentration of dTTP. The data were used to derive the $K_{d.dNTP}$ of incorrect nucleotide binding, the rate k_{pol} (using equations 1 and 3) and the efficiency of the misincorporation reaction ($k_{pol}/K_{d.dTTP}$).

Determination of *in vivo* Fidelity

ANGIE P cells, which contain a retroviral vector (GA-1) that encodes a bacterial β-galactosidase gene (*lacZ*) and a neomycin phosphotransferase gene, were plated ($5x10^6$ cells /100 mm dish) and after 24 hrs were transfected using the calcium phosphate precipitation method with a plasmid expressing either XMRV or amphotropic MLV (AM-MLV) (three independent transfections per vector). After 48 hrs, the culture medium with XMRV or (AM-MLV) was harvested, serially diluted, and used to infect D17 target cells ($2x10^5$ cells/60 mm dish) in the presence of polybrene. The infected D17 cells were selected for resistance to G418 (400 μg/ml) in the presence of 1 μM AZT to suppress reinfection, and characterized by staining with 5-bromo-4-chloro-3-indoyl-β-D-galacto-pyranoside (X-Gal) approximately 2 weeks after G418 selection. The frequencies of inactivating mutations in *lacZ* were quantified as described before (blue *vs.* white colonies) (*144*).

Processivity of DNA Synthesis – Trap Assay

Processivity reactions were carried out in Reaction Buffer containing 20 nM T_{d100}/P_{d18}, 100 μM of each dNTP, 30 nM HIV-1 RT, 50 nM MoMLV RT or 100 nM XMRV RT, and 1μg/μl unlabeled calf thymus DNA trap in 50 μL. Enzymes were pre-incubated with T_{d100}/P_{d18} for 1 min before adding dNTPs (100 μM each) together with the calf thymus DNA trap. Reactions were incubated at 37°C, and 10 μl aliquots were taken out at 3, 7.5, and 15 min for HIV-1 RT or at 7.5, 15, and 30 min for XMRV RT and MoMLV RT, and mixed with equal volume of loading dye. The effectiveness of the trap was determined by pre-incubating the enzyme with the trap before adding T_{d100}/P_{d18}. Control DNA synthesis was measured in absence of trap under the same conditions. Reaction products were resolved as above.

Single Turnover Processivity Assays

30 nM $T_{d31}/5'$-Cy3-P_{d18a} was pre-incubated for 10 min with 100 nM XMRV or 50 nM MoMLV RT in Reaction Buffer, then rapidly mixed with 100 μM dNTPs, 5 mM $MgCl_2$ for varying times (0.1-45 s) before quenching with EDTA (50 mM final). Single turnover processivity of HIV-1 RT was assayed with 40 nM enzyme, 20 nM DNA, and 50 μM of each nucleotide. The reaction products were resolved and quantified as described above. The data were fit to a one-phase exponential decay equation for the elongation of the 18-mer primer. The rates of appearance and extension of products from subsequent nucleotide incorporations (19- and 27-mer) were obtained by fitting the intensities of corresponding bands to double exponential (Equation 4):

$$P = A\left(1 - e^{-k_1 t}\right) + \left(e^{-k_2 t}\right) + C \qquad \text{(Eq.4)}$$

where A is the amplitude, P is the amount of 19-mer, 20-mer or higher length products, k_1 is the rate of product generation, k_2 the rate of subsequent elongation and C a constant (*37, 145*).

Assays for Reverse Transcriptase Inhibition

DNA synthesis by 50 nM XMRV RT or MoMLV RT was carried out in Reaction Buffer using 20 nM T_{d100}/5′-Cy3-P_{d18a}, 2.5 µM dNTP, 5 mM $MgCl_2$,and varying amounts of NRTI (0-100 µM). Reactions were quenched with 95% formamide after 1 hr incubation at 37ºC (*146*). In experiments with aptamers 10 nM XMRV RT, 20 nM T_{d31}/5'-Cy3-P_{d18a}, and 50 µM dNTPs were used in the presence of varying amounts of aptamer for 30 min (0-500 nM for m.1.3; 0-25 nM for m.1.4 and m.1.1FL). The inhibition of DNA polymerization was monitored by resolving the products on 15% polyacrylamide–7 M urea gels and visualized as described above. Bands corresponding to full extension products were quantified using MultiGauge Software and IC_{50}s were obtained from dose-response curves using GraphPad Prism.

PPi- and ATP-dependent Excision and Rescue of T/$P_{AZT\text{-}MP}$ or T/$P_{EFdA\text{-}MP}$

The ability of enzymes to use PPi or ATP to unblock template-primers that had AZT-MP (T/$P_{AZT\text{-}MP}$) or EFdA-MP (T/$P_{EFdA\text{-}MP}$) at their 3′ primer ends was measured as follows: 20 nM of T/$P_{AZT\text{-}MP}$ or T/$P_{EFdA\text{-}MP}$ were prepared as described before (*142*). They were incubated at 37°C with either 60 nM HIV-1 RT, or 200 nM XMRV RT in the presence of 0.15 mM PPi or 3.5 mM ATP for PPi- or ATP-dependent rescue reactions, respectively. Reactions were initiated by the addition of $MgCl_2$ (6 mM). Aliquots were removed at different times (0-90 min) and analyzed as above. Rescue assays were performed in the presence of 100 µM dATP to prevent EFdA-MP reincorporation, 0.5 µM dTTP, 10 µM ddGTP, and 10 mM $MgCl_2$.

Molecular Modeling

The sequence of XMRV RT from the VP62 clone was aligned with that of MoMLV RT (PDB: 1RW3) (*29*, *30*) using ClustalW. To generate the homology model of XMRV RT, we used the Prime protocol of the Schrödinger software suite (Schrödinger Inc. NY). The resulting molecular model prepared by Dr. Kamal Singh was further energy minimized by OPLS2005 force field using the Impact option of Schrödinger. The final model was validated with PROCHECK v.3.5.4.

C. RESULTS

Comparison of RT sequences

The XMRV and MoMLV enzymes are closely related (~95% sequence identity) with most of the differences between them being in the RNase H domain (Figure I.A-3(a)). While XMRV and MoMLV differ significantly from HIV-1 RT, the known polymerase motifs (A-F) are well conserved in all three enzymes (Figure I.A-3(a)). Specifically, the active site aspartates in Motifs A and C (Figure II-10) (D150, D224, D225 in XMRV RT; D150, D224, D225 in MoMLV RT; D110, D185, D186 in HIV-1 RT) are conserved in all three RTs. Also, the three enzymes are similar in Motif B, which is involved in dNTP binding and multidrug resistance (AZT and dideoxy-nucleoside drugs) through the decreased incorporation mechanism (*35*, *147-149*). Specifically, all three enzymes have a glutamine at the start of this motif (Q151 in HIV-1 RT, Q190 in XMRV RT and Q190 in MoMLV RT). Motif D includes HIV-1 RT residues L210 and T215, which when mutated they enhance excision of AZT from the AZT-terminated primer terminus. This motif is mostly different in XMRV and MoMLV RTs, where the corresponding residues are N226 and A231 (Figure I.A-3(a)). K219 of HIV-1 RT Motif D is proximal to the dNTP-binding pocket and is also conserved in the other enzymes (K235). The DNA primer grip (Motif E) (*150*) in HIV-1 RT ($M_{230}G_{231}Y_{232}$) is slightly different in the gammaretroviral enzymes ($L_{245}G_{246}Y_{247}$). Motif F at the fingers subdomain of all enzymes has two conserved lysines that bind the triphosphate of the dNTP (K65 and K72 in HIV-1 RT; K103 and K110 in XMRV and MoMLV RTs).

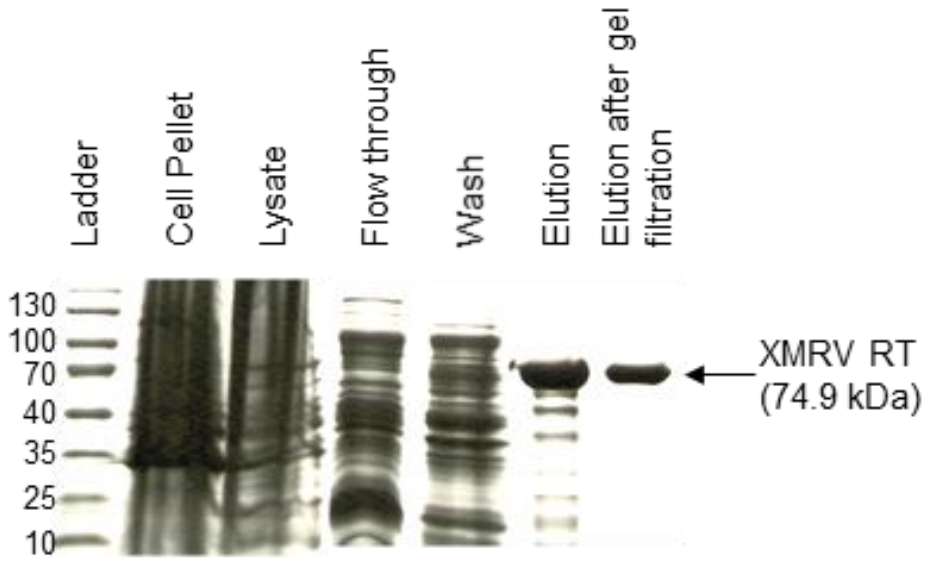
Ladder
Cell Pellet
Lysate
Flow through
Wash
Elution
Elution after gel filtration
130
100
70
40
35
25
10
XMRV RT
(74.9 kDa)

Figure II-1: Purification of XMRV RT. XMRV RT was expressed in E.coli BL21 pLysS cells and purified as described in 'Experimental Procedures'. The figure shows a representative SDS-PAGE gel with samples from various steps of the protein purification scheme. Lane 1 is a sample of the non-soluble fraction of the resuspended bacterial pellet; lane 2 shows the soluble fraction loaded on the nickel affinity column; lane 3 is the flow-through fraction with the proteins that did not bind to the nickel affinity column; lane 4 shows the proteins washed off before final elution; lane 5 is the main fraction eluted with 300 mM imidazole. All elution fractions containing XMRV RT were pooled, concentrated and passed through a gel filtration column to produce the final protein shown in lane 6.

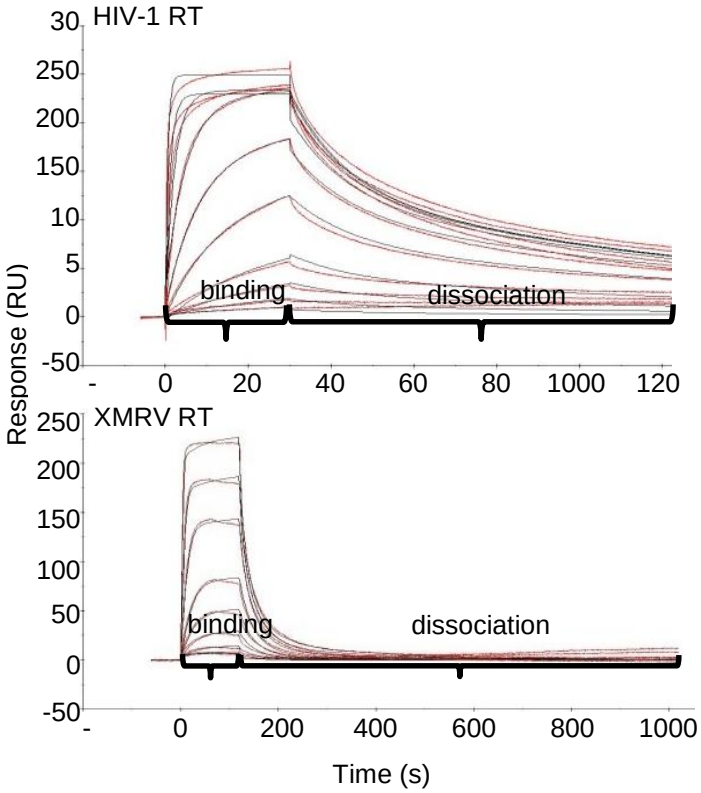
HIV-1 RT
30
250
200
150
10
5
0
-50
binding
dissociation
Response (RU)
- 0 20 40 60 80 1000 120
XMRV RT
250
200
150
100
50
0
-50
binding
dissociation
- 0 200 400 600 800 1000
Time (s)

Figure II-2: Assessment of $K_{D.DNA}$, k_{on} and k_{off} using Surface Plasmon Resonance (SPR). SPR was used to measure the binding affinity of RTs to a nucleic acid substrate. Increasing concentrations of each RT (0.2, 0.5, 1, 2, 5, 10, 20, 50, 100 and 200 nM) were injected over a streptavidin chip with biotinylated double-stranded DNA immobilized on its surface as described in Methods. The experimental trace (red) shown is the result of a subtraction of the data obtained from the channel containing the immobilized nucleic acid minus the signal obtained from an empty channel. The black curve represents the fitted data according to the "heterogeneous ligand" model that assumes two different binding modes for RT on the nucleic acid.

Several HIV-1 residues involved in NRTI resistance have the resistance mutations in XMRV and MoMLV RTs (Table 1). Hence, XMRV and MoMLV RTs have a Val as the X residue (codon 223) of the conserved YXDD sequence of Motif C. An M184V mutation at this position in HIV-1 RT causes strong, steric hindrance-based, resistance to 3TC and FTC (*151-153*), and to a lesser extent to ddI, ABC (reviewed in (*154*)), and translocation defective RT inhibitors (TDRTIs) (*151*) (Table 1). Similarly, the M41L mutation, which causes excision-based AZT resistance in HIV is already present in XMRV and MoMLV RT (L81, Table 1). The gammaretroviral enzymes differ from HIV-1 RT in several other HIV drug resistance sites (HIV residues 62, 67, 69, 70, 75, 77, 115, 210, 215) (Table 1). Finally, there are also differences in residues that are essential for NNRTI binding in HIV-1 RT: W229 changes to Y268 in XMRV RT, Y181 to L220, Y188 to L227, and G190 to A229 (Table 1) (*35, 36, 155-157*).

Preparation of MoMLV and XMRV RTs

The sequence coding for full-length XMRV RT from the VP-62 clone (NCBI RefSeq: NC_007815) (*1*) was optimized for expression in bacteria, synthesized by Epoch Biolabs and cloned as described in 'Methods'. Both XMRV RT and MoMLV RT were tagged with a hexahistidine sequence at the N-terminus and expressed with a yield of ~2 mg/liter of culture. Purified enzymes (>95% pure, Figure II-1) were stored at -20°C. The presence of NP-40 or glycerol was critical for enzyme stability.

Steady State Kinetics of Nucleotide Incorporation

Initial polymerase activity assays using $T_{d31}/5'$-Cy3-P_{d18a} displayed overall slower polymerase activity of XMRV RT compared to HIV-1 and MoMLV RTs. This observation led us to investigate the steady state nucleotide incorporation properties of XMRV RT using single nucleotide incorporation assays. The estimated values for k_{cat} (19.9 min^{-1} for HIV-1 RT (*142*), 3.3 min^{-1} for MoMLV RT, 0.6 min^{-1} for XMRV RT) and $K_{m.dNTP}$ (0.07 μM for HIV-1 RT (*142*), 3.3

Table 1: HIV-1 RT drug resistance mutations with wild-type XMRV RT and MoMLV RT residues

	HIV-1 Residue numbers	HIV-1 RT wt*	HIV-1 Resistance Mutations					XMRV RT wt*	MoMLV RT wt*
			3TC	ABC	TDF	D4T	EFdA		
Thymidine Analog Mutations (TAMs)	184	M	V	V	-	-	V	V223	V223
	41	M	-	L	L	L	-	L81	L81
	67	D	-	N	N	N	-	G105	G105
	210	L	-	W	W	W	-	N226	N226
	215	T	-	FY	FY	FY	-	A231	A231
	219	K	-			QE	-	K235	K235
Non-thymidine Analog Regimen Mutations	65	K	RN	RN	RN	RN	-	K103	K103
	70	K	EG	EG	EG	-	-	D108	D108
	74	L	-	VI	-	-	-	V112	V112
	75	V	-	TM	M	TM	-	Q113	Q113
	115	Y	-	F	F		-	F155	F155
	69	T	Ins	Ins	Ins	Ins	-	N107	N107
Multi-NRTI Resistance Mutations	151	Q	M	M	M	M	-	Q190	Q190
	62	A	V	V	V	V	-	P104	P104
	75	V	-	I	-	I	-	Q113	Q113
	77	F	-	L	-	L	-	L115	L115
	116	F	-	Y	-	Y	-	F156	F156
TDRTI Mutations	184	M	V	V	-	-	V	V223	V223
	165	T	-	-	-	-	R	H204	H204

The HIV-1 RT data are based on data from the Stanford HIV Database (*158*)
*****wt = wild-type

A.

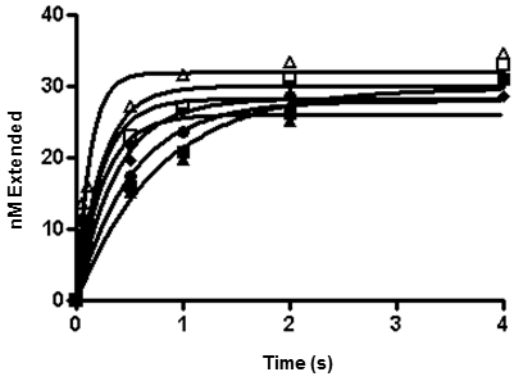
40
30
20
10
0
nM Extended
0
1
2
3
4
Time (s)

B.

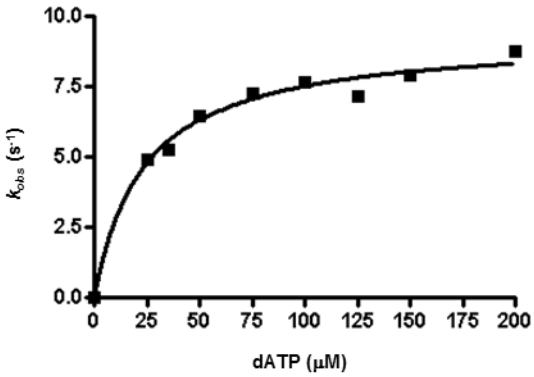
10.0
7.5
5.0
2.5
0.0
k_{obs} (s^{-1})
0
25
50
75
100
125
150
175
200
dATP (μM)

<u>Figure II-3</u>: Pre-steady state kinetics of nucleotide incorporation by XMRV RT. 150 nM enzyme was pre-incubated with 40 nM T_{d31}/5′-Cy3-P_{d18a} rapidly mixed with a solution containing $MgCl_2$ (5 mM) and varying concentrations of dATP: , 25 μM (■), 35 μM (▲), 50 μM (▼), 75 μM (♦), 100 μM (●), 125 μM (□), and 150 μM ( ); and incubated for 0.1 to 6 s before being quenched with EDTA. The DNA product for each dATP concentration was fit to the burst equation (A). The burst amplitudes generated for each dATP concentration were then fit to a hyperbola equation (B) yielding the kinetic parameters of dNTP incorporation: k_{pol} = 8.9 s^{-1} and dNTP binding to the RT-DNA complex: $K_{d.dATP}$ = 26.6 μM.

μM for MoMLV RT, 3.0 μM for XMRV RT) show that XMRV RT has a drastically reduced efficacy ($k_{cat}/K_{m.dNTP}$) at nucleotide incorporation, compared to both MoMLV and HIV-1 RTs.

DNA Binding Affinity

To assess whether the efficiency of XMRV RT was also affected by impaired interactions with DNA we measured the DNA binding affinity of the enzymes using three methods: gel-mobility shift assays, pre-steady state kinetics and SPR. Gel-mobility shift assays showed that the $K_{D\text{-}DNA}$ for XMRV RT was marginally higher (lower affinity) than that for HIV-1 RT and MoMLV RT (data not shown) (*159*) suggesting weaker binding to DNA.

DNA Binding Affinity using Pre-steady State Kinetics

Pre-steady state kinetics allow estimation of the fraction of active polymerase sites as well as the $K_{D.DNA}$ value for the enzyme. The amplitudes of DNA extensions using XMRV RT and/or MoMLV RT at varying DNA concentrations were plotted against the DNA concentration and the data were fit to the quadratic equation (Eq. 2), yielding a $K_{D.DNA}$ of 33 nM for XMRV RT, 19 nM for MoMLV RT (Table 2) and 12.5 nM for HIV-1 RT (*142*). These values did not change significantly when tested with DNA of different lengths (data not shown). Hence, the transient kinetic experiments confirmed the findings of the gel-mobility shift assays showing XMRV RT to have lower DNA binding affinity than HIV-1 RT.

Binding Kinetics of XMRV and HIV-1 RT to Double-Stranded DNA

Measurements of $K_{D.DNA}$ using gel-mobility shift assays and pre-steady state kinetic methods do not offer insights regarding the kinetics of binding and release of nucleic acid from the viral polymerases. Hence, we used SPR to measure directly DNA binding and the DNA dissociation components of the $K_{D.DNA}$. We attached on the SPR chip a nucleic acid biotinylated

Table 2: Kinetic parameters of DNA binding and synthesis by HIV-1 and XMRV RTs

Nucleotide affinity and incorporation	**HIV-1 RT***	**MoMLV RT**	**XMRV RT**
$K_{d.dNTP}$ (µM)	1.3±0.4	25±5.3	26.6±6.5
k_{pol} (s^{-1})	24.4±0.9	14.1±0.8	8.9±0.6
k_{pol}/Kd.dNTP (s^{-1}·μM^{-1})	18.8	0.56	0.33
DNA binding affinity: $K_{D.DNA}$ (nM)	12.5	19.0	32.5

* HIV-1 RT data published previously (*37*)

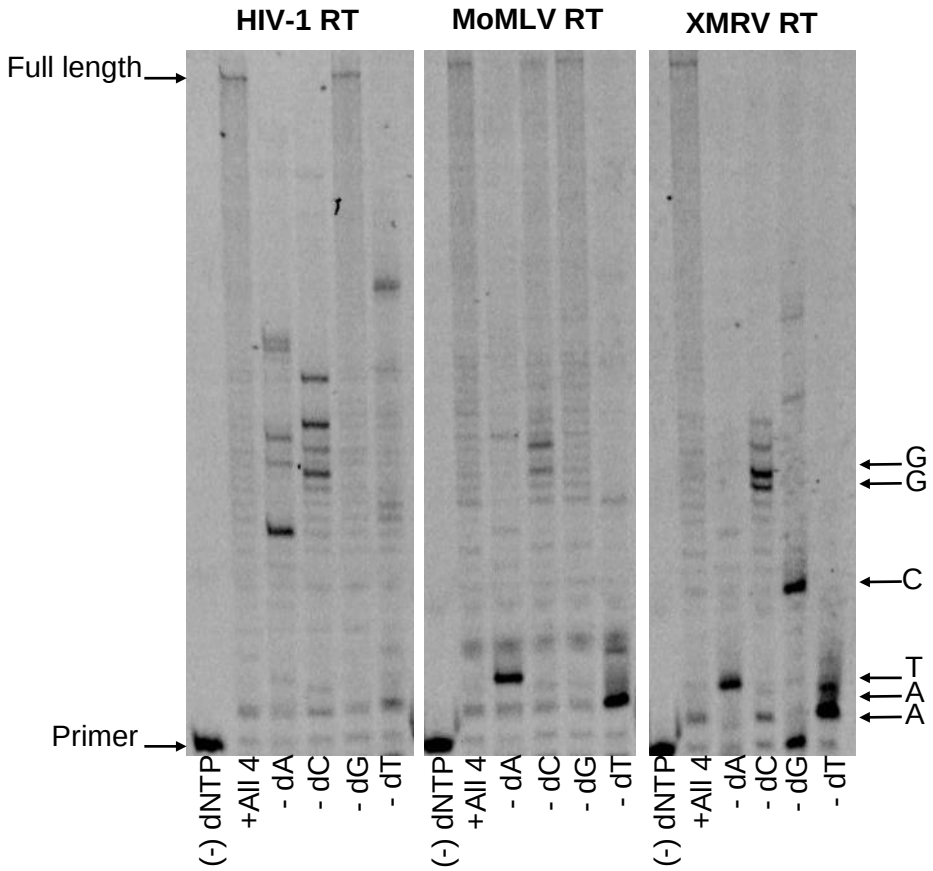
HIV-1 RT
MoMLV RT
XMRV RT
Full length
Primer
G
G
C
T
A
A
(-) dNTP
+All 4
- dA
- dC
- dG
- dT

Figure II-4: Comparison of *in vitro* fidelity of HIV-1, MoMLV, and XMRV RTs. Extension of 10 nM T_{d100}/5′-Cy3-P_{d18a} by HIV-1 RT, MoMLV RT or XMRV RT (20, 50, and 50 nM respectively) in the presence of 150 μM each of 3 out of four nucleotides (the missing nucleotide is marked at the bottom of each lane). Reactions were run for 30 min for HIV-1 RT and 45 min for XMRV RT and MoMLV RT. For each enzyme the first lane in each set shows the position of unextended primer, the second lane shows full extension in the presence of all four dNTPs, and each consecutive lane shows extension in the presence of 3 dNTPs. The arrows on the right mark the expected pauses based on the indicated composition of the template strand.

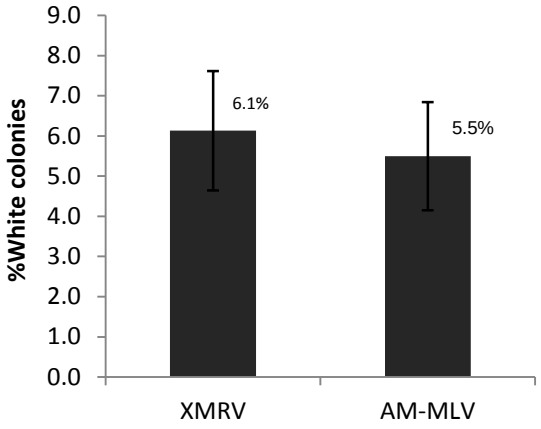
9.0
8.0
7.0
6.0
5.0
4.0
3.0
2.0
1.0
0.0
%White colonies
6.1%
5.5%
XMRV
AM-MLV

Figure II-5: Comparison of *in vivo* fidelity of XMRV with amphotropic MLV. The ANGIE P cells used for this assay contain a retroviral vector (GA-1), which encodes a bacterial β-galactosidase gene (*lacZ*) and a neomycin phosphotransferase gene. Replication fidelity is measured by the frequency of *lacZ* inactivation resulting in an increase in white colonies. The fidelity differences between the two viruses are not statistically significant (error bars represent standard error from 3 independent experiments).

at the 5′ template end and immobilized it on a streptavidin sensor chip. Various concentrations of either XMRV or HIV-1 RT were flowed over the chip to measure the association (k_{on}) and dissociation (k_{off}) rates of the enzymes in real time (Figure II-2). HIV-1 RT had considerably slower dissociation rates than XMRV RT, and longer dissociation phases were needed to obtain reliable values.

Several methods were tested to best fit our data. The "heterogeneous ligand" method gave the best fit for both XMRV and HIV-1 RT. In this model the x^2 values for DNA binding to XMRV and HIV-1 RT were 9.3 RU^2 and 48.1 RU^2, respectively, compared to 15.1 RU^2 and 152 RU^2 when we tried fitting the data in a "homogeneous ligand" model. The former model assumes that RT binds DNA in two different modes and provides two association (k_{on}) and two dissociation constants (k_{off}).

Our data show that XMRV RT has a slightly faster rate of association (k_{on}) than HIV-1 RT. We measured two k_{on} values of 7.3 X 10^6 $M^{-1}s^{-1}$ and 8.2 X 10^4 $M^{-1}s^{-1}$ for XMRV RT *versus* 7.6 X 10^5 $M^{-1}s^{-1}$ and 1.2 X 10^6 $M^{-1}s^{-1}$ for HIV-1 RT. Interestingly, the dissociation rate of XMRV RT was significantly faster than that of HIV-1 RT (0.28 s^{-1} and 0.0045 s^{-1} for XMRV RT and 7.8 X 10^{-4} $s^{-1}$and 0.0076 s^{-1} for HIV-1 RT) (Table 3). This difference in dissociation rate resulted in a K_D at least 1 order of magnitude higher for XMRV RT compared to HIV-1 RT (38 and 54 nM *vs.* 1.0 and 6.1 nM for XMRV and HIV-1 RT, respectively) (Table 3).

Nucleotide Binding Affinity and Optimal Incorporation Efficiency

A transient-state kinetics approach was used to estimate the dNTP binding affinity ($K_{d.dNTP}$) and maximum nucleotide incorporation rate (k_{pol}) (*160*). The rates at varying concentrations of next incoming nucleotide (dATP) were determined by plotting the amount of extended primer as a function of time. The rates were then plotted against dATP concentration. The data were fit to a hyperbola (Equation 3). The $K_{d.dNTP}$ for XMRV RT is 26.6 μM and the k_{pol}

Table 3: DNA binding constants for HIV-1 and XMRV RTs from surface plasmon resonance

	HIV-1 RT	**XMRV RT**
k_{on} (M^{-1}.s-1)	7.6 X 10^{5}	7.3 X 10^{6}
k_{off} (s^{-1})	7.8 X 10^{-4}	2.8 X 10^{-1}
K_{D1} (nM)	1	38 **(38-fold)***
k_{on} (M^{-1}.s-1)	1.2 X 10^{6}	8.2 X 10^{4}
k_{off} (s^{-1})	7.6 X 10^{-3}	4.5 X 10^{-3}
K_{D2} (nM)	6.1	54 **(9-fold)***

*Increase in K_d (decrease in affinity) with respect to HIV-1 RT
($K_{D1\text{-}XMRV\ RT}$/ $K_{D1HIV\text{-}1\text{-}RT}$ and $K_{D2\text{-}XMRV\ RT}$/ $K_{D2HIV\text{-}1\text{-}RT}$)

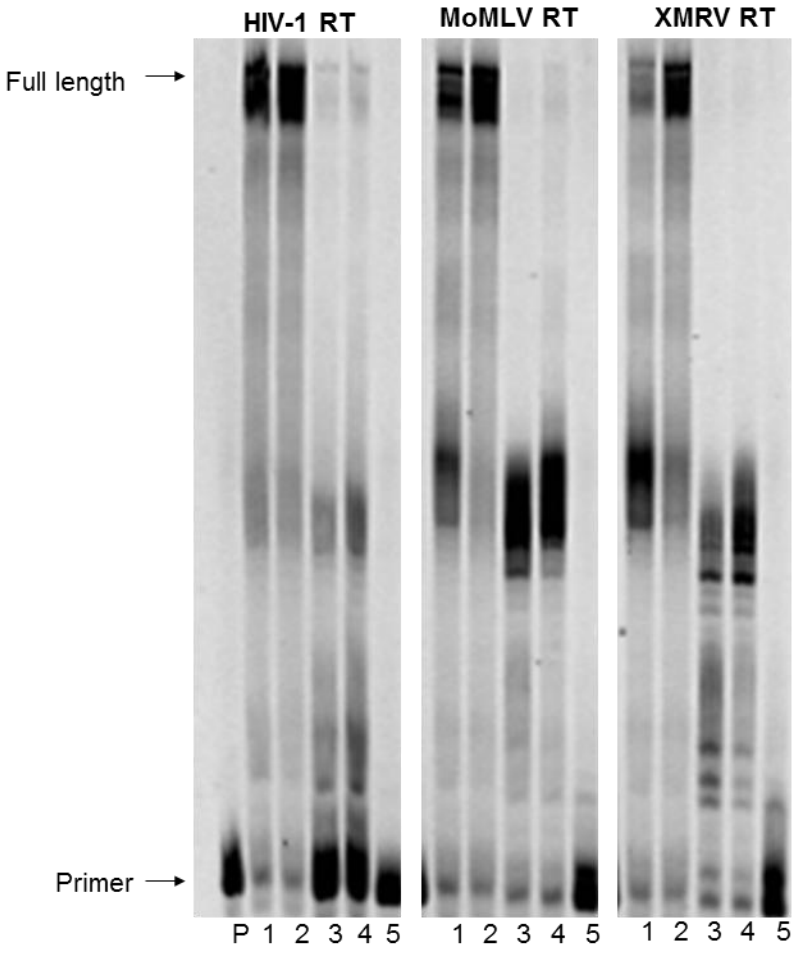
HIV-1 RT
MoMLV RT
XMRV RT
Full length
Primer
P 1 2 3 4 5
1 2 3 4 5
1 2 3 4 5

Figure II-6: Processivity (trap assay) of HIV-RT, MoMLV RT, and XMRV RT. DNA synthesis was monitored in the presence of calf thymus DNA as an enzyme trap. Each enzyme (30 nM HIV RT, 100 nM MoMLV RT or 100 nM XMRV RT) was pre-incubated with 40nM T_{d100}/Cy3-P_{d18a}. Lanes 1 and 2 of each set show unlimited DNA synthesis in the absence of trap for 5 and 10 min for HIV-1 RT and 10 and 40 min for XMRV RT and MoMLV RT. In Lanes 3 and 4 the reaction is initiated by the addition of dNTPs (100 µM each) together with the calf thymus DNA trap (0.5 µg/µl) such that the products generated represent a single processive synthesis event for the respective time points for each enzyme. Lane 5 shows the effectiveness of the trap determined by incubating the calf thymus DNA with the enzyme before addition of labeled template-primer. Processive primer extension by HIV-1 RT and MoMLV RT in lanes 4-6 of panel A and B is higher than by XMRV RT in lanes 4-6 of panel C.

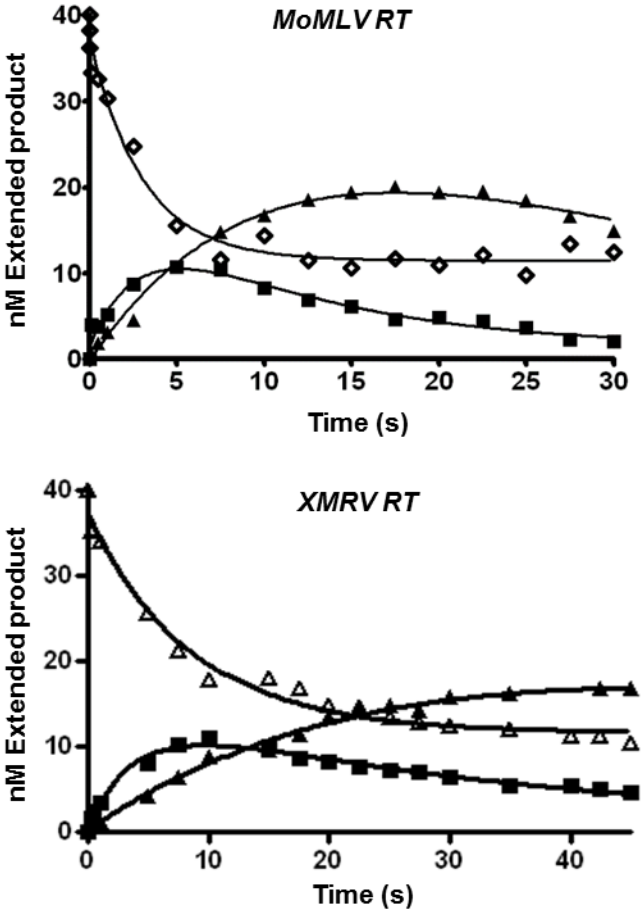
MoMLV RT
nM Extended product
Time (s)
XMRV RT
nM Extended product
Time (s)

Figure II-7: Single-turnover processivity assays. 30 nM T_{d31}/Cy3-P_{d18a} was combined with 100 nM XMRV RT or 50 nM MoMLV RT in RT buffer before rapidly mixing with all four dNTPs (100 μM each) and 5 mM $MgCl_2$ for varying incubation times (0.05 – 45 s) and quenching with EDTA. Extension of the 18-mer primer (◊) into 19-mer (■), and 22-mer (▲), by MoMLV RT (A) and XMRV RT (B) was fit to a double exponential equation to determine rates of product appearance, and subsequent processive extension of those products (rates shown in Table 5).

is 8.9 s^{-1} (Figure III-3) (Table 2). Under similar conditions the $K_{d.dNTP}$ and k_{pol} were 1.3 μM and 24.4 s^{-1} for HIV-1 RT (*37*), and 25 μM and 14.1 s^{-1} for MoMLV RT.

Fidelity of Nucleotide Incorporation

To assess whether XMRV RT displays high nucleotide incorporation fidelity we monitored the incorporation of three dNTPs by XMRV RT and compared with HIV-1 RT (*161*). The results of fidelity assay are shown in Figure III-4. The lanes marked "4dNTPs" for all enzymes represent the DNA synthesis using a T_{d100}/5′-Cy3-P_{d18a} template-primer in the presence of all four dNTPs. The subsequent lanes, marked '-dNTP', correspond to the synthesis of DNA in the absence of that specific deoxynucleotide triphosphate. The comparison of the DNA synthesis in the absence of one nucleotide by HIV-1 RT, MoMLV RT, and XMRV RT shows that HIV-1 and MoMLV RTs were able to misincorporate and extend the primer beyond the missing nucleotide more efficiently than XMRV RT, suggesting that the latter is a less error prone DNA polymerase. It should be noted that the higher fidelity of XMRV is not the result of measuring a smaller number of errors because of the decreased replication rate, as the assay conditions were optimized to allow production of the same amount of full length product in the presence of all four dNTPs for and MoMLV RTs. To further investigate the fidelity of DNA synthesis by XMRV RT, the kinetics of mismatch nucleotide incorporation were carried out in a quantitative manner by monitoring the incorporation of single mismatched nucleotide under pre-steady state conditions. The estimated $K_{d.dTTP}$ (mismatch) and k_{pol} values show that XMRV RT has a lower affinity for a mismatched nucleotide but comparable turnover number than MoMLV RT, suggesting that the observed higher fidelity over MoMLV RT is due to differences during the nucleotide binding step (Table 4). However, compared to HIV-1 RT, XMRV RT has decreased both affinity and incorporation rate, suggesting that its higher fidelity is the result of both decreased binding of mismatched nucleotides and slow rate of incorporation.

Table 4: Kinetics of mismatch incorporation for HIV-1, MoMLV, and XMRV RTs

Enzyme	**HIV-1 RT**	**MoMLV RT**	**XMRV RT**
$K_{d.dNTP}$ (μM)	9 ± 0.3	38.9 ± 11.6	256 ± 72
k_{pol} (s^{-1})	6.81 ± 1.2	0.16 ± 0.01	0.15 ± 0.018
$k_{pol}/K_{d.dNTP}$ (s^{-1}·μM)	0.756	0.0041	0.00058
Fidelity*	0.04	0.007	0.002

*Fidelity is the ratio of the incorporation efficiency (k_{pol}/K_d) of the mismatched nucleotide (dTTP) over that of the correct (dATP) ([k_{pol}/K_d]dTTP/[k_{pol}/K_d]dATP)

Intracellular Fidelity by Measuring LacZ Mutation Frequency

The ANGIE P cells used for this assay are a D17-based encapsidating cell line and contain an MLV-based retroviral vector (GA-1), which encodes a bacterial β-galactosidase gene (*lacZ*) and a neomycin phosphotransferase gene (*neo*). Replication fidelity is a measure of the frequency of *lacZ* inactivation and was determined by measuring *lacZ* nonexpressing white colonies. The results show that the number of white colonies was not statistically different in the case of XMRV as compared to AM-MLV, suggesting that under these conditions the fidelity of XMRV is not significantly different than that of AM-MLV (Figure II-5).

Processivity of DNA Synthesis

Processivity is the probability of translocation of a polymerase along a template and predicts the number of cycles of nucleotide incorporation during one productive enzyme-DNA binding event. We assessed XMRV RT's processivity of DNA synthesis in comparison to HIV and MoMLV RTs using both a gel-based trap assay and a quantitative pre-steady state assay. In the gel-based assay, the enzymes were pre-incubated with template-primer, then the reaction was initiated by the addition of all four nucleotides together with calf thymus DNA, which was used as a trap to bind free enzyme dissociated from the substrate during the course of the reaction (*146*). The length of the DNA product is an inverse measure of termination probability, as previously described. As a control, we used lanes where no trap was present; establishing that the same amount of total polymerase activity (processive and non-processive) is provided in all cases. The results indicate that XMRV RT is less processive than HIV-1 and MoMLV RTs with shorter DNA product after 30 min of reaction in the presence of trap (Figure II-7).

To measure processivity quantitatively we applied a single turnover processivity assay developed by Patel et al. (*145*). In this assay, the rates of consecutive nucleotide incorporations under single turnover conditions are monitored. The rate of elongation incorporation (k_1) and the rate of processive DNA synthesis (k_2) (Equation 4) were calculated at

Table 5: Single turnover processivity parameters of HIV-1, MoMLV, and XMRV RTs

Template site	Processivity Index (k_2/k_1)		
	HIV-1 RT	**MoMLV RT**	**XMRV RT**
1	6.98	0.31	0.12

```
                                          1
3′-   CAT TGA CAA GCT CGT GGT TAC GAT CGA TAC C
5′-Cy3-GTA ACT GTT CGA GCA CCT
```

The template site position monitored is underlined and labeled.

several template positions for each enzyme. The ratio of the rate of processive DNA synthesis to the rate of nucleotide incorporation (k_2/k_1) is referred to as the processivity index (*145*). The absolute values of these constants for HIV-1 RT, XMRV and MoMLV RT and their ratios are collected in Table 5. XMRV RT is clearly the least processive for each extension product. The difference in processivity varies significantly depending on sequence or sequence context (decrease in processivity from 3-fold up to 10-fold). While the current data do not allow generalization of rules for pausing at specific sites, this clearly shows consistently that XMRV is not as efficient as MoMLV RT in polymerizing processively through "difficult spots".

Susceptibility of XMRV RT to NRTIs, TDRTIs, and NNRTIs

Previous studies have shown that XMRV is inhibited by some antivirals (*162-165*). However, the susceptibility of XMRV RT has not been tested against a wide variety of nucleoside RT inhibitors (NRTIs) that block replication by chain-terminating the primer, or by preventing translocation after their incorporation into the nascent DNA chain (TDRTIs) (*142, 166, 167*). In addition, the susceptibility of XMRV RT to nonnucleoside RT inhibitors (NNRTIs) or RNA aptamers that can be selected to block reverse transcriptases (*168-172*) has not been established.

Hence, we performed gel-based primer extension assays in the presence of various inhibitors. As shown in Table 6, most of the HIV-1 RT inhibitors also block XMRV RT with significantly varying IC_{50}s. The most potent inhibitors tested were ENdA (4'-ethynyl-2-amino-2'-deoxyadenosine) followed by EFdA. EFdA was also potent at inhibiting wild-type XMRV replication in cell culture with an EC_{50} of 40 nM from 3 independent experiments (standard error was 10 nM).

Unlike HIV-1 RT, XMRV RT and MoMLV RT lack the two tyrosine residues (Y181 and Y188 in HIV-1 RT) that are known to contribute to NNRTI binding. Hence, the gammaretroviral enzymes were not inhibited by the NNRTIs tested (TMC-125 and efavirenz) (Figure II-9).

Table 6: Inhibition of XMRV and MoMLV RTs

Compound	IC_{50} (μM)	
	XMRV RT	**MoMLV RT**
Adefovir-DP	0.92	1.02
Tenofovir-DP	6.4	1.51
D4T-TP	0.77	2.37
3TC-TP	21	10
EFdA-TP	0.43	0.29
ENdA-TP	0.14	0.18

D4T; stavudine or 2′ ,3′ -dehydro-2′ ,3′ -deoxythymidine
3TC; lamivudine
EFdA; 4′ -ethynyl-2-fluoro-2′ -deoxyadenosine
ENdA; 4′ -ethynyl-2-amino-2′ -deoxyadenosine

A.

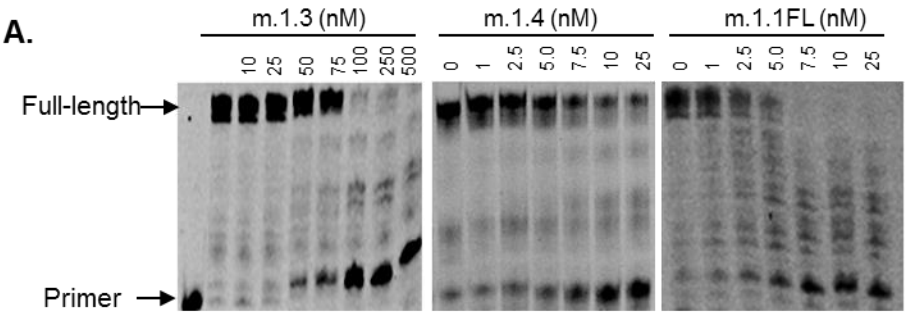

B.

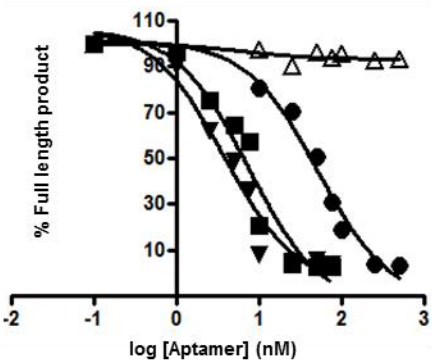

Aptamer	IC_{50} (nM)
m.1.1FL	2 ± 0.15
m.1.3	52 ± 0.27
m.1.4	7 ± 0.16

Figure II-8: Inhibition of XMRV RT by RNA aptamers. 10 nM XMRV RT was incubated with increasing amounts of RNA aptamer in Reaction Buffer for 5 min at 37°C followed by addition of 20 nM T_{d31}/Cy3-P_{d18a} and 50 µM of each dNTP. (A) The reactions were stopped after 30 min and resolved on a polyacrylamide gel. The predicted secondary structures of each aptamer were generated by mfold. (B) The percent full extension was quantified for m.1.1FL (▼), m.1.3 (●), and m.1.4 (■) and data points fit to one-site competition nonlinear regression using GraphPad Prism 4 to calculate IC_{50} (Errors represent data deviation from the fit).

Susceptibility of XMRV RT to RNA aptamers

We also tested XMRV RT's susceptibility to three independent RNA aptamers that had been previously selected against MoMLV RT (*169*). The aptamers inhibited XMRV RT to varying extents with IC_{50}s ranging from 2 to 52 nM (Figure II-8). Most notable was the m.1.1FL aptamer, which gave IC_{50}s of 2 and 4 nM for XMRV RT (Figure II-8) and MoMLV RT respectively, without inhibiting HIV-1 RT (data not shown). These inhibition assays utilized truncated forms of aptamers m.1.3 and m.1.4 lacking the original primer-binding segments of the aptamers, demonstrating that these 5′ and 3′ segments are not required.

PPi-mediated Excision Activity of XMRV RT

A key mechanism of NRTI resistance in HIV-1 RT is based on inhibitor excision from the primer end, using a pyrophospholytic reaction (*173, 174*). The pyrophosphate donor *in vivo* is likely to be ATP, although PPi can efficiently unblock NRTI-terminated primers. This excision activity is present in wild-type HIV-1 RT, and is enhanced in the presence of AZT-resistance mutations. We measured the ability of wild-type XMRV to unblock primers terminated with AZT or EFdA in the presence of PPi. We found that unlike HIV-1 RT, which excised AZT-MP efficiently under these conditions, XMRV RT had considerably lower excision activity (Figure II-10). Similar excision experiments where ATP was used instead of PPi showed that XMRV is very inefficient in ATP-based excision as compared to HIV-1 RT (data not shown).

Susceptibility of Mutant XMRV RTs to AZT-TP and Tenofovir-DP

The HIV-1 RT mutation Q151M confers resistance to AZT by enhancing discrimination of the nucleotide analog leading to its reduced incorporation (*175-178*). Another HIV-1 RT mutation, K65R, decreases susceptibility to tenofovir (*179, 180*). Since AZT and tenofovir are potent inhibitors of XMRV (Table 6) (*163-165*), we wanted to investigate whether the XMRV RT mutant equivalents of HIV Q151M and K65R (XMRV Q190M and K103R) would confer

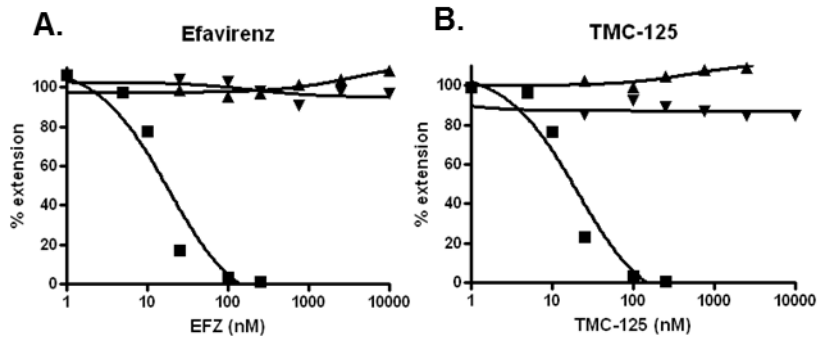

C.

	IC_{50} (μM)	
	Efavirenz	TMC-125
HIV-1 RT	0.02	0.02
MuLV RT	> 10	>10
XMRV RT	>10	>10

Figure II-9: Susceptibility of XMRV and HIV-1 RTs to NNRTIs. HIV-1 RT (20 nM) (■), MoMLV (30 nM) (▲) or XMRV RT (60 nM) (▼) were pre-incubated with 20 nM T_{d31}/5'-Cy3-P_{d18a}, 1 µM dNTPs in the presence of increasing concentrations of efavirenz (A) or TMC-125 (B) for 5 min. Reactions were initiated with 6 mM $MgCl_2$, run for 15 min at 37ºC and IC_{50} values were determined by quantifying the percent full extension and fitting data points to one-site competition nonlinear regression using GraphPad Prism 4.

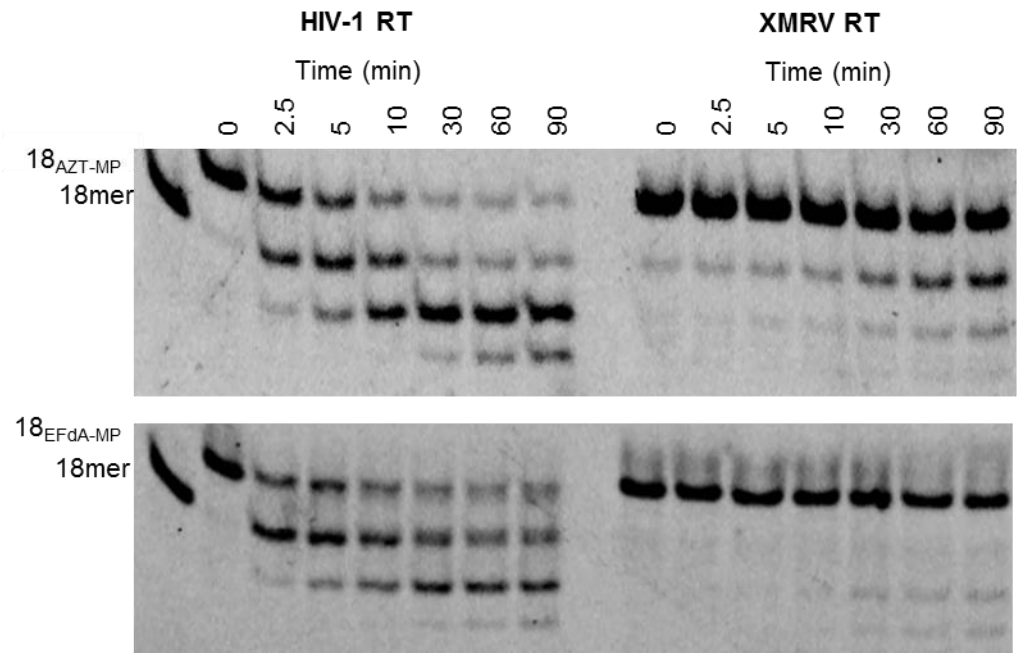
HIV-1 RT
XMRV RT
Time (min)
Time (min)
0
2.5
5
10
30
60
90
0
2.5
5
10
30
60
90
18AZT-MP
18mer
18EFdA-MP
18mer

Figure II-10: PPi-mediated unblocking of AZT-(A) and EFdA-(B) terminated DNA. 20 nM of AZT-(A) or EFdA-(B) terminated Td31/Cy3-Pd18c (T/PAZT-MP or T/PEFdA-MP) was incubated with HIV-1 RT (60 nM) or XMRV RT (200 nM) in the presence of 150 μM PPi and 6 mM $MgCl_2$. Aliquots of the reactions were stopped at different time points (0-90 min) and resolved on a 15% polyacrylamide–7M urea gel as described in the Methods section.

XMRV RT resistance to AZT and tenofovir. We constructed these mutant clones and tested their susceptibility to AZT and tenofovir in the same manner as wild-type XMRV RT. Interestingly, Q190M XMRV RT has a decreased susceptibility to AZT (~5-fold increase in the IC_{50}). Similarly, the K103R XMRV RT mutant enzyme was less susceptible to tenofovir, increasing the IC_{50} by at least 2-fold.

Molecular Model of XMRV RT

Given the significant sequence similarity between XMRV and MoMLV RTs, the resulting homology model of XMRV RT is highly similar to MoMLV RT (>1.5 *Å* rms) and of excellent quality. Since the input structure of MoMLV RT did not contain the RNase H domain of the enzyme, the XMRV RT model is also missing this domain. The molecular model of the polymerase domain of XMRV RT is shown in Figure II-11. An alignment of the MoMLV RT crystal structure (*30*) with the XMRV RT homology model highlights the few changes in the polymerase domain of XMRV RT. These are L29 (P in MoMLV), Q234 (L in MoMLV), R238 (Q in MoMLV), and N422 (D in MoMLV). From these, residue 422 is located in the nucleic acid binding cleft and may contribute to differences in the interactions with nucleic acid substrate. However, most of the differences between the gammaretroviral enzymes are in their RNase H domains and also in the first 30 N-terminal residues of the polymerase domain, for which we do not have structural information since they were not included in the original crystal structure of MoMLV RT. The differences between XMRV RT and HIV-1 RT are very significant. Unlike the HIV enzyme, XMRV RT appears to be a monomer in solution. Moreover, alignment of the HIV-1 RT-DNA complex with XMRV RT based on their active sites at the palm subdomains shows that the thumb subdomain of XMRV RT would have to be repositioned to be able to accommodate nucleic acid.

D. DISCUSSION

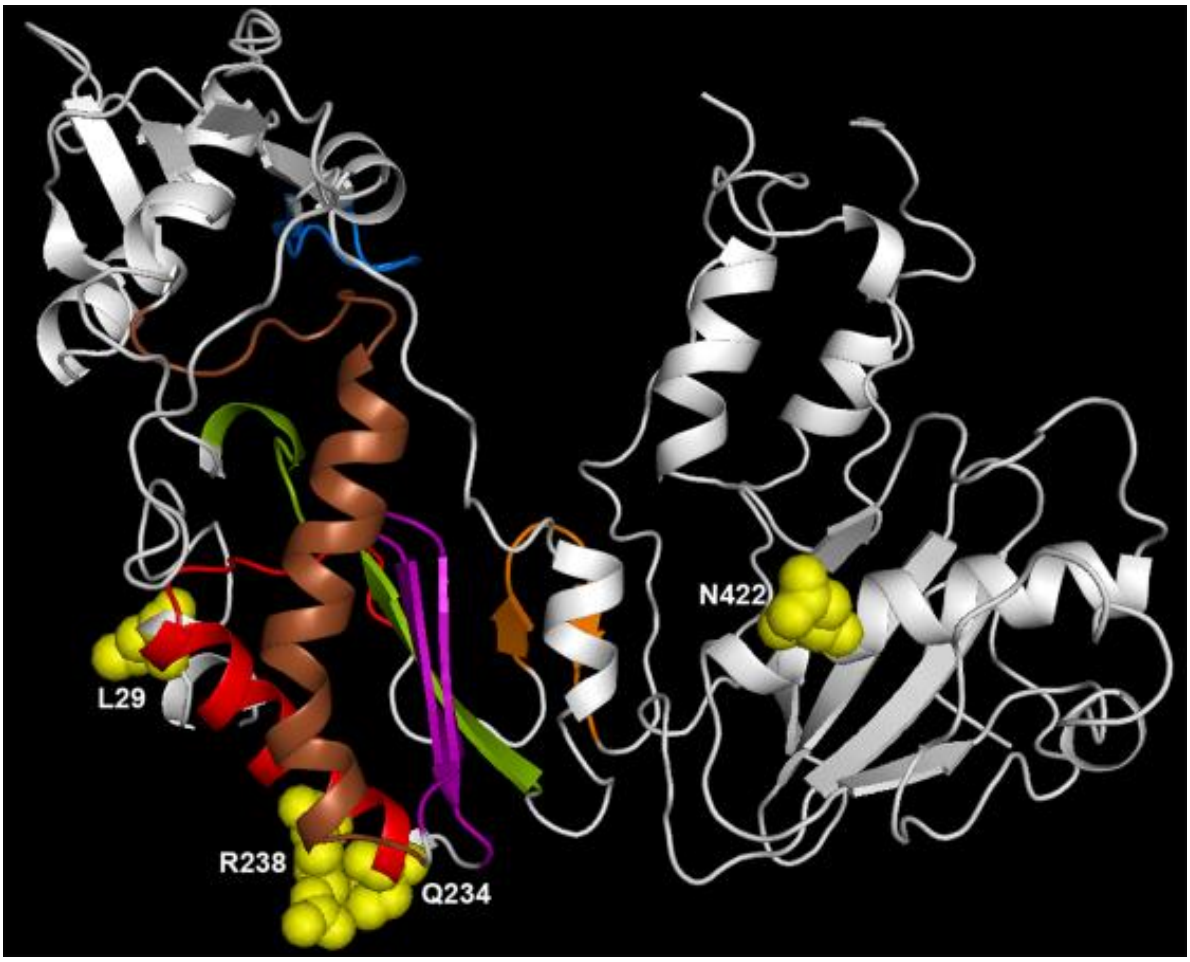
N422
L29
R238
Q234

Figure II-11: Molecular model of XMRV RT. Ribbons diagram of XMRV RT with the conserved polymerase Motifs color-coded: Motif A (green), B (brown), C (purple), D (red), E (orange), and F (blue). The residues that differ from MoMLV's polymerase domain are shown in ball and stick representation.

Polymerization and kinetics experiments	
T_{d100}	5′-ATG TGT GTG CCC GTC TGT TGT GTG ACT CTG GTA ACT AGA GAT CCC TCA GAC CCT TTT AGT CAG TGT GGA ATA TCT CAT AGC TTG GCG CCC GAA CAG GGA C-3′
P_{d18a}	5′Cy3-GTC CCT GTT CGG GCG CCA
T_{d31}	5′-CCA TAG CTA GCA TTG GTG CTC GAA CAG TGA C
T_{d43}	5′-CCA TAG ATA GCA TTG GTG CTC GAA CAG TGA CAA TCA GTG TAG A
P_{d18a}	5′Cy3-GTC CCT GTT CGG GCG CCA
T_{d26}	5′-CCA TAG ATA GCA TTG GTG CTC GAA CA
P_{d18b}	5'Cy3-TGT TCG AGC ACC AAT GCT
Footprinting assay	
T_{d43}	5′Cy3-CCA TAG ATA GCA TTG GTG CTC GAA CAG TGA CAA TCA GTG TAG A
P_{d30}	5′-CTA CAC TGA TTG TCA CTG TTC GAG CAC CA
Surface plasmon resonance assay	
T_{d37}	5′Biotin-TAG ATC AGT CAT GCT CCG CGC CCG AAC AGG GAC TGT G
P_{d25}	5′-CAC AGT CCC TGT TCG GGC GCG GAG C
PPi- and ATP-dependent excision	
T_{d31}	5'-CCA TAG CTA GCT ATG GTG CTC GAA CAG TGA C
P_{d18c}	5'Cy3-GTC ACT GTT CGA GCA CCA
Cloning primers	
Forward 1	5′-GGA ATT CCA TAT GACG CTG AAC ATC GAA GAC G
Reverse 1	5′-CCC AAG CTT TTA CAG CAG CGT ACT CGT TTC C
Mutagenesis primers	
Forward 2	5′-GGA CTC GTC TGC CAA TGG GTT TCA AGA ACA GC
Reverse 2	5′-GCT GTT CTT GAA ACC CAT TGG CAG ACG AGT CC
Forward 3	5′-GCT GCC GGT CAA GAG ACC TGG GAC GAA TG
Reverse 3	5′-CAT TCG TCC CAG GTC TCT TGA CCG GCA GC
RNA aptamers	
m.1.1FL	5′-GGAGGAUAUUUUCUCAGACCGUAACUUACCACgcgcUCUUAACUCG UAgcgcCAUGGCCAAAACUUUgcagcaUcgUgaacU
m.1.3	5′-GGGUUCCCAGCGAAAggAUACCGGCUGUGgcgcCCUCUUUCACAUu
m.1.4	5′-GGGAUCCCCGAUGAAgcgcGAUACCAUCGGgcgcGACUACCCCUGu

Table II-7 Sequences of oligonucleotides used in this study

Early studies reported the presence of XMRV in stromal cells from prostate cancer patient samples and also in CFS clinical samples. Some of the subsequent studies confirmed these findings whereas several others failed to identify XMRV in prostate cancer or in CFS patients, even when same samples were used (*181*). It was reported that human sample contamination with mouse DNA can occur frequently (*182-185*). Moreover, two coauthors from this study have recently demonstrated that XMRV is the product of recombination events between two MLV proviruses, suggesting that XMRV may not be relevant to human disease (*186*). Nonetheless, XMRV is still an important human retrovirus and comparisons with HIV can provide valuable insights into the fundamental mechanisms of DNA polymerization, RT inhibition and drug resistance (*187*).

There is high degree of sequence similarity between the XMRV and MoMLV RTs (95% amino acid identity), and much less so with HIV-1 RT (*187*). Based on gel filtration experiments we conclude that unlike HIV-1 RT, but similar to MoMLV RT, XMRV RT exists in solution primarily as a monomer. We also included comparisons with HIV-1 RT in this study as it has been extensively studied and provides an excellent frame of reference.

We report here that there are significant differences in the DNA polymerization efficiency of the three enzymes. Although the polymerase active sites of the XMRV and MoMLV enzymes are almost identical, there is a considerable decrease in the efficiency of nucleotide incorporation by XMRV RT. Most differences in sequence are at the RNase H domain and are likely to affect polymerization by changing the positioning of DNA at the polymerase active site. We have recently solved the crystal structure of the XMRV RNase H at high resolution (1.5 *Å*) (pdb 3P1G) (*188*). We observed major differences in affinity for nucleic acid that we determined with gel-mobility shift assays and with pre-steady state kinetics. SPR experiments dissected in more detail the specific defect of XMRV RT in binding DNA. Surprisingly, XMRV RT can associate very rapidly with DNA, even more so than HIV-1 RT (Figure II-2, Table 3). However, it dissociates from DNA much faster than the HIV enzyme, resulting in an overall reduced

binding affinity. A possible reason for the fast association and dissociation rates of XMRV RT may be the apparent monomeric state, which might offer facile access to the nucleic acid binding cleft, albeit with less contacts and lower affinity than HIV-1 RT, which is a heterodimer (*189-191*). This high rate of XMRV RT dissociation from DNA likely contributes to the decreased processivity observed in our study, and may have consequences in the recombination rates of this virus.

Previous sequences of XMRV from prostate cancer tumors showed low variability, suggesting that the virus may have a high fidelity of replication (*1, 15*). Our study demonstrated that HIV-1 RT and MoMLV RT incorporated mismatched nucleotides and extended past the mismatches more efficiently than XMRV RT. Pre-steady state kinetics established that the higher overall fidelity of XMRV RT over MoMLV RT is due to a lower affinity for mismatched nucleotides. When compared to HIV-1 RT, however, XMRV RT differs in both the nucleotide binding and incorporation steps. Nonetheless, XMRV did not have higher fidelity than a related amphotropic MLV virus or HIV-1 in a cell-based assay. It is possible that the high dNTP concentration in dividing cells can suppress mismatching events. We have previously shown (*147*) that as nucleotide concentrations vary in different cell lines, this can affect viral susceptibility to NRTIs, and possibly in this case also incorporation of mismatched nucleotides. Additional cell-based studies using multiple cell lines and a large panel of viruses should provide a better understanding of the relation between *in vivo* and *in vitro* fidelity.

Early studies have reported susceptibility of XMRV to some antiretrovirals that have been used in the treatment of HIV infection (*162-165*). In those studies the compounds were tested at the virus level. To better understand the interactions of inhibitors at their RT target level we tested here the ability of these and several more compounds to block the polymerase activity of XMRV RT. We found that two TDRTIs, EFdA-TP and ENdA-TP were potent RT inhibitors (IC_{50}s: 0.43 μM and 0.14 μM respectively). Unlike other NRTIs, these compounds have a 3′ OH group and are known to efficiently inhibit HIV replication by blocking translocation (*142, 167,*

192). Preliminary experiments demonstrated that they also block XMRV RT by the same mechanism (data not shown).

In HIV, moderate resistance to EFdA is conferred by the emergence of the M184V mutation at the conserved X position of the conserved YXDD motif of the polymerase active site. Interestingly, XMRV and MoMLV RTs already have a valine (V223) at this position. This difference is likely to contribute to the better potency of EFdA against HIV-1 RT than XMRV RT or MoMLV RT (*166, 167*). It may also contribute to the decreased ability of XMRV RT to unblock chain-terminated primers, as was also reported for M184V HIV-1 RT (*193*) and to the enhanced fidelity reported here for XMRV RT, which is also reminiscent of the previously reported high fidelity of M184V HIV-1 RT (*194, 195*). Nonetheless, despite the presence of a Val in the YMDD motif of XMRV RT we found EFdA to inhibit very efficiently replication-competent or pseudotyped XMRV, with submicromolar EC_{50}s (40 and 110 nM, respectively).

Previously, highly potent aptamers were selected to inhibit MoMLV RT (*169*). We demonstrate here that the three aptamers we tested have varying potency against XMRV RT. Aptamer m.1.1FL was the most potent inhibitor of XMRV RT and MoMLV RT in *in vitro* assays (IC_{50}=2 and 4 nM, respectively). The fact that XMRV and MoMLV RTs are inhibited by the same aptamers at comparable efficiencies suggests that the RT residues that are different in the two enzymes are not critical to the binding of the aptamer. In contrast, heterodimeric HIV-1 RT has a very different binding cleft and is not inhibited by these aptamers.

Tenofovir is an essential component of HIV therapies and is also a potent inhibitor of XMRV RT. HIV resistance to tenofovir is conferred by a single codon mutation (K65R). HIV-1 RT residue 65 is known to interact with the incoming dNTP or the activated tenofovir analog (tenofovir diphosphate) (*196*). K65R causes resistance to tenofovir by lowering the k_{pol} for the incorporation of the inhibitor into the nascent DNA. We prepared XMRV RT with the equivalent mutation, K103R, and determined that it has decreased susceptibility to tenofovir. Hence, it is possible for XMRV to develop tenofovir resistance through the same mechanism as HIV-1 RT.

HIV resistance to AZT can occur by either decreased binding/incorporation or increased excision of the chain-terminating NRTI (*143, 197*). HIV-1 RTs containing the M41L, D67N, K70R, T215Y/F, K219E/Q mutations show enhanced removal of AZT. Our experiments show that unlike wild-type HIV-1 RT, XMRV RT is not able to excise NRTI-terminated primers. Similarly, it was previously shown that MoMLV RT is not capable of unblocking chain-terminated primers (*143*).

In HIV, decreased binding of AZT is conferred initially in the presence of the primary Q151M mutation, followed by secondary mutations F77L, A62V, V75I, and F116Y (*35, 155, 198*). XMRV RT already differs from wild-type HIV-1 RT in the first three of these residues (P104, Q113, and L115 *vs.* A62, V75, and F77) (Table 1). We demonstrated that introducing the primary Q→M mutation at the equivalent XMRV RT site (Q190M) resulted in an enzyme with decreased susceptibility to AZT. Hence, it appears that these residues can confer AZT resistance to XMRV by reduced incorporation of nucleotide analogs, as is the case in HIV-2 (*149*). At this point we do not know if introduction of as yet unknown mutations could endow XMRV RT with the ability to unblock chain-terminated nucleic acids. The details of the molecular mechanism of XMRV resistance to tenofovir and AZT are under investigation.

In conclusion, our study provides detailed biochemical analysis of the mechanisms of polymerization, inhibition, fidelity, processivity, and drug resistance of XMRV RT and how it compares with the closely related enzyme MoMLV RT and the more distantly related HIV-1 RT. The findings enhance our understanding of the basic mechanisms of reverse transcription.

III. EFFECT OF P-BODY COMPONENT MOV10 ON HCV VIRUS PRODUCTION AND INFECTIVITY

A. ABSTRACT

Mov10 is an antiviral host factor that restricts replication of retroviruses, including HIV-1. Mov10 has also been reported to inhibit hepatitis C virus (HCV). However, the mechanism of this inhibition is unknown. Here we investigate the effect of Mov10 on HCV infection, and determine which steps of the virus life cycle are affected by changes in expression of Mov10. It is demonstrated that overexpression of Mov10 in human hepatoma cells restricts HCV RNA production from a sub-genomic replicon (genotype 1a) and fully infectious virus (genotype 2a). Inhibition of RNA replication in the infectious virus system leads to decreased virus production over time, as measured by HCV RNA levels in cell culture media by RT-qPCR, and released virus titer ($TCID_{50}$/ml). In addition to decreasing virus production, Mov10 overexpression decreases the infectivity of the produced virus. In contrast, overexpression of a control P-body protein, Dcp1a, had no effect on HCV RNA production, virus production, or infectivity of progeny virus. Confocal imaging of uninfected cells shows endogenous Mov10 to be localized at P-bodies. However, HCV infection results in redistribution of Mov10 to circular structures surrounding lipid droplets where it co-localizes with HCV NS5A and the core protein. Similar experiments with Mov10 active site mutants demonstrated that neither Mov10's helicase function nor localization to P-bodies was required for antiviral activity. Finally, decreasing Mov10 protein expression levels using CRISPR-Cas9 genome editing decreased HCV replication and infection levels, consistent with disruption of Mov10-Ago2/miR122 binding, which would destabilize the HCV

genome. Hence, our data reveal a complex balance between Mov10 and HCV, with Mov10 knockdown data suggesting optimum levels of Mov10 are required for HCV infection, whereas Mov10 overexpression is detrimental to the virus.

.

B. MATERIALS AND METHODS

Cell lines and reagents

All experiments described in this study were performed using human hepatoma cells (Huh7.5.1) provided by Dr. Charles M. Rice (Rockefeller University, NY). The cells were maintained in Dulbecco's modified Eagle medium (DMEM, Invitrogen) supplemented with 10% fetal bovine serum (FBS, Hyclone).

Virus constructs and *in vitro* RNA production

The virus constructs Jc1378.1-NS5A-Ypet and Jc1378.1-FLAG (nsGluc2A) were provided by Dr. Charles M. Rice (Rockefeller University, NY) and encode fully infectious chimeric genotype 2a hepatitis C virus (*199*). In these virus chimeras the core, E1, E2, and 33 amino acids of NS2 are from the J6 clone, and the remaining proteins are from JFH1. Jc1378.1-NS5A-Ypet expresses fluorescent Ypet fused within the NS5A protein, while Jc1378.1-FLAG (nsGluc2A) contains *Gaussia* luciferase within the NS2 protein. The luciferase gene is flanked by FMDV ns2A protein. Upon HCV infection and translation and processing of viral proteins, the luciferase protein is expressed and secreted into cell culture media. To generate RNA for transfection, the plasmid DNA was purified from *E.coli* using a plasmid midi-prep kit (Qiagen). The DNA (2 µg) was linearized by *XbaI* or *ScaI* cleavage (New England Biolabs) at a site upstream of a T7 promoter for 4 hours at 37°C. The linearized DNA was purified using the QIAquick® PCR-clean up kit (Qiagen) and transcribed into RNA using the MegaScript Ampliscribe T7 kit (Invitrogen) with 0.5 µg of linearized DNA per reaction incubated for 5 hours at 37°C. DNase I was added

and the reaction mixture was incubated for an additional 20 minutes. The integrity of the RNA was checked by agarose gel electrophoresis and the concentration determined by measurement of the optical density at 260 nm. After purification by RNeasy kit (Qiagen) the RNA was stored in RNase-free water at -80°C, in 10 µg aliquots.

Overexpression plasmids and transfection

Plasmids expressing YFP-Dcp1a, FLAG-Dcp1a, mRFP-Mov10, and FLAG-Mov10 were constructed as has been previously described (*134*). Briefly, the plasmids express human Dcp1a or Mov10 N-terminally tagged with FLAG epitope (DYKDDDDK) or fluorescent Venus yellow fluorescent protein (YFP). Expression plasmids for mutant Mov10 proteins (G527A, R730A/N731A, V866A, and DQAG) were constructed as described and proteins tagged N-terminally with eYFP were expressed as previously published (*139*).

Transfections were performed using Fugene HD reagent (Promega) in 60-80% confluent cells. For dose-response experiments cells were transfected with 0.05-0.3 ng of plasmid DNA per µl of growth media, in 24-well plates with 1 ml per well. In experiments to determine the effect on virus production, 0.4 ng of plasmid per µl of media was used, in T25 flasks with 4 ml media each.

Electroporation and virus production

To produce HCV virus 10 µg of HCV RNA was transfected into Huh7.5.1 cells by electroporation as previously described (*200*). Briefly, ~70% confluent Huh7.5.1 cells were detached from a T75 flask, washed twice with ice cold DPBS and resuspended in cold DPBS to $1.5x10^6$ cells per ml. 700 µl of this suspension was added to a tube containing 10 µg HCV RNA, mixed briefly and transferred to a 0.4 cm cuvette (Fisher Scientific) and electroporated using a Gene Pulser II (Bio-Rad). The cells were allowed to rest for 10 minutes at room temperature then transferred into a T75 flask containing 10 ml growth media. The next day, the media was changed

and the cells were incubated for two more days. Beginning 72 hours after electroporation, the now virus-containing media was collected and replaced every 6-8 hours, filtered through a 0.45 µm filter and stored in aliquots at -80°C.

To determine the effect of Mov10 on virus production 10 µg HCV RNA (Jc1378.1-NS5A-Ypet construct) was electroporated into Huh7.5.1 cells as described above. $5x10^6$ electroporated cells were diluted into 20 ml media and plated onto T25 flasks (4 ml per flask). After 16 hours the media was replaced with fresh media and transfected with 1 µg pFLAG-Mov10 or control plasmids (empty vector/pFLAG-Dcp1a). Virus-containing media was collected and replaced 24, 48, and 72 hours after transfection and assayed for virus titers ($TCID_{50}$/ml values) and HCV RNA levels (by RT-qPCR).

Determining virus titers by $TCID_{50}$ assay

A previously described limiting dilution assay was used to determine viral titer (*200*). For virus released from the cells into the media, $3x10^3$ cells were plated onto a 96-well plate, and the next day infected with 100 µl of undiluted virus-containing media (8 wells) or 100 µl diluted virus (five serial dilutions, from 10^{-1} to 10^{-5}, 8 wells per dilution). For cell-associated virus infected cells were detached from 6-well plates and washed twice with DPBS then resuspended in media (a volume equal to the virus-containing media collected). The cells were then subjected to four freeze-thaw cycles using a dry-ice ethanol bath and a 37°C water bath, and centrifuged to remove cellular debris. The supernatant was used to make dilution and infect cells as above. For both intra- and extracellular virus titers the cells were fixed 72 hours post infection with cold methanol, for 30 mins at -20°C, followed by blocking with 1% BSA and 0.2% non-fat milk in 1x PBS-T. To identify infected cells, we probed the cells for HCV NS5A using the NS5A monoclonal antibody 9E10 (provided by Dr. Charles M. Rice) detected by an HRP anti-mouse secondary antibody (ImmPRESS, Vector Laboratories) followed by addition of an HRP substrate,

diaminobenzene, DAB (Invitrogen). NS5A positive cells were detected under a light microscope to score infection positive wells.

RNA levels by quantitative RT-qPCR

For HCV RNA levels in released virus, 100 µl TRIzol reagent (Sigma) was added to 300 µl virus-containing media and total RNA purified according to the manufacturer's instructions. For intracellular HCV RNA and IFNβ mRNA, cells were detached by addition of TRIzol then also processed according to the manufacturer's instructions. Quantitative reverse transcription PCR was performed with the ABI 7700 machine (Perkin-Elmer Biosystems) using the Power SYBR Green RNA-to-CT 1-Step kit (Applied Biosystems) as per kit instructions with 100 ng total RNA per reaction. The sequence of the primers used to amplify the 5' untranslated region of the HCV genome are given in Table III-1. To determine HCV RNA copy numbers a standard curve was generated by amplifying dilutions of *in vitro* transcribed HCV RNA ($2x10^7$ to $2x10^1$ genome copies per reaction). The sequences of the forward and reverse primers used to detect IFNβ and IFNα2 transcripts are given in Table III-1. Cellular RNA samples were also analyzed in parallel for GAPDH levels. GAPDH CT values were used to normalize samples using: $\Delta CT = CT_{sample} - CT_{GAPDH}$ (where $CT_{sample} = CT_{HCV\ RNA}$ or $CT_{IFN\beta\ mRNA}$). For IFNβ mRNA levels fold expression/relative quantity ($2^{(-\Delta\Delta CT)}$) was calculated using $\Delta\Delta CT = \Delta CT_{sample} - \Delta CT_{untreated\ control}$.

***Gaussia* luciferase activity assay**

To measure HCV replication of the *Gaussia* luciferase-secreting virus we used the *Gaussia* Glow Assay kit (Thermo Scientific) as per the manufacturer's instructions. Briefly, 30 µl of the cell culture media was collected and mixed with 30 µl 1 x lysis buffer, and incubated at room temperature for 15 minutes. 50 µl of this mixture was added to 50 µl *Gaussia* glow assay buffer containing 1 x substrate (coelentrazine). Luminescence was read using the Enspire™ 2300

Multilabel Reader (Perkin-Elmer Biosystems), and normalized to an uninfected control (cell culture media).

Virus infectivity

To determine the effect of Mov10 on virus infectivity naïve Huh7.5.1 cells were infected with HCV virus-containing media collected from cells overexpressing Mov10, Dcp1a, or transfected with the empty vector at 72 hours post transfection (hpt). The amount of each virus was normalized by HCV RNA levels from RT-qPCR ($6.25x10^3$ HCV RNA copy numbers). 48 and 72 hours post infection (hpi) the cells were imaged by fluorescent microscopy for HCV NS5A-Yet expression. After imaging at 72 hpi, the media and cells were collected and the cells were divided into two fractions. One was probed for HCV core protein levels (and GAPDH as a loading control) by Western blot analysis. Total RNA was isolated from the second fraction and along with the media collected at 72 hpi, analyzed by RT-qPCR for HCV RNA levels.

Western blot analysis

Cells for analysis were detached and lysed with Triton lysis buffer (0.1% Triton-X, 0.1% SDS, 1 x Roche protease inhibitor cocktail). 50 to 100 µg of total protein was ran on SDS-PAGE gels, then transferred onto immobilon-p nitrocellulose membrane (Millipore), blocked for non-specific binding in 5% non-fat milk, and then probed for specific proteins. Primary antibodies: HCV NS5A 9E10 1:5,000 dilution; HCV core 1:2,000 (Abcam, Cat #ab2740), GAPDH 1:10,000 (Santa Cruz, Cat #sc-365062), or Mov10 1:3,500 (Abcam, Cat #ab80613). HRP-tagged secondary antibodies were purchased from Sigma; anti-mouse cat #A5278, anti-rabbit cat #A0545. Bound antibodies were visualized by adding Luminata Forte Western HRP substrate (Millipore) to the membrane and imaged with a Fuji camera system.

Confocal microscopy

Huh7.5.1 cells were plated on 8-well chambered #1 borosillicate coverglass (Thermo Scientific,

Cat # 155411) at 2 x 10^4 cells per well. Cells were infected with either Jc1378.1-NS5A-Ypet or Jc1378.1-FLAG (nsGluc2A) for 48 hours then washed with DPBS and incubated at 4 degrees overnight in 4% paraformaldehyde. The cells were then permeabilized with 1% BSA, 0.1% skim milk, 0.1% Triton-X in PBS for 30 minutes at room temperature. Primary antibodies were bound at room temperature for 1.5 hours at the following dilutions: NS5A (9E10) 1:500, core (Abcam, Cat #ab2740) 1:500, dsRNA (J2 antibody from Scicons, Hungary) 1:500 or Mov10 (Abcam, Cat #ab80613) 1:1,000. Staining for cytoplasmic lipid droplets was with BODIPY 493/503 (Invitrogen, Cat #D3922) at a 1:500 dilution for 30 minutes at room temperature. All samples were also counterstained for nuclei using Hoechst 33342 (Invitrogen, Cat #H3570) at a 1:10,000 dilution for 15 minutes at room temperature. Following the primary antibodies; anti-mouse Alexa 647 (Invitrogen, Cat #A21235) was used for NS5A, core, and dsRNA. Alexa 568 (Invitrogen, Cat #A11036) was used for Mov10 (both at 1:1,500 dilutions for 1 hour at room temperature).

Knocking out endogenous Mov10

Endogenous Mov10 protein levels were modified using CRISPR-Cas9 gene editing technology (*201, 202*). We designed guide-RNA sequences to target Sp-Cas9 to the 5'-end of the Mov10 gene. Target 1: 5'-TGTCCAGTCCCCGAACGACC-3' and Target 2: 5'-GAGAGTTTCCTGGTCGTTCG-3'. A plasmid containing the designed gRNA, Sp-Cas9, and GFP as a reporter (pCas9-GFP-Mov10_T1 or T2) was purchased from OriGene Technologes (Rockville, MD). pCas9-GFP-Mov10_T1 was transfected into Huh7.5.1 cells at 0.5 ng of plasmid per µl of growth media. 48 hpt the cells were collected and the GFP positive cells sorted and collected by flow cytometry. Half of this population was cultured and expanded as is (Huh7.5.1_Mov10_CRISPR1), whereas the other half was diluted to a single cell per well of a 96 well plate and expanded as individual clones. Huh7.5.1_Mov10_CRISPR1 and the individual clones were evaluated for Mov10 protein expression by western blot, or immunocytochemistry. The cell line Huh7.5.1_Mov10_CRISPR1 was used for HCV infection and replication assays as

is. Clones with decreased levels of Mov10 (1E9) or undetectable levels of Mov10 (1D6) were selected and expanded into individual cell lines for HCV infection and replication assays.

Flow cytometry analyses

To determine transfection efficiencies Huh7.5.1 cells were transfected with 0.4 µg of plasmid DNA in 12-well culture plates containing 1 ml of growth media. 72 hours after transfection, the cells were detached, washed once with cold DBPS, and fixed in 4% paraformaldehyde at room temperature for 20 minutes. The cells were pelleted to remove the fixative and resuspended in 200 µl 1 x PBS. A BD Accuri® C6 CFlow SAMPLER was used to determine the percentage of cells expressing eYFP-tagged Mov10 (wild-type or mutant) protein. 20,000 cells were analyzed per sample. To determine the percentage of cells infected with HCV, cells were infected with the Jc1378.1-NS5A-Ypet virus and collected 72 hours post infection. The cells were prepared as detailed above, and analyzed for the percentage of cells expressing Ypet-tagged HCV NS5A.

C. RESULTS

Overexpression of Mov10 inhibits HCV

The antiviral activity of Mov10 against retroviruses and more in-depth HIV-1 has been well documented (*134, 137, 139, 140, 203, 204*). Mov10 has also been shown to have antiviral activity against HCV (*131*). We investigated whether overexpression of Mov10 would restrict HCV infection in Huh7.5.1 cells and whether this inhibition would be dose-dependent. Twenty-four hours after transfecting Huh7.5.1 cells with varying amounts of p-mRFP-Mov10 the cells were infected with HCV virus (Jc1-378.1-p7(nsGluc2A) at 0.2 multiplicity of infection (M.O.I). The Jc1-378.1-p7(nsGluc2A) construct expresses fully infectious genotype 2a HCV and upon viral replication *Gaussia* luciferase is expressed and secreted into the culture media, as previously described (*199*). Three days after infection we assayed the culture media for *Gaussia* luciferase activity to determine the level of HCV replication. In cells overexpressing Mov10, HCV replication was restricted in a dose dependent manner (Figure III-1).

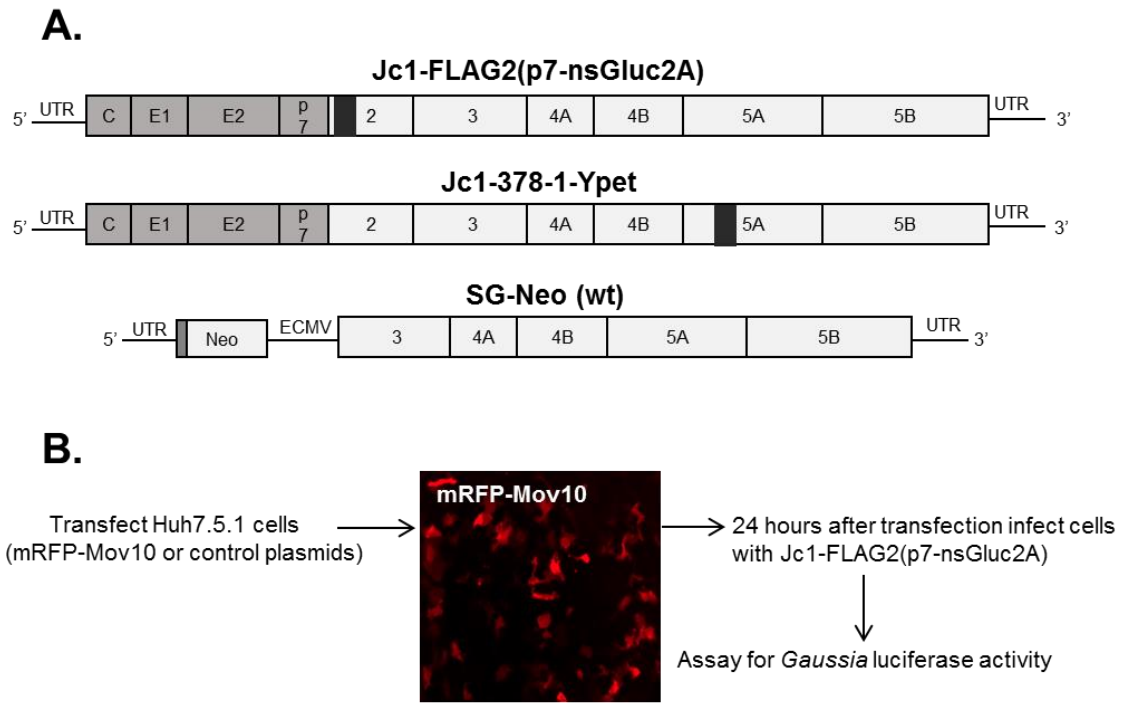
A.
Jc1-FLAG2(p7-nsGluc2A)
5' UTR C E1 E2 p7 2 3 4A 4B 5A 5B UTR 3'
Jc1-378-1-Ypet
5' UTR C E1 E2 p7 2 3 4A 4B 5A 5B UTR 3'
SG-Neo (wt)
5' UTR Neo ECMV 3 4A 4B 5A 5B UTR 3'
B.
Transfect Huh7.5.1 cells
(mRFP-Mov10 or control plasmids)
mRFP-Mov10
24 hours after transfection infect cells
with Jc1-FLAG2(p7-nsGluc2A)
Assay for Gaussia luciferase activity
C.
48 hpi
72 hpi
HCV Replication
(relative luciferase units)
70000
60000
50000
40000
30000
20000
10000
0
0 0.05 0.1 0.2 0.3 0 0.05 0.1 0.2 0.3
mRFP-Mov10 DNA transfected (μg)

Figure III-1: Genetic organization of HCV RNAs used and effect of Mov10 overexpression on HCV. (A) Schematic representation of HCV RNA used in this study. The 5' and 3' NTR regions are shown as thick black lines; the viral poly protein is depicted as an open box, with individual proteins separated by vertical lines. Chimeric clones Jc1378.1-NS5A-Ypet and Jc1378.1-FLAG(nsGluc2A) encode full length HCV genomes, expressing fully infectious genotype 2a virus. The structural proteins are from the J6 clone (white fill) and non-structural proteins from the JFH1 clone (gray fill). SG-neo(wt) is a sub-genomic replicon (genotype 1a) encoding a neomycin resistance gene. **(B)** Huh7.5.1 cells were transfected with varying amounts (0.05, 0.1, 0.2, and 0.3 µg) of an mRFP-Mov10 expression plasmid. 24 hours after transfection cells were checked for Mov10 expression and infected with the *Gaussia* luciferase expressing virus (Jc1378.1-FLAG(nsGluc2A)). 72 hours post infection cell culture media was collected and assayed for luciferase activity in **(C)**. Results are shown as the mean of three independent experiments ± the standard deviation (SD) of the mean.

Mov10 inhibits HCV RNA replication in both infectious virus and sub-genomic replicon systems

To begin characterizing the antiviral activity of Mov10 against HCV and determine which step(s) in the virus lifecycle were affected by overexpression of Mov10 we investigated HCV RNA levels in cells overexpressing Mov10. We transfected a plasmid expressing FLAG-Mov10 into Huh7.5.1 cells harboring HCV RNA (encoding the entire HCV genome, introduced by electroporation) and 24, 48, and 72 hours after transfected assayed the cells for HCV RNA levels. As shown in Figure III-2A, overexpression of Dcp1a had no significant effect on HCV RNA levels. Overexpression of Mov10, however, decreased viral RNA (21% inhibition), beginning at 24 hours after transfection. This inhibition increased over time to 74% at 48 hpt and 82% by 72 hpt.

To probe this further we assayed the replication of a sub-genomic HCV replicon in cells overexpressing Mov10. The replicon 'SG-wt-neo'(*205*) expresses HCV viral proteins NS3 to NS5B, which are necessary for RNA replication, but lacks the structural proteins and NS2 required to assemble and produce infectious virions. The replicon system eliminates other stages of infection except for RNA replication and translation, namely entry, assembly, maturation, viral release, and secondary infections. This allowed us to specifically determine the effect of Mov10 on HCV RNA replication. We overexpressed Mov10 or Dcp1a in cells harboring the HCV sub-genomic replicon (introduced by electroporation) and assayed HCV RNA levels at 48 hours after transfection by RT-pPCR. The levels of HCV RNA were normalized to GAPDH mRNA levels. Overexpression of Mov10 inhibited HCV RNA replication in a dose-dependent manner (Figure III-2B). Expression of Dcp1a on the other hand, had no effect on HCV RNA levels. Mov10 has several reported functions involving RNA modulation: it has been shown to be an RNA helicase, a component of mRNA processing bodies, and it has been implicated in RNA interference signaling complex (RISC) functions. All these functions would be expected to involve RNA binding capability. This RNA binding function of Mov10 has been shown to contribute to its

antiviral activity against HIV-1 (*134, 139*). Moreover, the RNA binding domains of Mov10 are required to be intact for inhibition of HIV-1 (*139*). Mov10 restricting HCV replicon replication might be due to Mov10 interacting with or binding to the HCV RNA genome.

Inhibition of HCV replication by Mov10 leads to decreased virus production

Next we investigated whether restriction of HCV RNA replication by Mov10 affected the later stages of the HCV life-cycle. To probe the effect of Mov10 on HCV virus production we transfected FLAG-Dcp1a/Mov10 expression plasmids into cells electroporated with HCV RNA (NS5A-Ypet virus) and collected virus-containing media at 24, 48, and 72 hpt. The media was filtered and assayed for HCV RNA levels and HCV virus titers to determine the amount of virus released into the media. Overexpression of Mov10 restricted the levels of HCV RNA released into the media, beginning at 24 hours post transfection of the expression plasmid. The level of inhibition at 24 hpt (~10-20%) (Figure III-3A) was similar to that seen with the sub-genomic replicon (Figure III-2A). This inhibition increased with time to ~50% inhibition at 48 hpt and ~80% by 72 hpt. Mov10 restricts single cycle RNA replication (replicon), and this restriction increases with multiple cycles of replication (replication competent virus).

To eliminate the possibility that the decreased virus production from Mov10-overexpressing cells was due to cell death we assayed whether overexpression of Mov10 was cytotoxic. Transfection of the Mov10 expression plasmids and/or overexpression of Mov10 had no effect on cell viability (data not shown).

To further investigate the effect of Mov10 on virus production, we assayed the titer ($TCID_{50}$/ml) of the virus produced in cells overexpressing Mov10. Similar to the restriction of released HCV RNA, overexpression of Mov10 decreased the titer of the virus produced (Figure III-3B). Also similar to the RNA levels, the restriction increased over time or with multiple cycles of replication.

HCV 5'UTR	5'-TGCGGAACCGGTGAGTACA-3'
	5'-TGC GGAACCGGTGAGTACA-3'
IFNα2	5'-TGAAGGACAGGCAGGACTTTGGAT-3'
	5'-AGGAGGGTTGTATTCCAAGCAGCA-3'
IFNβ	5’-TCC AGCTCCAAGAAAGGACGAACA-3’
	5’-TCTGGATCTCTTGGATGGCAA-3’
GAPDH	5'-CGCTCTCTG CTCCTCCTGTTC-3'
	5'-CGCCCAATACGACCAAATCCG-3'
Mov10	5'-AATTCCAAGGCCAAGAACGA-3'
	5'-CCAGATCCAGCTGCACAAA-3'

Table III-1: RT-qPCR primers used in this study.

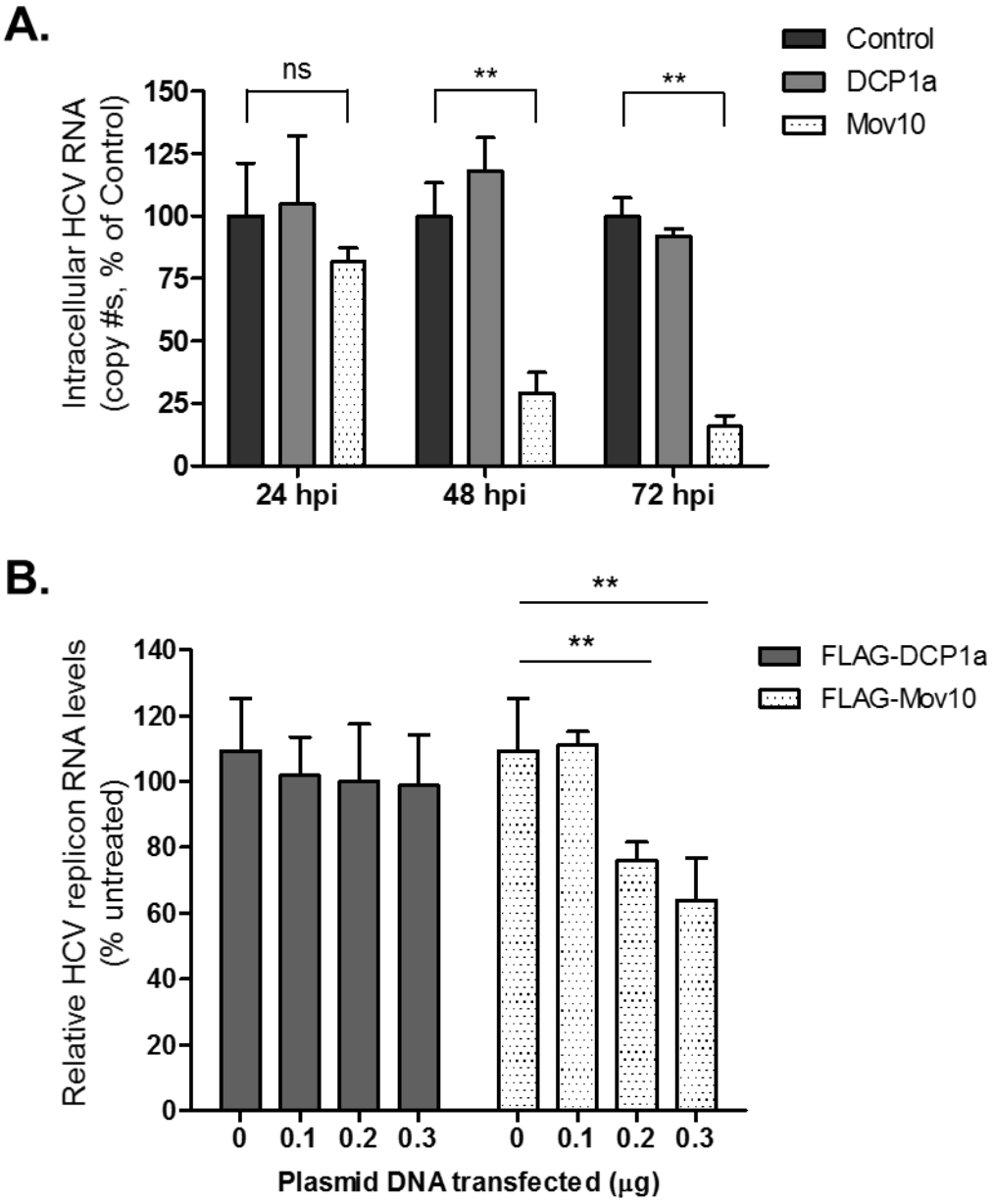
A.
Control
DCP1a
Mov10
ns
**
**
Intracellular HCV RNA
(copy #s, % of Control)
150
125
100
75
50
25
0
24 hpi
48 hpi
72 hpi
B.
**
**
FLAG-DCP1a
FLAG-Mov10
Relative HCV replicon RNA levels
(% untreated)
140
120
100
80
60
40
20
0
0
0.1
0.2
0.3
0
0.1
0.2
0.3
Plasmid DNA transfected (μg)

Figure III-2: Mov10 inhibits HCV RNA production from fully infectious virus and a sub-genomic replicon. (A) Huh7.5.1 cells were transfected with an empty vector (Control), YFP-Dcp1a plasmid, or mRFP-Mov10 plasmid (final concentration of 0.6 ng/µl) and 24 hours after transfection, infected with HCVcc-Gluc (at 0.1 MOI). HCV replication 24 hours post infection was assessed by measuring *Gaussia* luciferase activity in cell culture media. To determine the effect of Mov10 overexpression on HCV RNA levels, Huh7.5.1 cells were electroporated with HCVcc RNA and 8 hours post electroporation transfected with pUC18 (Control)/YFP-Dpc1a/mRFP-Mov10 plasmids. 24 hours post transfection; total RNA was isolated from the cells (intracellular HCV RNA levels) and culture media (extracellular HCV RNA levels) and analyzed for HCV RNA levels by RT-pPCR. **(B)** SG-neo-wt replicon RNA (1µg) was transfected into Huh7.5.1 cells by electroporation. 16 hours post electroporation empty vector or plasmids expressing FLAG-Dcp1a or FLAG-Mov10 (0.1, 0.2 or 0.3µg) were transfected into the cells. The cells were collected 24 hours after plasmid transfection and analyzed for: HCV RNA levels by RT-pPCR. Experiments were performed three times independently. Results are expressed as the mean ± the Standard Deviation (SD) of the percent of the control sample.

HCV produced in Mov10 overexpressing cells has decreased infectivity.

$TCID_{50}$/ml values are a measure of both the amount of virus produced and its infectivity, to explore the infectivity of HCV produced in cells overexpressing Mov10, we transfected empty vector/pFLAG-Mov10/Dcp1a into cells electroporated with HCV RNA (Jc1-378.1-NS5A-Ypet construct). 72 hours post transfection the virus-containing media was collected, and assayed for HCV RNA levels by RT-pPCR. Naïve Huh7.5.1 cells were infected with equal amounts of the virus-containing media, normalized by HCV RNA levels to $6.25x10^3$ copy numbers per well. Imaging of the cells by fluorescent microscopy (under the YFP channel for NS5A-Ypet) at 48 and 72 hours after infection showed decreased HCV protein expression from the virus produced in cells overexpressing Mov10 (Figure III-4A). The virus produced in cells overexpressing Dcp1a was fully infectious and expressed NS5A-Ypet to the same extent as the control virus (Figure III-4A).

Western blot analysis of the HCV core protein levels in the cells confirmed the decreased HCV viral protein from the Mov10 virus (Figure III-4B). After imaging at 72 hours post infection the virus-containing media and infected cells were collected and assayed for HCV RNA levels. The virus produced in Mov10 overexpressing cells had ~3-fold less HCV RNA produced in the cells and less virus released into the media (Figure III-4C).

Mov10 localization to P-bodies is not required for the antiviral activity of Mov10 against HCV

To further characterize the antiviral activity of Mov10 against HCV we sought to investigate whether all of Mov10's putative assigned capabilities were required for its effect on HCV. In a recent report Izumi *et al.* generated Mov10 variants with mutations that disrupt the putative functions of Mov10 (*139*). In the case of HIV-1 restriction some of these Mov10 mutants lost their antiviral activities. As shown in Figure III-5C, the Mov10 mutants were expressed to similar levels in Huh7.5.1. However, their cytoplasmic distribution differed slightly from the

wild-type Mov10 (Figure III-5A), similar to the previous report (*139*). The wild-type Mov10 is distributed into distinct foci with multiple foci in most of the cells. These foci co-localize or correlate with Dcp1a foci as shown in Figure III-5C and with Dcp2 (*139*) or APOBEC3G (*134*). Mutants G527A, V866A, and DQAG, however, had less foci per cell, and were not localized to P-bodies as efficiently as the wild-type Mov10 (data not shown). Interestingly, it has been reported (*139*) that overexpression of the double mutant R730A/N731A results in diffused distribution throughout the cytoplasm with no granules seen in cells that express the mutant protein. To investigate which of the Mov10 mutants retained or lost antiviral activity we overexpressed individual Mov10 variants in Huh7.5.1 cells that had been electroporated with viral RNA from Jc1-378.1-NS5A-RFP. 72 hours after transfection we imaged the cells for NS5A-RFP expression. We found that mutants G527A, V866A, and DQAG retained antiviral activity resulting in decreased NS5A-RFP expression to levels similar to wild-type Mov10 (Figure III-6A). Cells overexpressing the double mutant R730A/N731A, however, showed NS5A-RFP expression levels similar to the mock transfected control. Next we collected virus-containing culture media and the infected cells, to analyze released and intracellular HCV RNA levels by RT-pPCR. As shown in Figure III-6B, mutants G527A, V866A, and DQAG retained their antiviral activity, decreasing HCV RNA production as efficiently as the wild-type Mov10. This suggests that as in the case of HIV-1 restriction recruitment of Mov10 to P-bodies was not required for its inhibition of HCV. The double mutant R730A/N731A, however, lost some of its antiviral activity. Overexpression of Mov10 R730A/N731A did not decrease HCV RNA and NS5A protein levels to a similar extent as wild-type Mov10 and overexpression of Mov10 R730A/N731A did not affect the levels of released RNA. Intriguingly, this mutant also lost its antiviral activity against HIV-1 (*139*), suggesting that residues R730 and N731 are required for the antiviral properties of Mov10 and that these residues may be directly involved in the specific mechanism(s) of Mov10 action.

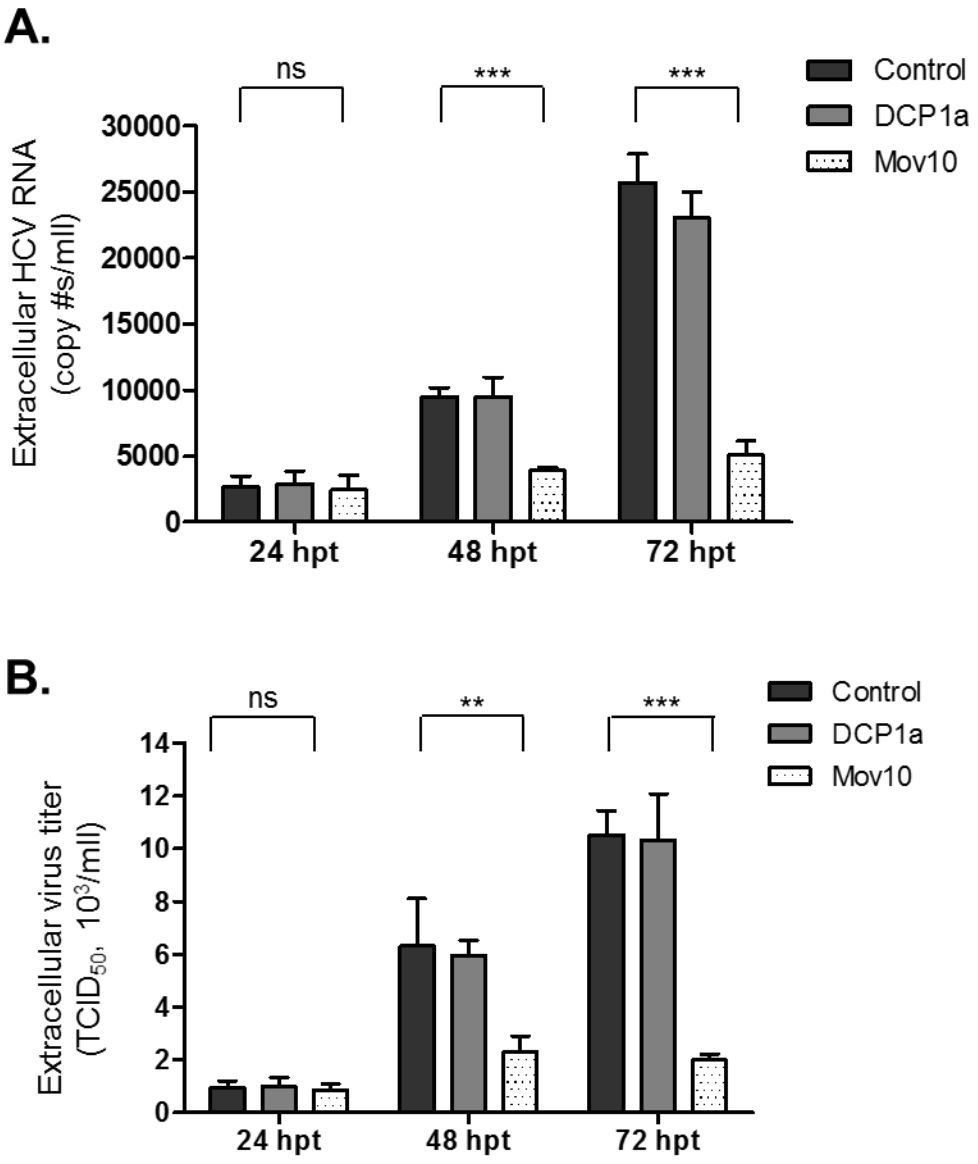
A.
ns
***
***
Control
DCP1a
Mov10
Extracellular HCV RNA
(copy #s/ml)
30000
25000
20000
15000
10000
5000
0
24 hpt
48 hpt
72 hpt
B.
ns
**
***
Control
DCP1a
Mov10
Extracellular virus titer
(TCID50, 10^3/ml)
14
12
10
8
6
4
2
0
24 hpt
48 hpt
72 hpt

Figure III-3: Mov10 overexpression decreases virus production. HCVcc-Ypet RNA was electroporated into Huh7.5.1 cells. 16 hours later the cells were transfected with empty vector plasmid (Control)/YFP-Dcp1a/mRFP-Mov10 plasmid. Virus-containing cell culture medium and cells were collected at 24, 48, and 72 hours post transfection. **(A)** To determine the extracellular HCV RNA levels of released virus (RNA levels in released virus) total RNA was isolated from the culture media and analyzed by RT-pPCR. **(B)** To determine extracellular virus titers, the medium was filtered and used to infect naïve Huh7.5.1 cells by limiting dilution, and the $TCID_{50}$/ml values determined as described in Materials and Methods. Experiments were performed three independent times and results are expressed as the mean ± SD of the percent of the control sample.

A.

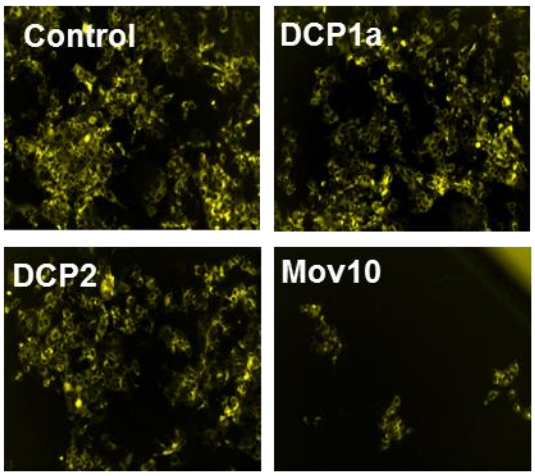
Control
DCP1a
DCP2
Mov10

B.


Control
DCP1a
DCP2
Mov10
HCV core
GAPDH

C.

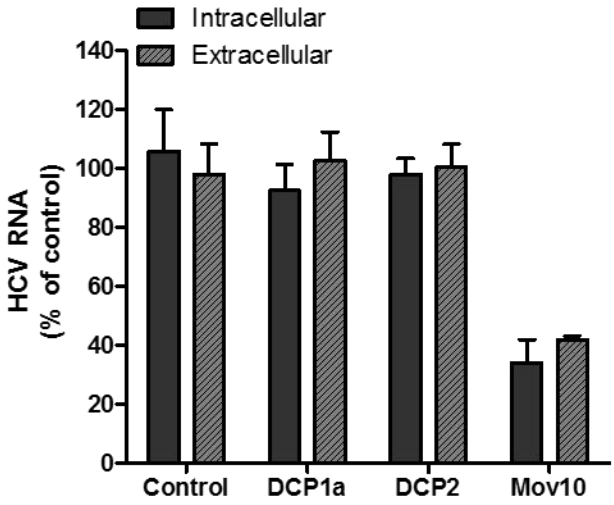
Intracellular
Extracellular
HCV RNA
(% of control)
140
120
100
80
60
40
20
0
Control
DCP1a
DCP2
Mov10

Figure III-4: HCV virus produced in Mov10 overexpression cells has decreased infectivity. To determine the infectivity of the virus produced in Mov10 overexpressing cells; (A) Naïve Huh7.5.1 cells were infected with HCV virus-containing media collected from cells overexpressing Mov10, Dcp1a, or transfected with empty vector at 72 hours post transfection. The amount of each virus was normalized by HCV RNA levels from RT-pPCR (6.25x103 HCV RNA copy numbers). 48 and 72 hours post infection the cells were imaged by fluorescent microscopy for HCV NS5A-Yet expression. After imaging at 72 hpi, the media and cells were collected. Cells were collected into two fractions. (B) One was probed for HCV core protein levels (and GAPDH as a loading control) by Western blot analysis. (C) Total RNA was isolated from the second fraction and along with the media collected at 72 hpi, analyzed by RT-pPCR for HCV RNA levels.

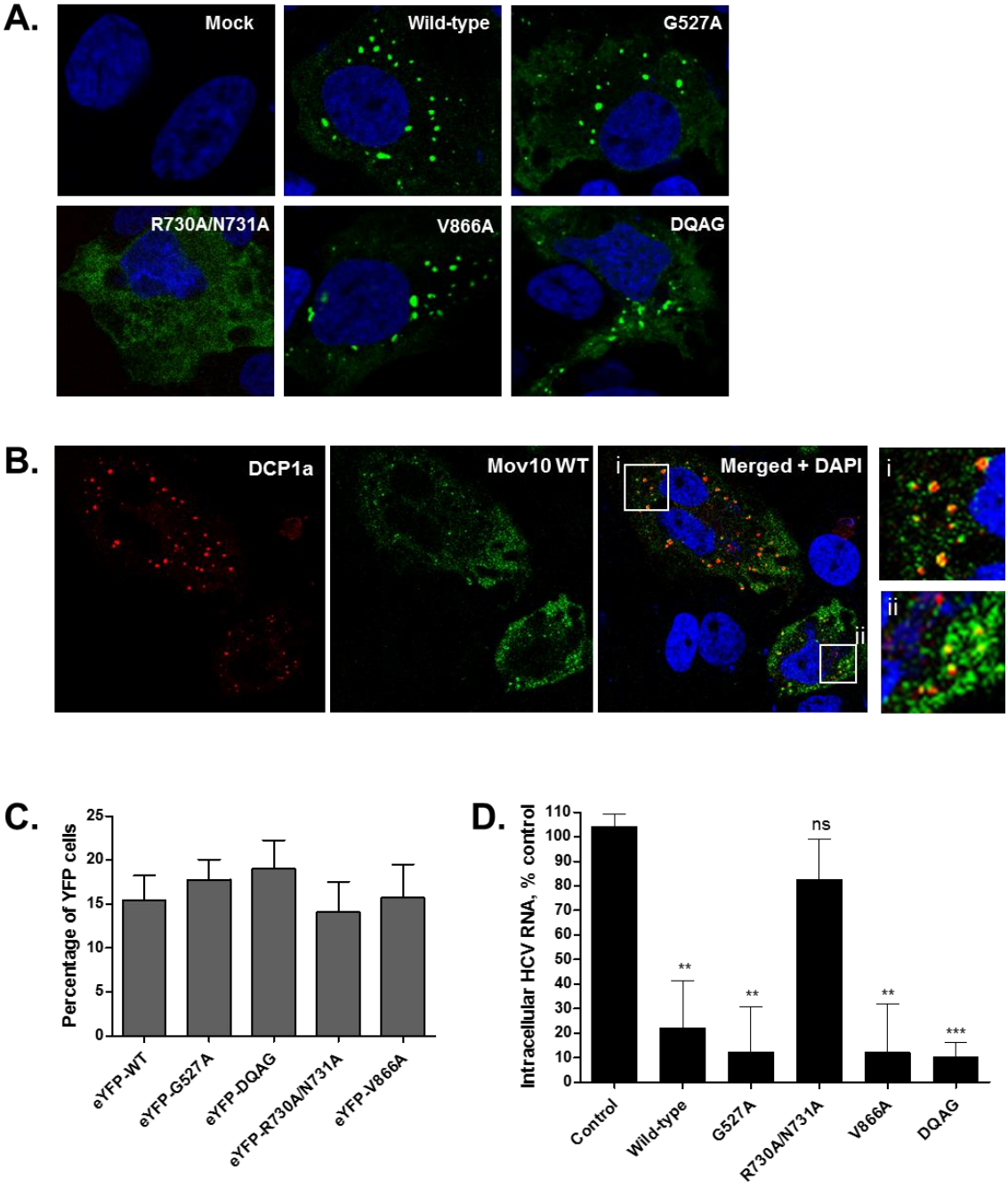
A.
Mock
Wild-type
G527A
R730A/N731A
V866A
DQAG
B.
DCP1a
Mov10 WT
i
Merged + DAPI
i
ii
ii
C.
Percentage of YFP cells
25
20
15
10
5
0
eYFP-WT
eYFP-G527A
eYFP-DQAG
eYFP-R730A/N731A
eYFP-V866A
D.
Intracellular HCV RNA, % control
110
100
90
80
70
60
50
40
30
20
10
0
ns
**
**
**
***
Control
Wild-type
G527A
R730A/N731A
V866A
DQAG

Figure III-5: P-body localization or intact helicase active site are not required for the antiviral activity of Mov10 against HCV. (A) 0.3 ug of plasmid (eYFP-tagged Mov10 wild-type or mutants) was transfected into Huh7.5.1 cells. 48 hours later, the cells were fixed and after staining for nuclei, imaged by confocal microscopy using 63x oil objectives. **(B)** eYFP-tagged Mov10 wild-type and mRFP-Dcp1a (0.3 ug of each) was transfected into Huh7.5.1 cells. 48 hours later, the cells were fixed and after staining for nuclei, imaged by confocal microscopy using 63x oil objectives. **(C)** Transfection efficiencies for the Mov10 plasmids used. **(D)** HCV RNA (Jc1378.1-FLAG(nsGluc2A)) was electroporated into Huh7.5.1 cells, 16 hours later the cells were transfected with eYFP-Mov10 expression plasmids (0.4 μg/well, wild-type or mutants). 72 hours post transfection the cells were assayed for intracellular HCV RNA levels by RT-pPCR (experiments were performed three times independently and results are expressed as the mean ± SD of the percent of the mock transfected sample).

HCV infection redistributes endogenous Mov10, to co-localize with viral proteins NS5A and core

In uninfected cells endogenous or overexpressed Mov10 is distributed throughout the cytoplasm, with occasional foci. These foci co-localize or correlate with canonical mRNA processing body (p-body) proteins; Dcp1a (shown in Figure III-5), APOBEC3G, or Dcp2 (*134, 139*). To determine if this distribution was altered during HCV infection, uninfected and infected cells were fixed then stained for endogenous Mov10 and HCV proteins (NS5A and core) as outlined in 'Materials and methods.' Imaging by confocal microscopy showed Mov10 distributed throughout the cytoplasm in uninfected cells (Figure III-6, orange arrows). Infected cells (white arrows) show more Mov10 puncta, with the number of foci proportional to the amount of infection in the cell (labeled by viral protein staining). These new foci co-localized with HCV NS5A and core protein, shown in Figure III-7.

HCV infection redistributes endogenous Mov10 to lipid droplets

HCV viral packaging and assembly presumably occurs on cytosolic lipid droplet (cLD) structures in the cytoplasm (*90*). cLDs are made up of a phospholipid monolayer that is derived from outer endoplasmic reticulum, around a hydrophobic core of neutral lipids and cholesterol esters. During infection, HCV proteins NS5A and core localize to cLDs at the later stages of the virus' lifecycle (*85, 86, 89*). HCV has been shown to hijack some p-body proteins during infection, redistributing them from P-bodies to HCV pre-assembly sites; cLDs (*126*). As shown in Figure III-7 endogenous Mov10 co-localizes with NS5A and core protein. To determine whether Mov10 this co-localization was occurring at cLDs; uninfected and infected cells were stained for endogenous Mov10, viral proteins, and cLDs (using a lipid droplet marker as described in 'Materials and methods').

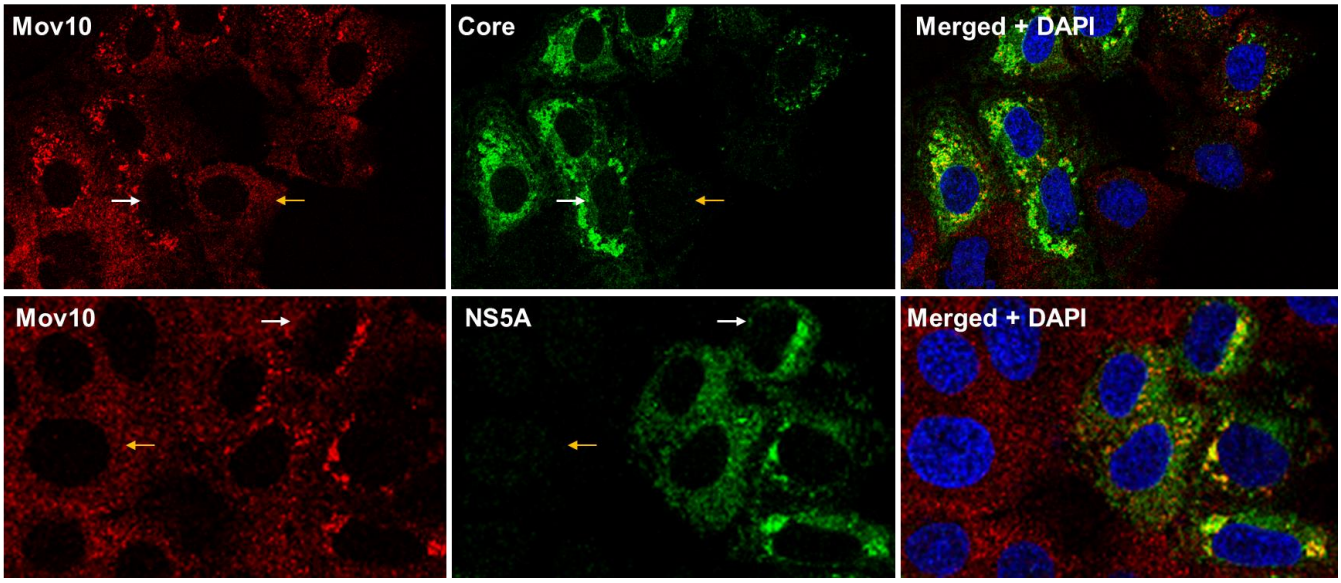
Mov10
Core
Merged + DAPI
Mov10
NS5A
Merged + DAPI

Figure III-6: HCV infection redistributes endogenous Mov10 into concentrated perinuclear foci. Huh7.5.1 cells were infected with Jc1378.1-FLAG(nsGluc2A) (at an M.O.I of 0.5). 48 hours after infection the cells were fixed in 4% paraformaldehyde and stained for endogenous Mov10; in combination with HCV core, or NS5A. The cells were imaged on a Leica TCS SP8 microscope with a 40x water objective. Representative images are shown.

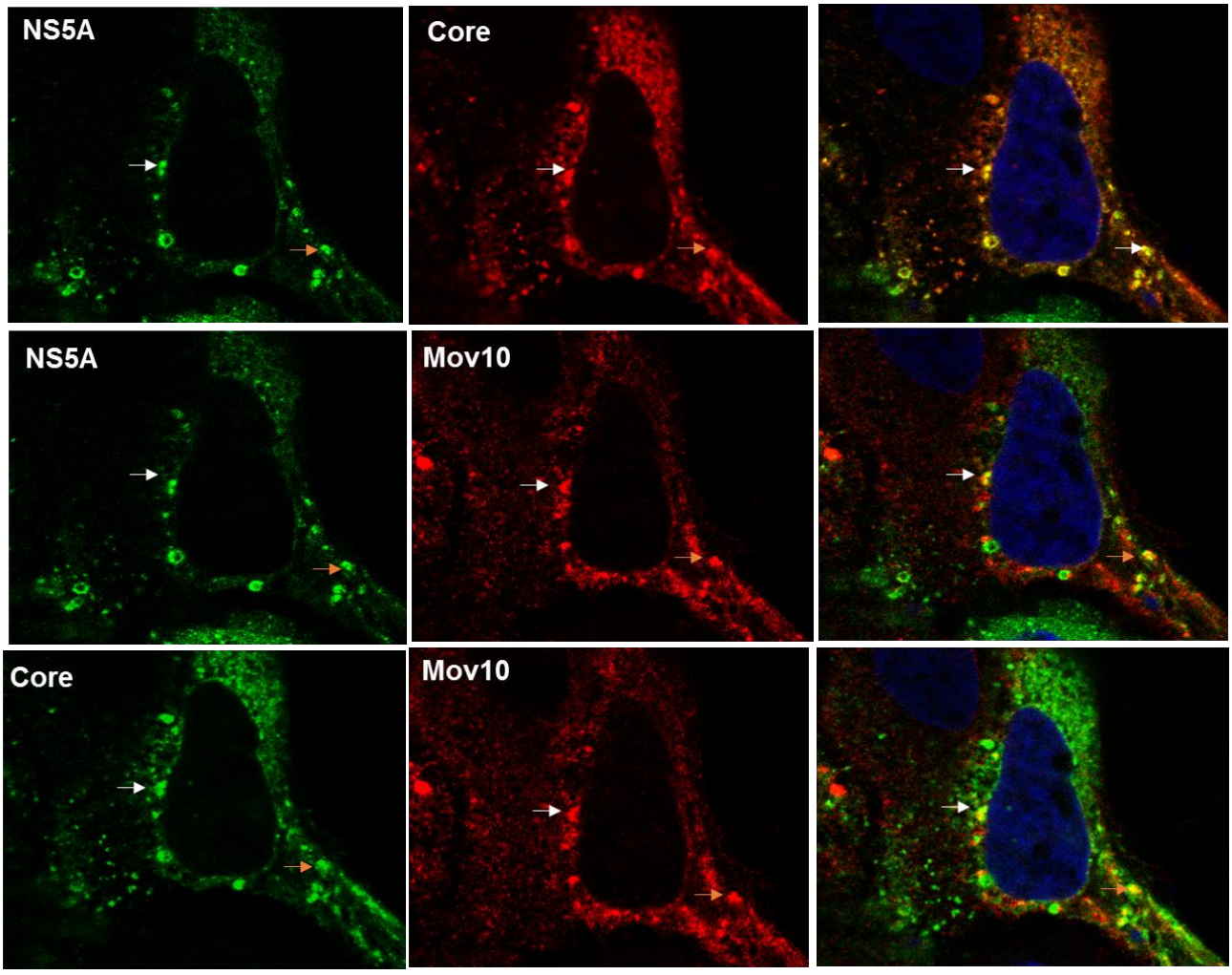
NS5A
Core
NS5A
Mov10
Core
Mov10

Figure III-7: Endogenous Mov10 co-localizes with HCV viral proteins NS5A and core Huh7.5.1 cells were infected with Jc1-378.1-NS5A-Ypet (at an M.O.I of 0.5). 48 hours after infection the cells were fixed in 4% paraformaldehyde and stained for the HCV core protein and Mov10. The cells were imaged on a Leica TCS SP8 microscope with a 63x oil objective. One representative image is shown.

Figure III-8A shows endogenous Mov10 does not localize at or around cLDs in uninfected cells. As expected, NS5A and core protein localize around cLDs. In infected cells, Mov10 formed round or crescent-shaped foci around cLDs (Figure III-8B). These Mov10 crescents co-localize with the core protein, but are also independently around cLDs. The presence of Mov10 at lipid droplets, the sites for HCV viral assembly could explain the protein's effect on HCV virion infectivity.

Mov10 knockout decreases HCV replication

To explore the effects of Mov10 depletion on HCV infection and replication, we used the CRISPR-Cas9 technology (*201, 206*) to knockdown endogenous Mov10 from the hepatoma cell line Huh7.5.1. We designed a guide-RNA that was complementary to the 5'-end of the Mov10 gene; expressed together with the Cas9 endonuclease the guide-RNA would recruit Cas9 to the Mov10 gene. Huh7.5.1 cells were transfected with a plasmid expressing the guide-RNA, Cas9, and reporter GFP. At the peak of GFP expression, the cells were collected and the GFP-positive cells collected by flow cytometry. Half of these cells were expanded as is (Huh7.5.1-round 1 (R1)) and the other half plated at one cell per well, and expanded. After screening for Mov10 protein levels *via* immunocytochemistry and immunoblotting, clones E9 and D6 (Huh7.5.1_E9, and Huh7.5.1_D6) were selected for further assays. As shown in Figure 9A, Huh7.5.1-R1 showed decreased levels of Mov10 compared to the parent cell line Huh7.5.1 (40% decrease by Western blot analysis). Huh7.5.1-E9 had much less Mov10 expressed (85% decrease), and Huh7.5.1-D6 had the least Mov10 expressed (~90% decrease).

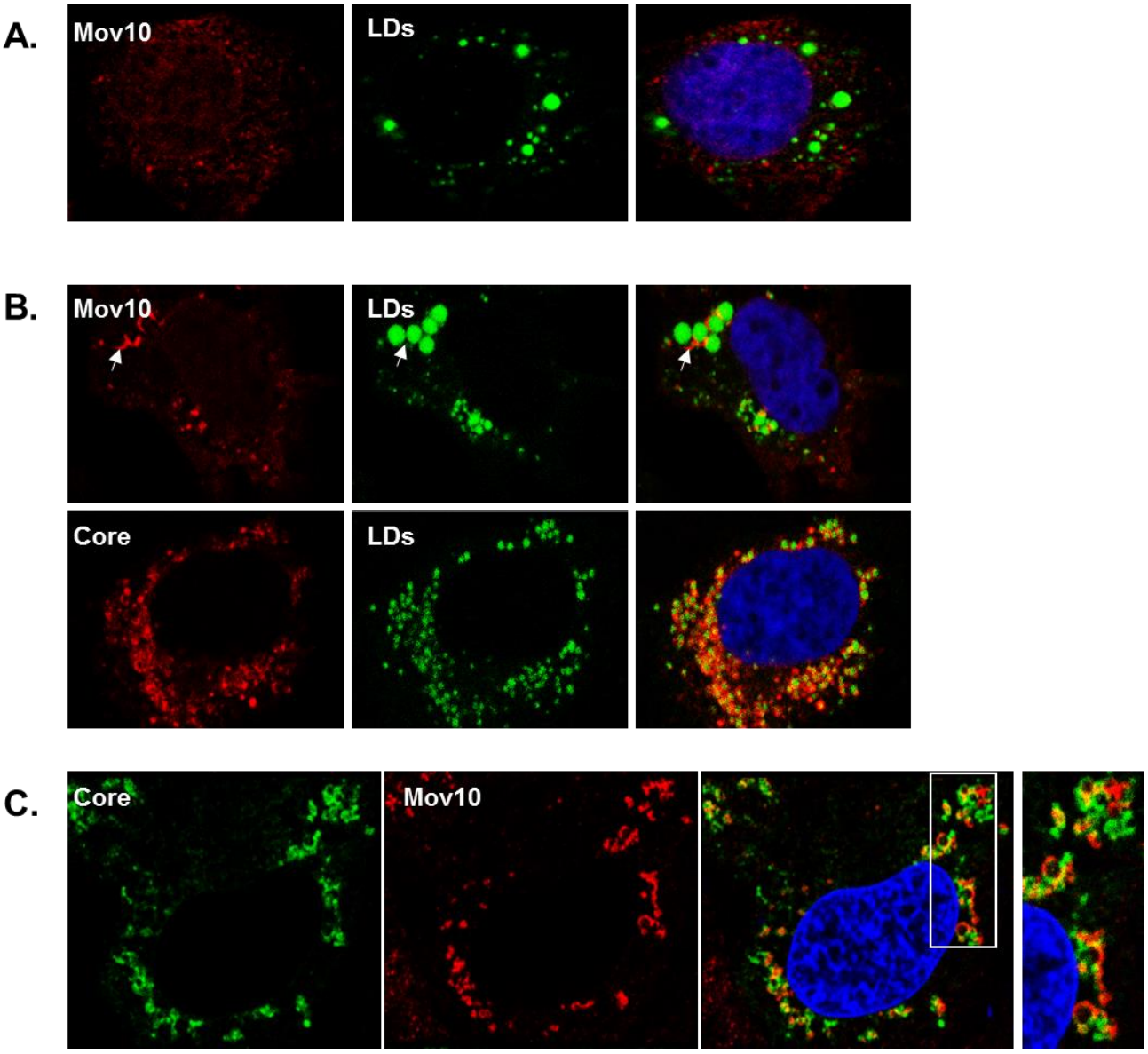
A.
Mov10
LDs
B.
Mov10
LDs
Core
LDs
C.
Core
Mov10

<u>Figure III-8:</u> Endogenous Mov10 localizes to cytoplasmic lipid droplets in HCV infected cells.

Huh7.5.1 cells were infected with Jc1378.1-FLAG(nsGluc2A) (at an M.O.I of 0.5). 48 hours after infection the cells were fixed in 4% paraformaldehyde and stained for lipid droplets using BODIPY 493/503, in combination with HCV core, Mov10, or NS5A. The cells were imaged on a Leica TCS SP8 microscope with a 63x oil objective. One representative image is shown.

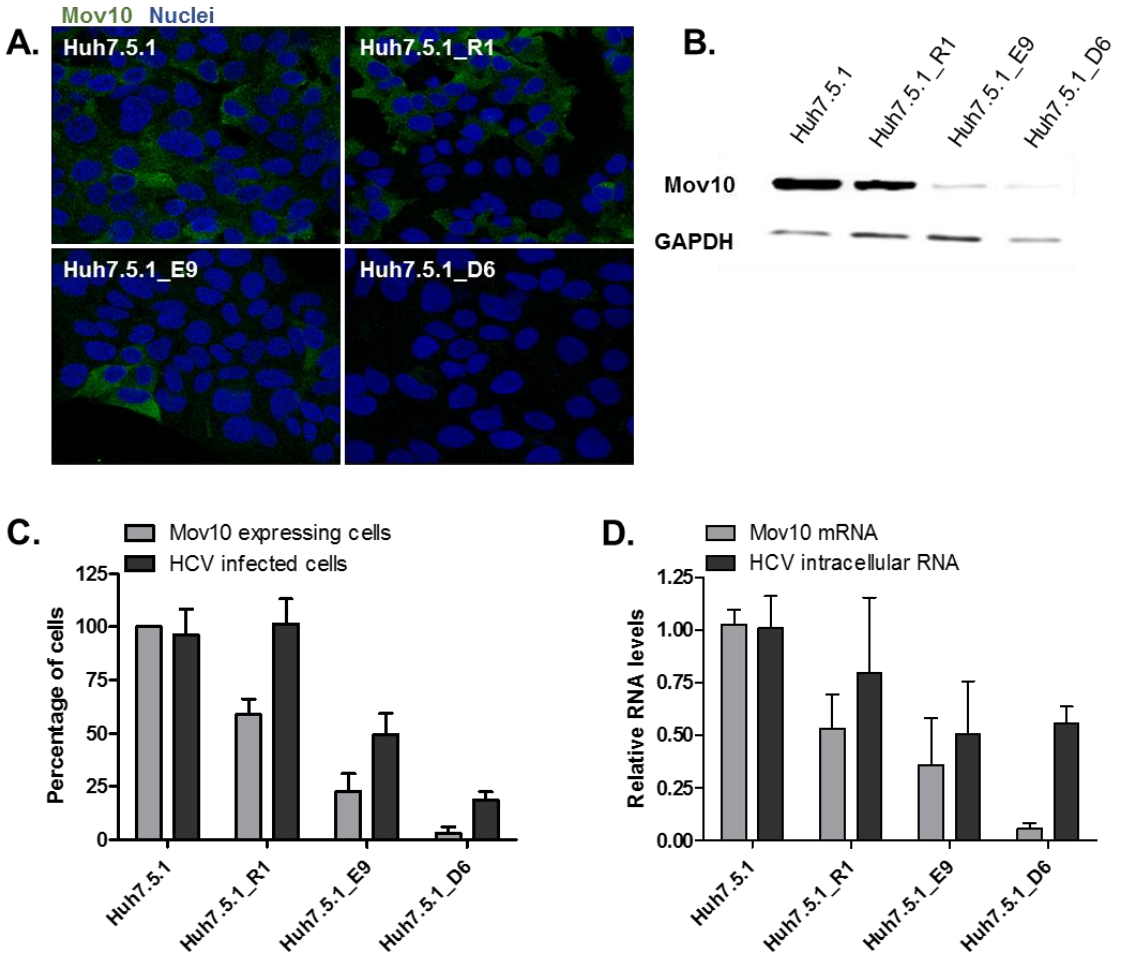
A.
Mov10 Nuclei
Huh7.5.1
Huh7.5.1_R1
Huh7.5.1_E9
Huh7.5.1_D6
B.
Huh7.5.1
Huh7.5.1_R1
Huh7.5.1_E9
Huh7.5.1_D6
Mov10
GAPDH
C.
Mov10 expressing cells
HCV infected cells
Percentage of cells
125
100
75
50
25
0
Huh7.5.1
Huh7.5.1_R1
Huh7.5.1_E9
Huh7.5.1_D6
D.
Mov10 mRNA
HCV intracellular RNA
Relative RNA levels
1.25
1.00
0.75
0.50
0.25
0.00
Huh7.5.1
Huh7.5.1_R1
Huh7.5.1_E9
Huh7.5.1_D6

Figure III-9: Decreasing endogenous Mov10 protein levels decreases HCV replication.

(A) CRISPR/Cas9 genome editing decreased endogenous Mov10 protein levels. Huh7.5.1 cells were transfected with pCas9-GFP-Mov10_T1, a plasmid expressing Cas9 endonuclease and a guide-RNA to target the endonuclease to the 5'end of the Mov10 gene. Cells transiently expressing GFP were selected and expanded as described in Materials and Methods. The selected clones were fixed and stained for endogenous Mov10 (green), and nuclei (DAPI, blue). Images were taken on a TCS Leica SP8 confocal microscopy using a 40x water objective. Representative images are shown. **(B)** Equal numbers of the cells imaged in A were collected for western blot to analyze Mov10 protein levels, and loading control GAPDH. **(C)** Several images from (A) where collected. Cells expressing Mov10 were counted and expressed as a percentage of the total number of cells. 400-500 cells were counted per cell line. In parallel, the same cell lines were infected with Jc1-378.1-NS5A-Ypet (at an M.O.I of 0.5) for 3 days, and collected for flow cytometry analysis to quantify the percentage of cells expressing NS5A-Ypet. Results are shown normalized to the parental cell line Huh7.5.1. **(D)** Cells were infected with Jc1-378.1-NS5A-Ypet (at an M.O.I of 0.5) 72 hours after infection, total RNA was purified from the cell lines shown as detailed in Materials and Methods followed by RT-pPCR analysis for Mov10 and GAPDH mRNA levels.

Mov10 protein levels were also analyzed on a per cell basis by staining fixed cells for Mov10 followed by confocal microscopy, shown in Figure III-9A and quantified in Figure III-9C. In addition to a decrease in Mov10 protein levels, the cell lines described above also had decreased levels of Mov10 mRNA measured by RT-pPCR (Figure III-9D). The RT-pPCR primers used bind to the 5'-end of the gene in close proximity to the Cas9 endonuclease cleavage site. The decreased Mov10 detected is likely due to nucleotide changes in that region following DNA damage repair resulting in decreased binding of the primers.

To investigate HCV infection in these cell lines, the cells were infected with Jc1378.1-NS5A-Ypet for 72 hours then collected to determine HCV infection by flow cytometry and HCV RNA levels by RT-pPCR shown in Figure III-9C and 9D. Decreasing the mRNA and protein levels of Mov10 led to decrease in HCV infection and viral RNA.

D. DISCUSSION

In this study, we investigated the effect of the Mov10 host restriction factor on HCV infection. We show that Mov10overexpression decreases HCV virus production by inhibiting the production of viral RNA. Moreover, overexpression of Mov10 in virus producer cells decreases the infectivity of the progeny virions. Furthermore, we observed that with the exception of Mov10 with mutations designed to affect RNA binding, all other Mov10 variants with mutations designed to disrupt putative Mov10 enzymatic activities retained their restriction effect against HCV.Overexpression of Mov10 decreased viral RNA production in cells infected with fully infectious HCV. This decrease was also observed with a sub-genomic replicon that is capable of only RNA production and primary protein translation. In contrast, overexpression of control P-body protein Dcp1a had no significant effect on HCV RNA replication or virus production. The fact that Mov10 affects both the replicon and fully infectious systems suggests that Mov10 affects early steps in viral replication present in both systems. However, it does not preclude the possibility that Mov10 affects later steps of viral. Mov10 has RNA binding and unwinding

capabilities through a 5'-3' helicase activity (*207*). In addition, Mov10 has been reported to associate with HIV-1 RNA (*134, 139*). Overexpression of the double mutant Mov10 protein R730A/N731A fails to inhibit HCV RNA replication and virus production to the same extent as the wild-type Mov10 or the rest of the mutant Mov10 panel of proteins. The Mov10 R730A/N731A protein showed similar expression levels to the wild-type protein, and the other mutants. It is also likely that the protein is properly folded as the eYFP-fused protein fluoresces, which requires proper folding. The Mov10 double mutant also failed to inhibit HIV-1 and was also shown to have lost its capability to interact with HIV-1 RNA. Taken together, these results suggest that (i) the RNA binding function of Mov10 is required for inhibition of viral replication in both HIV-1 and HCV, and (ii) residues R730 and N731 are involved in, and required for viral RNA binding. However, these hypotheses remain to be further tested.

HCV virus produced in cells overexpressing Mov10 had decreased infectivity, with up to a 4-fold decrease in HCV RNA and protein production. The observed decreased infectivity (tested in cells with normal amounts of Mov10) of HCV virions produced in cells overexpressing Mov10 suggests that it is possible that Mov10 is packaged into HCV virions, and impairs the HCV RNA replication. In fact we observe Mov10 in Western blots of virus-enriched supernatants from Mov10 overexpressing, HCV-infected cells (not shown). However, we could not rule out that the observed Mov10 was present in these supernatants because of possible presence in exosomes. It is also possible that Mov10 overexpression results into a somehow aberrant HCV genome packaging that prevents efficient replication. In fact, interactions of the 3'end of the HCV genome with upstream regions of the viral RNA, have been reported to be important for HCV infectivity, and it is possible that Mov10 may affect these interactions. Further studies will be required to determine the precise defect(s) of assembled virions and the specific role of Mov10 in this process.

Mov10 was predicted to have helicase activities based on the presence of ATP binding (residues 524 to 531), and unwinding domains (residues 645 to 648). A recent published study

and also work in our laboratory confirmed its 5'-3' unwinding capabilities (*207*), and shows that the predicted ATP binding and active site residues are required for Mov10's helicase activity. We tested whether Mov10's putative helicase activity interfered with RNA replication, possibly by disrupting RNA hybrids or secondary structures of the viral RNA genome. The DQAG Mov10 mutant contains an E->Q active site mutation that is designed to disrupt the helicase catalytic activity of Mov10. In addition, the G527A mutation is designed to disrupt the ATP binding function of the enzyme. Interestingly, both the DQAG and G527A mutants retained their antiviral properties against HCV as they did with HIV-1 (*138, 139*), suggesting that neither ATP binding nor helicase activity is involved in Mov10's mechanism of inhibition of both HIV-1 and HCV. Mutant V866A and R730A/N731A Mov10 proteins, when compared to wild-type Mov10, were distributed more diffusely throughout the cytoplasm, forming a smaller number of distinct foci, which were found in a smaller number of cells as we have previously shown (*139*). In addition, these mutants did not localize to P-bodies as efficiently as wild-type Mov10, as we have shown by decreased co-localization with Dcp2, a marker for P-bodies (*139*). Since Mov10 V866A retained its antiviral activity, it seems that localization to P-bodies is not a requirement for Mov10 inhibition of HCV infection.

HCV viral packaging and assembly is known to occur on cytosolic lipid droplet (cLD) structures in the cytoplasm (*90*). cLDs are made up of a phospholipid monolayer derived from outer endoplasmic reticulum, around a hydrophobic core of neutral lipids and cholesterol esters. During infection, HCV proteins NS5A and core localize to cLDs at the later stages of the virus life cycle (*85, 86, 89*). HCV has been shown to hijack some P-body proteins during infection, redistributing them from P-bodies to cLD pre-assembly sites (*124-126*) although the purpose for this relocalization is unknown. Although in uninfected cells endogenous Mov10 localizes in P-bodies, during infection Mov10 changes localization at and around cytoplasmic lipid droplets together with HCV proteins NS5A and core. Further studies are required to understand the

precise s function of Mov10 in lipid droplets and whether there is a specific effect of this host protein on virus assembly.

Previous studies have shown that an optimum concentration of Mov10 is required for HIV-1 infection and infectivity (*134, 138*). Both overexpressing and decreasing Mov10 protein levels decrease HIV-1 infection. Interestingly, we observe that decreasing Mov10 levels also decreases HCV infection levels, both at the protein and RNA levels. Notably, Mov10 is a component of the RNA interference silencing complex (RISC) where it has been reported to interact with Ago2 (*133, 208, 209*). Moreover, suppression of Mov10 levels affects RISC formation and functionality. Abrogating Mov10's interaction with Ago2 inhibits RISC's repression of translation (*210*). Because HCV utilizes microRNAs (primarily miR-122) in complex with Ago2 in order to bind and stabilize its viral RNA (*68-70*), it is possible that a decrease in Mov10 levels disrupts the beneficial interactions of HCV RNA genome with Ago2 and miRNA leading to a destabilization of HCV RNA and a decrease in infection levels.

In summary. Mov10 overexpression potently inhibits HCV replication by decreasing HCV RNA production and virus infectivity, leading to an overall drastic reduction in infectious virus production.

IV. INSIGHTS INTO NOVEL DIRECT-ACTING ANTIVIRAL AGENTS (DAAS), HOST RESTRICTION FACTORS, AND MECHANISMS OF CLINICALLY ADVANCED DAAS

A. ABSTRACT

Work in this Chapter aims at studying the inhibition of HCV by (i) screening for novel small molecule inhibitors of the HCV helicase, (ii) discovering novel host restriction factors, and (iii) providing insights into the mechanism(s) of action of approved and clinically advanced direct-acting antiviral agents (DAAs). There are currently no approved drugs targeting the helicase function of HCV NS3. We screened a chemical library for inhibitors of NS3's helicase domain (NS3h) and discovered two compounds that inhibited NS3h *in vitro*. We validated the antiviral properties of these copounds by showing that they can suppress HCV replication in cell-based assays. These preliminary hits can lead to more potent inhibitors by future chemical modification of the leads in structure activity relationship studies, or through computational *in silico* searches for bioactive analogs. Targeting NS3h in addition to other viral proteins may lead to new therapies that decrease or delay the emergence of drug resistance.

Host proteins can act as restriction factors without directly interacting with viruses, but by indirectly affecting the IFN response pathway. We discovered one such factor Dcp2. Overexpression of Dcp2 restricts HCV replication (by up to 60%); by causing a profound (30-fold) increase in IFN transcription. This inhibition of HCV replication led to a decrease in virus production, but did not affect the infectivity of the virus produced.

Recently several DAAs have advanced in clinical trials and been approved for HCV treatment. NS5A-targeting drugs rapidly eliminate HCV RNA, however their exact mechanism(s) of action are not clear. We show that similar to daclatasvir (DCV), treatment with ledipasvir (LDV) and cyclosporine A (CsA) redistributes NS5A into circular structures. We determined these circular structures to be NS5A at lipid droplets, where it co-localized with the core protein. However, the three drugs had distinctly different effects on the size and number of circular

structures and lipid droplets per cell. Additionally, LDV treatment disrupted the localization of HCV dsRNA to lipid droplets and its association with NS5A. These data provide insights into differences in the antiviral mechanism of action of DCV, CsA, and LDV, and their effects on viral complexes and processes.

B. MATERIALS AND METHODS

HCV helicase expression and purification

The helicase domain portion of HCV protein NS3 (NS3h) was expressed from the pET-SUMO-NS3h plasmid (provided by Dr. CM Rice, Rockefeller University). The construct expresses hexahistidine-tagged NS3h from the HCV Con1 clone (genotype 1a). The protein was expressed as previously described (*211*). Briefly, pET-SUMO-NS3h plasmid was transformed into Rosetta DE3 pLysS *E. coli* cells and grown in LB containing Kanamycin and Chloramphenicol at 37°C to an O.D of ~0.8. Expression was induced by addition of 1 mM IPTG (isopropyl β-D-1-thiogalactopyranoside) followed by growth at 25°C for 5 hours.

A cell pellet from a 3L culture was incubated with 40 ml lysis buffer (50 mM Tris-HCl, pH 7.8, 500 mM NaCl, 1 mM PMSF, 0.1% NP-40, 1% sucrose, and 2 mg/ml lysozyme) then sonicated and centrifuged at 15,000 x g for 30 min. The supernatant was diluted 2-fold in Buffer A (50 mM Tri-HCl pH 7.8, 1 mM PMSF, 4% streptomycin sulfate, and 10% sucrose), stirred on ice for 30 min and centrifuged. The supernatant was loaded on a Ni-NTA column and bound proteins were washed with 20 ml Buffer B (20 mM Tris-HCl pH 7.5, 500 mM NaCl) and 5 mM imidazole, followed by 20 ml Buffer B with 75 mM imidazole. RT was eluted in 2 ml fractions with 20 ml buffer B containing 300 mM imidazole. Fractions with RT were pooled and further purified by size exclusion chromatography (Superdex 75; GE Healthcare). NS3h protein was stored in 50 mM Tris-HCl pH 7.0, 100 mM NaCl, 1 mM DTT, 0.1% NP-40, and 30% glycerol in 10 µl aliquots at -20°C.

FRET-based microplate fluorescence assay for HCV helicase activity and Inhibitor library screening

To monitor the unwinding activity of HCV NS3h we used a fluorescence-based assay that our lab previously described for the discovery of SARS-CoV helicase inhibitors (*212*). The assay uses a dsDNA substrate with two chromophores (Fluorescein-Acceptor and Black Hole quencher-Donor) at the 5'- and 3'-ends of each strand. An active helicase will separate the two strands and fluorescence signal will be observed as a result of photon emission from the fluorescein chromophore (FAM). No fluorescence will be observed if there is no strand separation because the emitted photons from the black hole quencher (BHQ) are absorbed by the fluorescein, thereby quenching the release of a fluorescein signal.

The assay was optimized to give fluorescence values at least 4-fold over the background in the absence of helicase protein. 0.2 μM NS3h was incubated with 60 nM fluorogenic DNA substrate, in a reaction mixture containing 20 mM HEPES pH 7.5, 20 mM NaCl, 5 mM MgCl, and 1 mM DTT, 0.1 mg/ml BSA, 5% glycerol, and 1 mM ATP. The reactions were incubated at 37°C for 60 mins. Fluorescence signals were obtained by excitation at 520 nm and by measuring emission at 495 nm. To identify novel inhibitors of NS3h helicase activity we screened the Maybridge Hitfinder Library using the FRET assay above. 40 μM of each compound was pre-incubated with NS3h for 5 minutes before the addition of the reaction mixture.

Gel-based helicase activity assay

Hits were further validated by gel-based helicase assays. For these assays we monitored the unwinding activity of 0.2 μM NS3h that was incubated with 10 nM of dsDNA (5'-Cy3-labeled 31/18-mer) in a reaction mixture containing 20 mM HEPES pH 7.5, 20 mM NaCl, 5 mM MgCl, and 1 mM DTT, 0.1 mg/ml BSA, 5% glycerol, and 1 mM ATP. The reactions were incubated at 37°C for 60 mins, followed by the addition of an equal volume of stop buffer (1% SDS, 30% glycerol). The samples were electrophoresed at 100 V for 1.5 h at 4 °C on a 5% nondenaturing

polyacrylamide gel, using 89 mM Tris borate pH 8.2. Gels were scanned in a phosphorimager (FLA 5000, FujiFilm).

For inhibition assays, varying concentration of the inhibitors were pre-incubated with NS3h at 37°C for 5 minutes, before the addition of dsDNA and continued incubation for 60 minutes. The reaction was stopped and the products were resolved as described above.

Cell-based helicase inhibitor assays

The initial hits were tested in hepatoma cells Huh7.5.1 for their ability to inhibit fully infectious HCV. Cells were incubated with varying drug concentrations and virus-containing (Jc1378.1-FLAG (nsGluc2A) construct described below) media. Following a 30 minute incubation at 37°C the cells were washed and infected with the drug containing media. 24- and 48-hours after infection, culture media was collected and assayed for *Gaussia* luciferase activity. Protocol also shown in Figure IV-4 (top panel).

Cell lines and reagents

All experiments described in this study were performed using human hepatoma cells (Huh7.5.1) (provided by Dr. Charles Rice,Rockefeller University, NY). The cells were maintained in Dulbecco's modified Eagle medium (DMEM, Invitrogen) supplemented with 10% fetal bovine serum (FBS, Hyclone).

Virus constructs and *in vitro* RNA production

The virus constructs Jc1378.1-NS5A-Ypet and Jc1378.1-FLAG (nsGluc2A) were provided by Dr. C. M. Rice (Rockefeller University). Jc1378.1-FLAG (nsGluc2A) has been previously described (*199*) and encodes fully infectious chimeric genotype 2a hepatitis C virus. In these virus chimeras the core, E1, E2, and 33 amino acids of NS2 are from the J6 clone, and the remaining proteins are from JFH1. Jc1378.1-NS5A-Ypet expresses fluorescent Ypet fused within

the NS5A protein, while Jc1378.1-FLAG(nsGluc2A) contains *Gaussia* luciferase within the NS2 protein. The luciferase gene is flanked by FMDV ns2A protein. Upon HCV infection and translation and processing of viral proteins, the luciferase protein is expressed and secreted into cell culture media. To generate RNA for transfection, the plasmid DNA was purified from *E.coli* using a plasmid midi-prep kit (Qiagen). The DNA (2 µg) was linearized by *XbaI* or *ScaI* cleavage (New England Biolabs) at a site upstream of a T7 promoter for 4 hours at 37°C. The linearized DNA was purified using the QIAquick® PCR-clean up kit (Qiagen) and transcribed into RNA using the MegaScript Ampliscribe T7 kit (Invitrogen) with 0.5 µg of linearized DNA per reaction incubated for 5 hours at 37°C. DNase I was added and the reaction mixture incubated for an additional 20 minutes. The integrity of the RNA was checked by agarose gel electrophoresis and the concentration determined by measurement of the optical density at 260 nm. After purification by RNeasy kit (Qiagen) the RNA was stored in RNase-free water at -80°C, in 10 µg aliquots.

Overexpression plasmids and transfection

Plasmids expressing YFP-Dcp1a, FLAG-Dcp1a, mRFP-Mov10, and FLAG-Mov10 were provided by Dr. Vinay Pathak (Center for Cancer Research, National Cancer Institute, Frederick, MD). Details on the plasmid construction have been previously described (*134*). Briefly, the plasmids express human Dcp1a or Mov10 N-terminally tagged with FLAG epitope (DYKDDDDK) or fluorescent Venus yellow fluorescent protein (YFP). Expression plasmids for mutant Mov10 proteins (G527A, R730A/N731A, V866A, and DQAG) were constructed as described (*139*), and express proteins tagged N-terminally with eYFP.

Transfections were performed by use of Fugene HD reagent (Promega), using 60-80% confluent cells. For dose-response experiments cells were transfected with 0.05-0.3 ng per µl of growth media, in 24-well plates with 1 ml per well. In experiments to determine effect on virus production 0.4 ng of plasmid per µl of media was used, in T25 flasks with 4 ml media each.

Electroporation and virus production.

To produce HCV virus, 10 µg of HCV RNA was transfected into Huh7.5.1 cells by electroporation as previously described (*200*). Briefly, ~70% confluent Huh7.5.1 cells were detached from a T75 flask, and washed twice with ice cold DPBS and resuspended in cold DPBS to $1.5x10^6$ cells per ml. 700µl of this suspension was added to a tube containing 10µg HCV RNA, mixed briefly and transferred to a 0.4cm cuvette (Fisher Scientific) and electroporated using a Gene Pulser II (Bio-Rad). The cells were allowed to rest for 10 minutes at room temperature then transferred into a T75 flask containing 10 ml growth media. The next day, the media was changed and the cells were incubated for two more days. Beginning 72 hours after electroporation, the now virus-containing media was collected and replaced every 6-8 hours, filtered through a 0.45 µm filter and stored in aliquots at -80°C.

To determine the effect of Mov10 on virus production 10 µg HCV RNA (Jc1378.1-NS5A-Ypet construct) was electroporated into Huh7.5.1 cells as described above. $5x10^6$ electroporated cells were diluted into 20 ml media and plated onto T25 flasks (4 ml per flask). After 16 hours the media was replaced with fresh media and transfected with 1 µg pFLAG-Mov10 or control plasmids (empty vector/pFLAG-Dcp1a). Virus-containing media was collected and replaced 24, 48, and 72 hours after transfection and assayed for virus titers (TCID50/ml values) and HCV RNA levels (by RT-pPCR).

Determining virus titers by TCID50 assay

A previously described limiting dilution assay was used to determine viral titer (*200*). For virus released from the cells into the media, $3x10^3$ cells were plated onto a 96-well plate, and the next day infected with 100µl of undiluted virus-containing media (8 wells) or 100µl diluted virus (five serial dilutions, from 10^{-1} to 10^{-5}, 8 wells per dilution). For cell associated virus; infected cells were detached from 6-well plates and washed twice with DPBS then resuspended in media (a volume equal to the virus-containing media collected). The cells were then subjected to four

freeze-thaw cycles using a dry-ice ethanol bath and a 37°C water bath, and centrifuged to remove cellular debris. The supernatant was used to make dilution and infect cells as above. For both intra- and extracellular virus titers the cells were fixed 72 hours post infection with cold methanol, for 30 mins at -20°C, followed by blocking with 1% BSA and 0.2% non-fat milk in 1x PBS-T. To identify infected cells, we probed the cells for HCV NS5A using the NS5A monoclonal antibody 9E10 (provided by Dr. Rice) detected by an HRP anti-mouse secondary antibody (ImmPRESS, Vector Laboratories) followed by addition of an HRP substrate, diaminobenzene, DAB (Invitrogen). NS5A positive cells were detected under a light microscope to score infection positive wells.

RNA levels by quantitative RT-PCR

For determining HCV RNA levels in released virus, 100µl TRIzol reagent (Sigma) was added to 300µl virus-containing media and total RNA purified according to the manufacturer's instructions. For measuring intracellular HCV RNA and IFNβ mRNA, cells were detached by addition of TRIzol then also processed according to the manufacturer's instructions. Quantitative reverse transcription PCR was performed with the ABI 7700 machine (Perkin-Elmer Biosystems) using the Power SYBR Green RNA-to-CT 1-Step kit (Applied Biosystems) as per kit instructions with 100 ng total RNA per reaction. The sequence of the primers used to amplify the 5' untranslated region of the HCV genome are given in Table III-1. To determine HCV RNA copy numbers a standard curve was generated by amplifying dilutions of *in vitro* transcribed HCV RNA ($2x10^7$ to $2x10^1$ genome copies per reaction). The sequences of the forward and reverse primers used to detect IFNβ and IFNα2 transcripts are given in Table III-1. Cellular RNA samples were also analyzed in parallel for GAPDH levels. GAPDH CT values were used to normalize samples using: $\Delta CT = CT_{sample}$ minus CT_{GAPDH} (where $CT_{sample} = CT_{HCV\ RNA}$ or $CT_{IFN\beta\ mRNA}$). For IFNβ mRNA levels fold expression/relative quantity ($2^{(-\Delta\Delta CT)}$) was calculated using

$\Delta\Delta CT = \Delta CT_{sample}$ minus $\Delta CT_{untreated\ control}$.

Gaussia luciferase activity assay

To measure HCV replication of the *Gaussia* luciferase secreting virus we used the *Gaussia* Glow Assay kit (Thermo Scientific) as per the manufacturer's instructions. Briefly, 30µl of the cell culture media was collected and mixed with 30 µl 1x Lysis buffer, and incubated at room temperature for 15 minutes. 50 µl of this mixture was added to 50 µl *Gaussia* glow assay buffer containing 1x substrate (coelentrazine). Luminescence was read using the Enspire™ 2300 Multilabel Reader (Perkin-Elmer Biosystems), and normalized to an uninfected control (cell culture media).

Virus infectivity

To determine the effect of Mov10 on virus infectivity, naïve Huh7.5.1 cells were infected with HCV virus-containing media collected from cells overexpressing Mov10, Dcp1a, or transfected with the empty vector at 72 hours post transfection. The amount of each virus was normalized by HCV RNA levels from RT-pPCR ($6.25x10^3$ HCV RNA copy numbers). 48- and 72 hours post infection the cells were imaged by fluorescent microscopy for HCV NS5A-Yet expression. After imaging at 72 hpi, the media and cells were collected and the cells were split into two fractions. One was probed for HCV core protein levels (and GAPDH as a loading control) by Western blot analysis. Total RNA was isolated from the second fraction and along with the media collected at 72 hpi, it was analyzed by RT-pPCR for HCV RNA levels.

Confocal microscopy

Huh7.5.1 cells were plated on 8-well chambered #1 borosillicate coverglass (Thermo Scientific, Cat # 155411) at $2x10^4$ cells per well. Cells were infected with either Jc1378.1-NS5A-Ypet or

Jc1378.1-FLAG (nsGluc2A) for 48 hours then treated with various compounds (or the vehicle DMSO) for 16 hours. Subsequently, the cells were washed with DPBS and incubated at 4 degrees overnight in 4% paraformaldehyde. The cells were then permeabilized with 1% BSA, 0.1% skim milk, 0.1% Triton-X in PBS for 30 minutes at room temperature. Primary antibodies were bound at room temperature for 1.5 hours at the following dilutions: NS5A (9E10 antibody) 1:500, core (Abcam, Cat #ab2740) 1:500, dsRNA (J2 antibody from Scicons, Hungary) 1:500 or Mov10 (Abcam, Cat #ab80613) 1:1,000. Staining for cytoplasmic lipid droplets was with BODIPY 493/503 (Invitrogen, Cat #D3922) at a 1:500 dilution for 30 minutes at room temperature. All samples were also counterstained for nuclei using Hoechst 33342 (Invitrogen, Cat #H3570) at a 1:10,000 dilution for 15 minutes at room temperature. Following the primary antibodies anti-mouse Alexa 647 (Invitrogen, Cat #A21235) was used for NS5A, core, and dsRNA; and Alexa 568 (Invitrogen, Cat #A11036) was used for Mov10 (both at 1:1,500 dilutions for 1 hour at room temperature).

C. RESULTS

Discovery of novel helicase inhibitors using a high-throughput FRET-based assay

We expressed the helicase domain of HCV NS3h in *E.coli* and purified it by nickel affinity as described in the Materials and Methods (Figure IV-1). HCV NS3h was over 95% pure after size exclusion chromatography. We were able to purify ~20 mg per littre of expression culture. A previously described FRET-based assay from our laboratory (*212*) (outlined in Figure IV-2) was used to determine and optimize the unwinding activity of HCV NS3h. The assay conditions were optimized to achieve fluorescence counts six times over the background (no enzyme controls). Following optimization we began screening the Maybridge Hitfinder Library for compounds that inhibited ≥50% of the helicase activity at 40 μM of compound and 4% DMSO final concentration. More than 2,000 compounds have been screened so far. 6 compounds were identified as ‘hits’ in this initial screening. These compounds were used in dose-response

assays and 2 of them were selected for further validation. One of these, compound 32A3, had an IC_{50} of 11 μM using the FRET-based assay (Figure IV-3).

Validation of hit using a gel based assay

The two selected compounds were validated using a gel-based assay. This was done to exclude the possibility that the compounds were somehow interfering with fluorogenic substrate used in the FRET assay. A 5'-Cy3-labelled dsDNA substrate with 13 annealed bases, and an 18 nucleotide overhang was used (31/18-mer). Using a non-denaturing acrylamide gel, unwound single stranded DNA migrates faster than the dsDNA substrate. An unlabeled DNA strand, complementary to the 31-mer strand was used as a 'trap' to prevent re-annealing of the substrate after helicase unwinding. The inhibition assays were carried out as described in Materials and Methods and both compounds 32A3 and 34B8 inhibited the NS3h unwinding activity of HCV. As shown in Figure IV-4, however, even in the presence of the higher concentrations of 34B8 (last two lanes) the helicase activity of HCV NS3h was not completely suppressed.

Inhibition of HCV NS3h by 34B8 depends on ATP

HCV NS3h requires ATP binding and hydrolysis to unwind DNA or RNA substrates (*213*). To begin to understand the compounds' mechanism(s) of action, we sought to determine whether either one of the compounds would compete with ATP, suggesting the compound binding to the helicase's ATP-binding site or interfering with ATP hydrolysis. To this end, we investigated the inhibitory action of 34B8 in the presence of increasing amounts of ATP. Data shown in Figure IV-4B, show that increasing amounts of ATP do not suppress the inhibitory effect of 34B8. Instead, there appears to be an increase in the inhibitory activity of the compound as the ATP concentration is increased, suggesting that ATP may assist or improve the compound's binding. The data suggest that 34B8 does not compete with ATP for binding, which makes it less likely to promiscuously bind at ATP-binding pockets of cellular proteins.

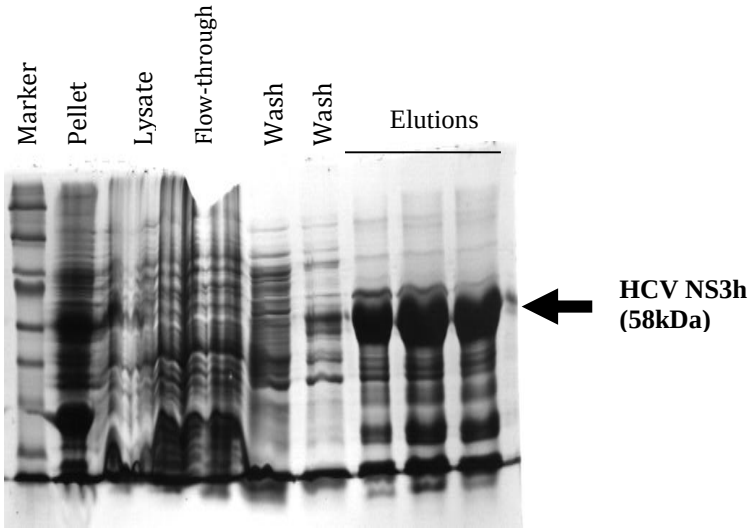
Marker
Pellet
Lysate
Flow-through
Wash
Wash
Elutions
HCV NS3h
(58kDa)

Figure IV-1: HCV NS3h purification. The helicase domain of HCV non-structural protein 3 (NS3) was expressed and purified as outlined in Materials and Methods. Aliquots from steps in the purification process were run on a 10% denaturing SDS acrylamide gel, followed by Coomassie blue staining. Elution fractions containing HCV NS3h were pooled and further purified by size-exclusion chromatography.

34B8 and 32A3 inhibit infectious HCV in a cell-based assay

Next, we tested the ability of the two compounds to inhibit fully infectious HCV in hepatoma cells. We pre-treated the cells with compound for 3 hours. In parallel, virus-containing media was incubated with the compound (or just DMSO in controls) for the same amount of time. Then the compound was removed from the cells, and the cells infected with the pre-treated virus One and two days after infection, we collected virus supernatants and assayed for *Gaussia* luciferase activity. Although both compounds decreased HCV replication at both 24- and 48-hours after infection, the compounds were not as efficient at blocking the virus as they were at inhibiting the helicase protein *in vitro* (Figure IV-6). This might be due to the compounds not entering the cells efficiently, or having a short half-life once in the cells.

Dcp2 as a HCV restriction factor

Overexpression of Dcp2 inhibits HCV replication

A plasmid expressing mRFP-tagged Dcp2 protein was transfected into Huh7.5.1 cells. 24 hours after transfection the cells were infected with HCV virus (*Gluc* reporter virus). 72 hours after infection culture media was collected and assayed for luciferase activity. As shown in Figure IV-7 overexpression of Dcp2 inhibited HCV replication. However, inhibition was not in a dose-dependent manner, suggesting minimum amounts of Dcp2 were required for the maximum effect, and increasing Dcp2 plasmid amounts or protein expression did not increase the effect on HCV replication.

Overexpression of Dcp2 restricts HCV virus production

To determine whether the inhibition of HCV replication led to a decrease in virus production we electroporated HCV RNA (NS5A-Ypet virus) into Huh7.5.1 cells.16 hours later these cells were transfected with the mRFP-Dcp2 plasmid. Three days after transfection the cell culture media was collected and assayed for extracellular HCV RNA levels and virus titer levels ($TCID_{50}$/ml) were

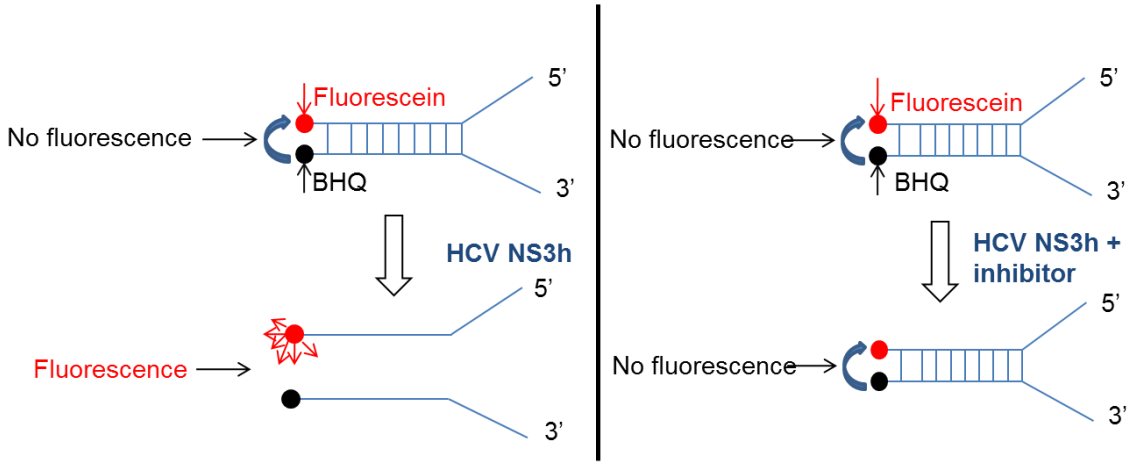
No fluorescence
Fluorescein
5'
BHQ
3'
HCV NS3h
Fluorescence
5'
3'
No fluorescence
Fluorescein
5'
BHQ
3'
HCV NS3h +
inhibitor
No fluorescence
5'
3'

Figure IV-2: FRET-based assay for helicase activity and inhibitor screening. In the presence of an active helicase, the dsDNA substrate is unwound, separating the Fluorescein from the Black Hole Quencher (BHQ) and allowing for fluorescence signal. In the presence of a helicase inhibitor, the helicase is unable to unwind the substrate, and no fluorescence is observed.

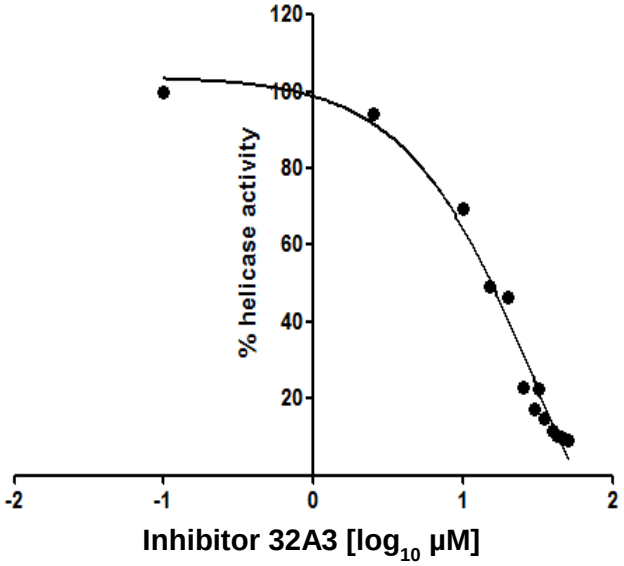
120
100
80
60
40
20
% helicase activity
-2
-1
0
1
2
Inhibitor 32A3 [log10 µM]

Figure IV-3: Validation of 32A3 as an inhibitor using the FRET assay. 200 nM of HV NS3h was incubated with varying amounts of inhibitor 32A3 at 37°C for 5 minutes. A reaction mixture containing 5 mM ATP and 5 mM $MgCl_2$ and the reactions incubated for a further 60 mins. Fluorescence signals were measured at excitation and emission wavelengths of 520 nm and 495 nm, respectively.

determined using a limiting dilution assay. As shown in Figure IV-8, overexpression of P-body marker protein Dcp1a had no effect on virus production. However, overexpression of Dcp2 resulted in a 60-70% decrease in virus production.

The infectivity of HCV virus is not affected by Dcp2 overexpression

The decrease in virus production observed could have been due to a decrease in the infectivity of the virus being produced. This would affect or decrease subsequent infections and lead to a perceived decrease in virus production. The cell culture media collected in Figure IV-8 was used to infect naïve Huh7.5.1 cells.

The amount of virus-containing media used to infect cells was normalized to result in equal amounts of HCV RNA copies per sample. 72 hours after infection, cells and cell culture media was collected and subjected to RT-pPCR for intracellular and extracellular HCV RNA levels, respectively (Figure IV-9). Virus produced in Dcp2-overexpressing cells was equally infectious as the virus from Dcp1a-overexpressing and mock transfected cells. This indicated that Dcp2 overexpression inhibited HCV replication by affecting virus production but had no effect on the infectivity of the virus produced.

Overexpression of Dcp2 profoundly induces IFNβ mRNA transcription in Huh7 cells, and moderately in Huh7.5.1 cells

As described above Dcp2 overexpression decreased HCV replication and viral production, but not in a dose-dependent manner. Overexpression of Dcp2 also had no effect on the assembly and infectivity of the virus produced. These results suggested that Dcp2 did not have a direct effect on HCV, but rather induced an intracellular response against the virus. To investigate this we quantified IFNβ mRNA levels upon Dcp2 overexpression in Huh7 *vs.* Huh7.5.1 cells. Huh7 cells are hepatoma cells that have been selected for permissiveness to HCV

.

A.

34B8 (uM):	–	–	–	–	–	2.5	5	7.5	10	20
ATP (mM):	–	–	5	5	5	5	5	5	5	5
HCV ns3h:	–	–	+	+	+	+	+	+	+	+
95°C:	+	–	–	–	–	–	–	–	–	–

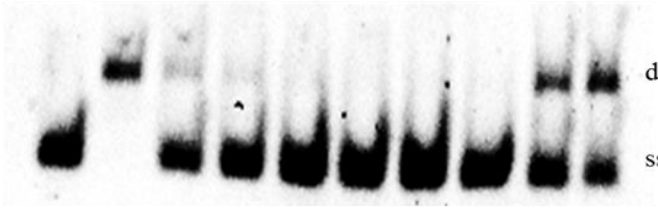

B.

34B8 (uM):	–	–	10	10	10	20	20	20
ATP (mM):	–	–	1	2.5	5	1	2.5	5
HCV ns3h:	–	–	+	+	+	+	+	+
95°C:	+	–	–	–	–	–	–	–

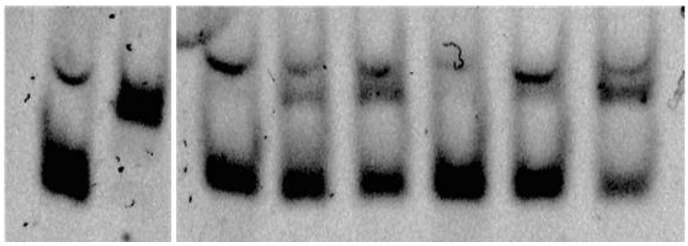

Figure IV-4A: Validation of 34B8 as an inhibitor using the gel-based assay. 200 nM of HCV NS3h was incubated with varying amounts of inhibitor 34B8 at 37°C for 5 minutes. A reaction mixture containing 5 mM ATP and 5 mM $MgCl_2$ was set and the reactions were incubated for a further 60 minutes. After addition of stop buffer the samples were resolved on a non-denaturing polyacrylamide gel as outlined in Material and Methods.

Figure IV-4B: Inhibition of HCV NS3h by 34B8 is depends on ATP. 200 nM of HV NS3h was incubated with either 10 or 20 μM of inhibitor 34B8 at 37°C for 5 minutes. A reaction mixture containing varying amounts of ATP and 5 mM $MgCl_2$ was set and the reactions were incubated for a further 60 minutes. After addition of stop buffer, the samples were resolved on a non-denaturing polyacrylamide gel as outlined in Material and Methods.

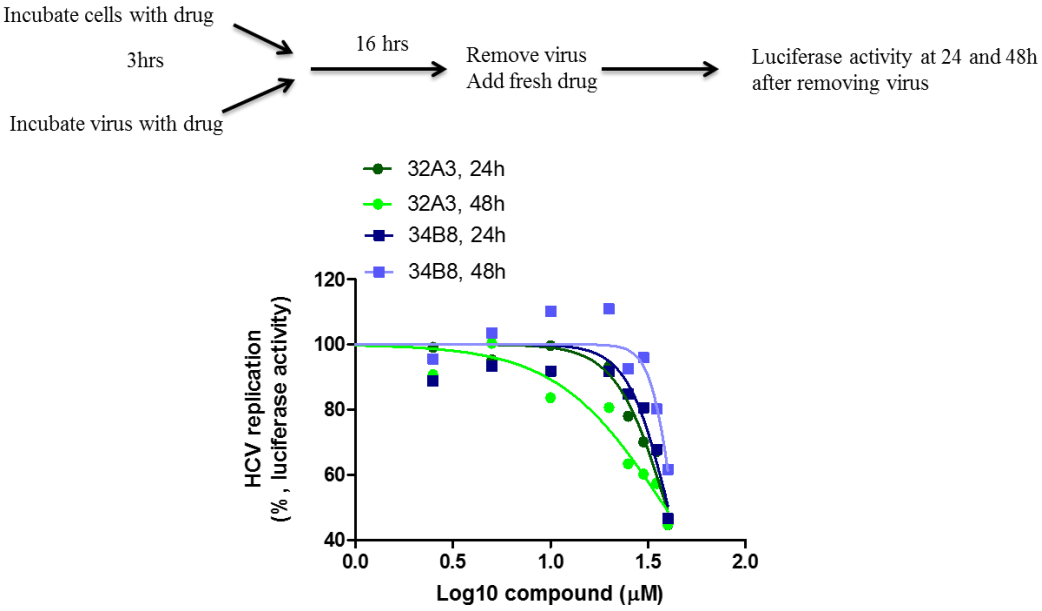
Incubate cells with drug
3hrs
Incubate virus with drug
16 hrs
Remove virus
Add fresh drug
Luciferase activity at 24 and 48h
after removing virus
32A3, 24h
32A3, 48h
34B8, 24h
34B8, 48h
HCV replication
(% , luciferase activity)
120
100
80
60
40
0.0
0.5
1.0
1.5
2.0
Log10 compound (μM)

Figure IV-5: 34B8 and 32A3 inhibit infectious HCV in a cell-based assay. Huh7.5.1 cells were incubated with varying drug concentrations; in parallel virus-containing (Jc1378.1-FLAG (nsGluc2A) construct described below) media was incubated with drug. Following a 3 hour incubation at 37° the cells were washed and infected with the drug containing media. 16 hours later the virus-containing media was replaced with fresh media. 24- and 48-hours after removing virus, culture media was collected and assayed for *Gaussia* luciferase activity.

infection. These cells have been shown to have decreased levels of toll-like receptors 3 and 7 (TLR3 and TLR7) (*214*). This in turn would decrease induction of the antiviral response upon infection. Huh7.5.1 cells are a derivative of Huh7 cells that is even more permissive to HCV infection due to the expression of a deficient form of RIG-I protein and because they have been previously infected (and treated) with HCV (*205, 215, 216*). Thus, Huh7.5.1 cells have a defunct RIG-I, which is unable to detect HCV infection. As shown in Figure IV-10 overexpression of Dcp2 in Huh7 cells induced a profound increase in IFNβ mRNA, compared to mock and Dcp1a expressing cells. Interestingly, in the presence of virus, this induction was decreased by more than 50%. This is likely due to the several mechanisms that HCV has developed to decrease and prevent induction of the anti-viral response. On the other hand, overexpression of Dcp2 in Huh7.5.1 cells induced a modest increase in IFNβ mRNA, which was again decreased in the presence of virus. Taken together our results suggest that Dcp2 plays a role in IFN induction in the absence of infection. In infected cells Dcp2 still induced IFNβ mRNA role in IFN induction which was countered by HCV's mechanisms to decrease and affect IFN induction.

Treatment with NS5A-targeting drugs redistributes NS5A into circular structures

Recently several highly potent compounds have entered clinical trials for the treatment of HCV and several of these have been approved for use in the United States and in Europe. These drugs target HCV viral proteins (direct-acting antiviral agents, DAAs) or host proteins involved in the virus life cycle. Although these drugs cause rapid clearance of the viral RNA it is not clear what effect have on viral replication and assembly complexes, and whether they cause changes in cellular protein complexes and processes. Daclatasvir (DCV) has been shown to cause alterations in the cytoplasmic distribution of NS5A (*115, 116*). DCV treatment results in the disruption of replication complex formation leading in NS5A being redistributed disproportionally to pre-assembly sites in cytoplasmic lipid droplets (cLDs). We sought to determine the effect of other NS5A-targeting compounds.

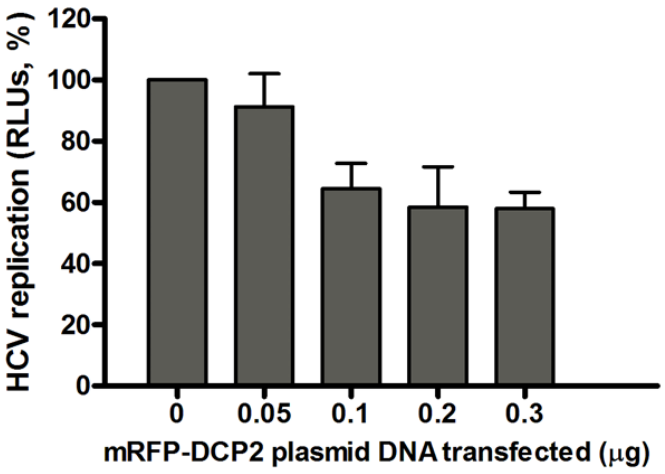
HCV replication (RLUs, %)
120
100
80
60
40
20
0
0
0.05
0.1
0.2
0.3
mRFP-DCP2 plasmid DNA transfected (μg)

Figure IV-6: Overexpression of Dcp2 inhibits HCV replication. Varying amounts of a plasmid expressing mRFP-Dcp2 were transfected into Huh7.5.1 cells. After 24 hours the cells were infected with HCV virus (Jc1-378.1 Gluc construct). Culture media was collected 48 hours post infection and assayed for *Gaussia* luciferase activity. Error bars represent the mean ± SD values from 3 independent experiments.

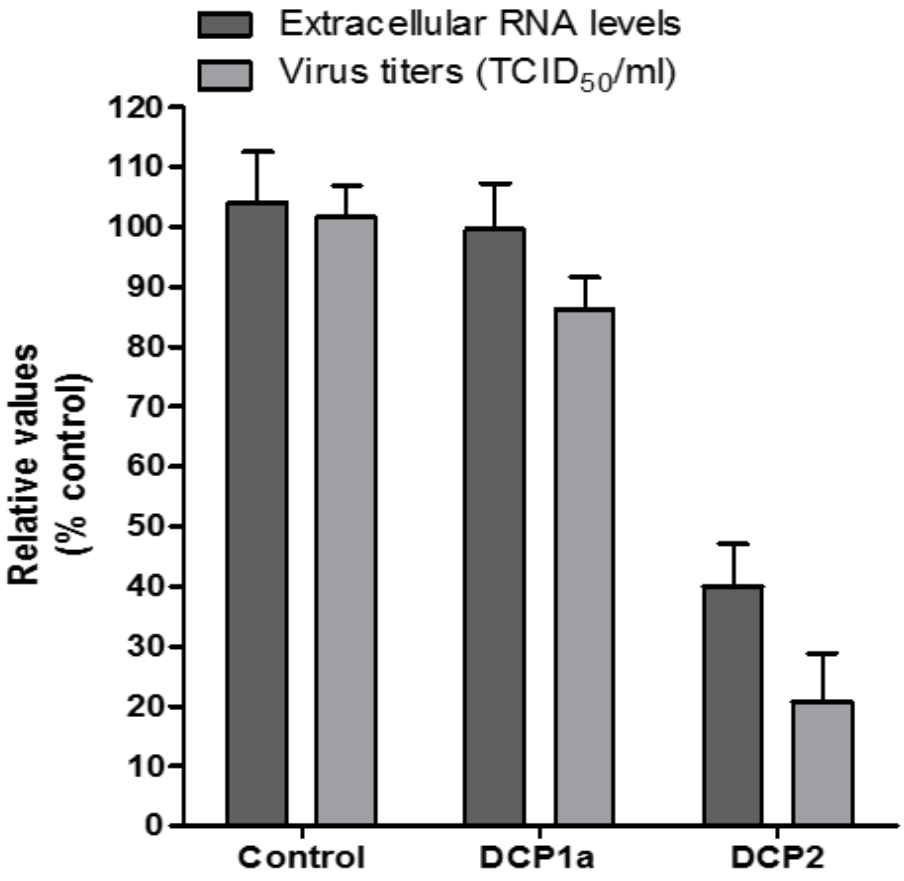
Extracellular RNA levels
Virus titers (TCID50/ml)
Relative values
(% control)
120
110
100
90
80
70
60
50
40
30
20
10
0
Control
DCP1a
DCP2

Figure IV-7: Overexpression of Dcp2 decreases HCV virus production. HCV RNA (Jc1 Ypet clone) was electroporated into Huh7.5.1 cells. 16 hours later, 0.4 µg of either empty plasmid (control), FLAG-Dcp1a or FLAG-Dcp2 were transfected into the cells. Culture media was collected 72 hours post transfection and assayed for HCV RNA levels by RT-pPCR and viral titer levels by a limiting dilution assay. Error bars represent the mean ± SD values from 3 independent experiments.

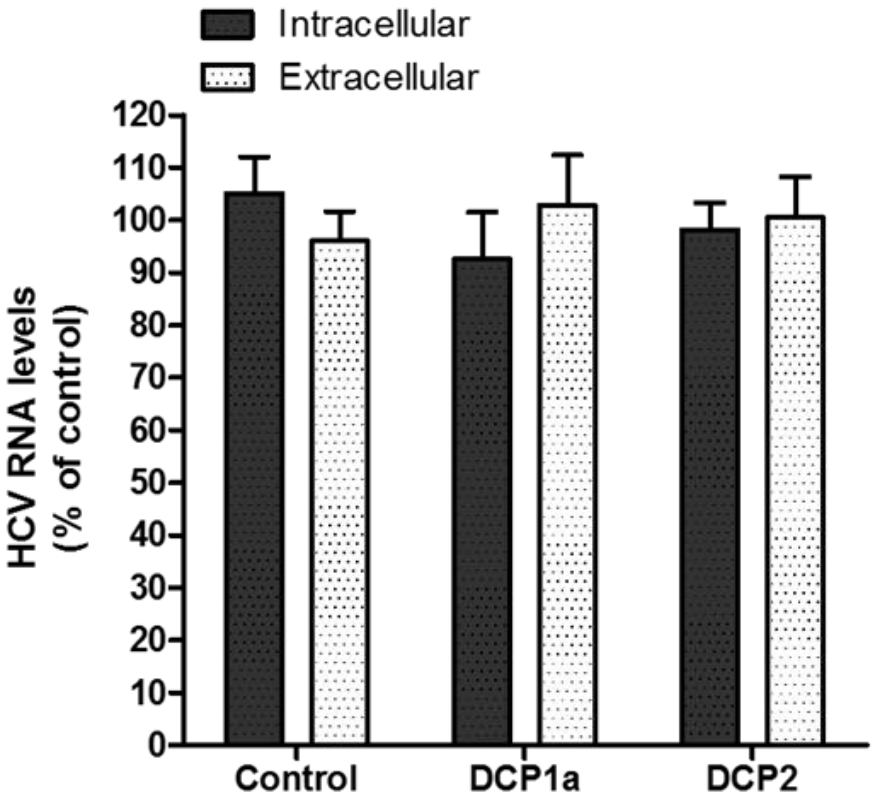
Intracellular
Extracellular
HCV RNA levels
(% of control)
120
110
100
90
80
70
60
50
40
30
20
10
0
Control
DCP1a
DCP2

Figure IV-8: Overexpression of Dcp2 does not affect the infectivity of produced virus. The virus-containing media from Figure IV-8 was used to infect naïve Huh7.5.1 cells. Equal amount of HCV copy numbers were used for the 3 different samples. 72 hours after infection, the culture media and cells were collected and assayed for HCV RNA levels by RT-pPCR. Error bars represent the mean ± SD values from 3 independent experiments.

Specifically, we tested cyclosporine A (CsA), which targets the host factor cyclophilin A, and ledipasvir (LDV), which targets NS5A. We determoined the effect of these antivirals on NS5A distribution, replication complexes, and pre-assembly sites (cLDs). To this end, we treated HCV infected cells with 5-times the EC_{50} of each drug, or the vehicle DMSO as a mock treated control. After a 16 hour treatment, the cells were fixed and stained for viral proteins NS5A and core. As shown in Figure IV-11A, in infected, by mock treated cells, NS5A shows mostly a diffuse distribution, consistent with its expression in the ER, and as part of the replication complex also on the ER. In some cells, NS5A is found in circular structures, and co-localizes with the core protein. This circular distribution has been reported to be NS5A and core protein at, and surrounding cLDs. In the presence of CsA, DCV, or LDV, most of the NS5A visualized is distributed in these circular structures where it still co-localizes with the core protein. This suggests that similar to DCV, CsA and LDV treatment redistributes NS5A from the endoplasmic reticulum (ER) to cytoplasmic lipid droplets. We also, however, observed that the size and quantity of the circular structures seen differed among the different drug treatments. As shown quantified in Figure IV-11B and C, treatment with CsA resulted in larger structures (average area of ~170 $pixels^2$), with less of them per cell (average of ~50/cell). LDV treatment on the other hand, resulted in much smaller structures (~100 $pixels^2$), with more of them per cell (~110/cell). Measurements were done manually using the cellSens (Olympus USA) program.

NS5A-targeting drugs change the appearance of lipid droplets

As described above, treatment with NS5A-targeting drugs redistributes NS5A to cLDs. We investigated whether the drugs had any effect on the cLDs themselves and whether the circular structures we observed were indeed NS5A around cLDs. Using a marker for cLDs we were able to visualize changes in both NS5A and cLDs. Studies have found that in HCV infected cells cLDs are small, and infection increases the number of droplets per cell (*217, 218*). As shown

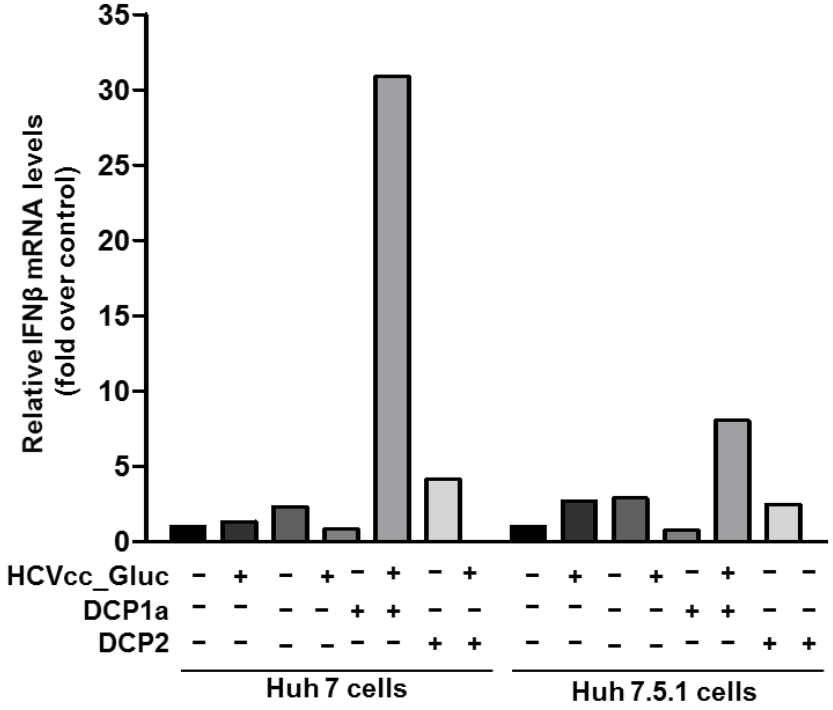
Relative IFNβ mRNA levels
(fold over control)
35
30
25
20
15
10
5
0
HCVcc_Gluc
DCP1a
DCP2
Huh 7 cells
Huh 7.5.1 cells

Figure IV-9: Overexpression of Dcp2 induces IFNβ moderately in Huh7.5.1 cells, and profoundly in Huh7 cells. 0.4 μg of either empty plasmid (control), FLAG-Dcp1a or FLAG-Dcp2 was transfected into Huh7 or Huh7. 5.1 cells. After 24 hours, the cells were collected and assayed foR IFNβ and GAPDH mRNA levels by RT-pPCR.

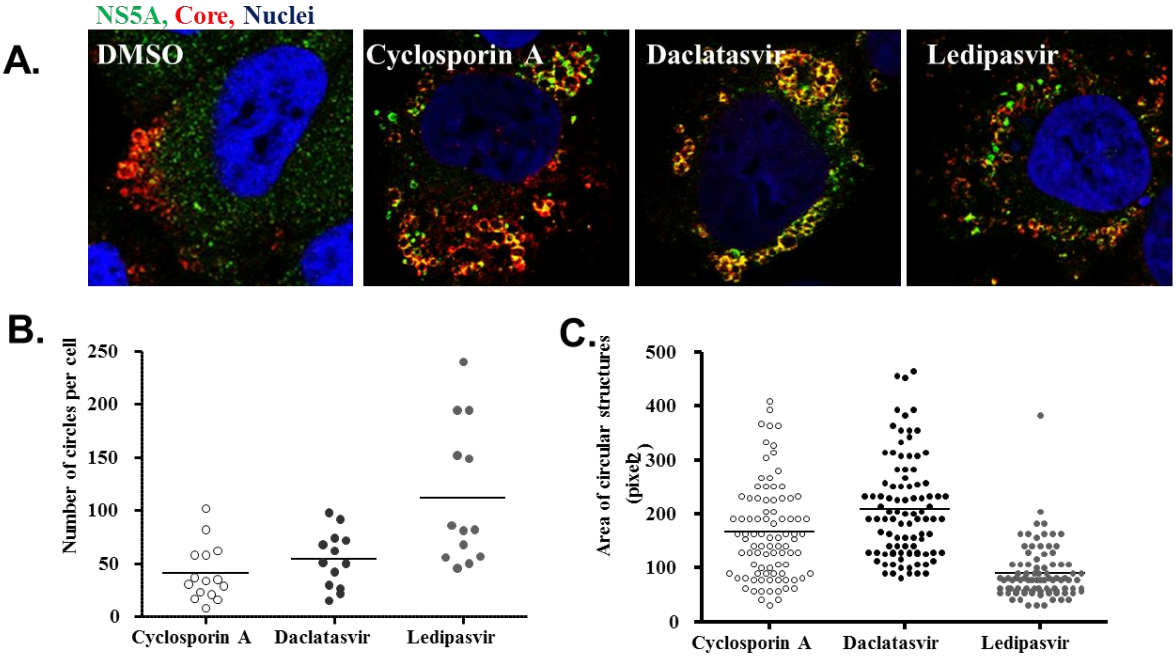
NS5A, Core, Nuclei
A.
DMSO
Cyclosporin A
Daclatasvir
Ledipasvir
B.
Number of circles per cell
250
200
150
100
50
0
Cyclosporin A
Daclatasvir
Ledipasvir
C.
Area of circular structures (pixel2)
500
400
300
200
100
0
Cyclosporin A
Daclatasvir
Ledipasvir

Figure IV-10: Treatment with NS5A-targeting drugs redistributes NS5A into circular structures. Huh7.5.1 cells were infected with HCV (Jc1-378.1-NS5A-Ypet construct) for 72 hours before being treated with cyclosporin A, daclatasvir, ledipasvir, or DMSO as a control. The drugs were removed after 16 hours, and the cells fixed in paraformaldehyde. The cells were stained for HCV core protein and nuclei as outlined in Materials and Methods and imaged on a TCS Leica SP8 confocal microscope using a 63x oil objective lens. The resulting images were quantified for the number of circular structures per cell, and the area of each circular structure. 20 cells were quantified per treatment.

in Figure IV-12, in mock-treated cells, NS5A (red) was mostly diffused in the cytoplasm, and in circular structures in some of the cells. This distribution was mostly the same for cells treated with NS5B-targeting drug sofosbuvir (Sof) and protease inhibitor danoprevir (Dano). In cells treated with CsA, DCV, or LDV, however, most of the NS5A observed shows a spotty distribution, and at higher magnification, circular distribution. In terms of cLDs, as expected in DMSO treated cells, they were small, numerous in number, and in most cases perinuclear. This was mostly maintained in Sof and Dano treated cells and also in DCV and LDV treated cells. In CsA, treated cells as previously described (*219*) cLDs were larger, fewer in number, and not strictly perinuclear.

Ledipasvir treatment disrupts localization of HCV dsRNA with NS5A

Double-stranded RNA is formed during replication of HCV RNA. Using an antibody that has been reported to recognize long (at least 80bp) stretches of double stranded RNA (dsRNA), we visualized viral dsRNA and any changes in its localization that occur during drug treatment. Previous reports have shown dsRNA localizes at cLDs where it partially co-localizes with NS5A and core protein (*115, 116*). As shown in Figure IV-13, in control DMSO-treated cells, dsRNA (red) and NS5A (green) are both mostly diffused throughout the cytoplasm. However, in parts of some cells the two form circular structures and co-localize. In CsA-treated cells, as previously shown there are more of these structures, which consistently appear to be larger than in the control samples (quantification shown in Figure IV-10). In CsA-treated cells, there is less dsRNA detected due to the compound's inhibitory action, and the remaining dsRNA still co-localizes with NS5A. However, in LDV-treated cells the circular structures formed by NS5A consistently appear to be smaller in size but more in number. Surprisingly, in the case of LDV the dsRNA no longer localizes to these circular structures or co-localizes with NS5A. Instead, dsRNA is seen in distinct foci throughout the cytoplasm.

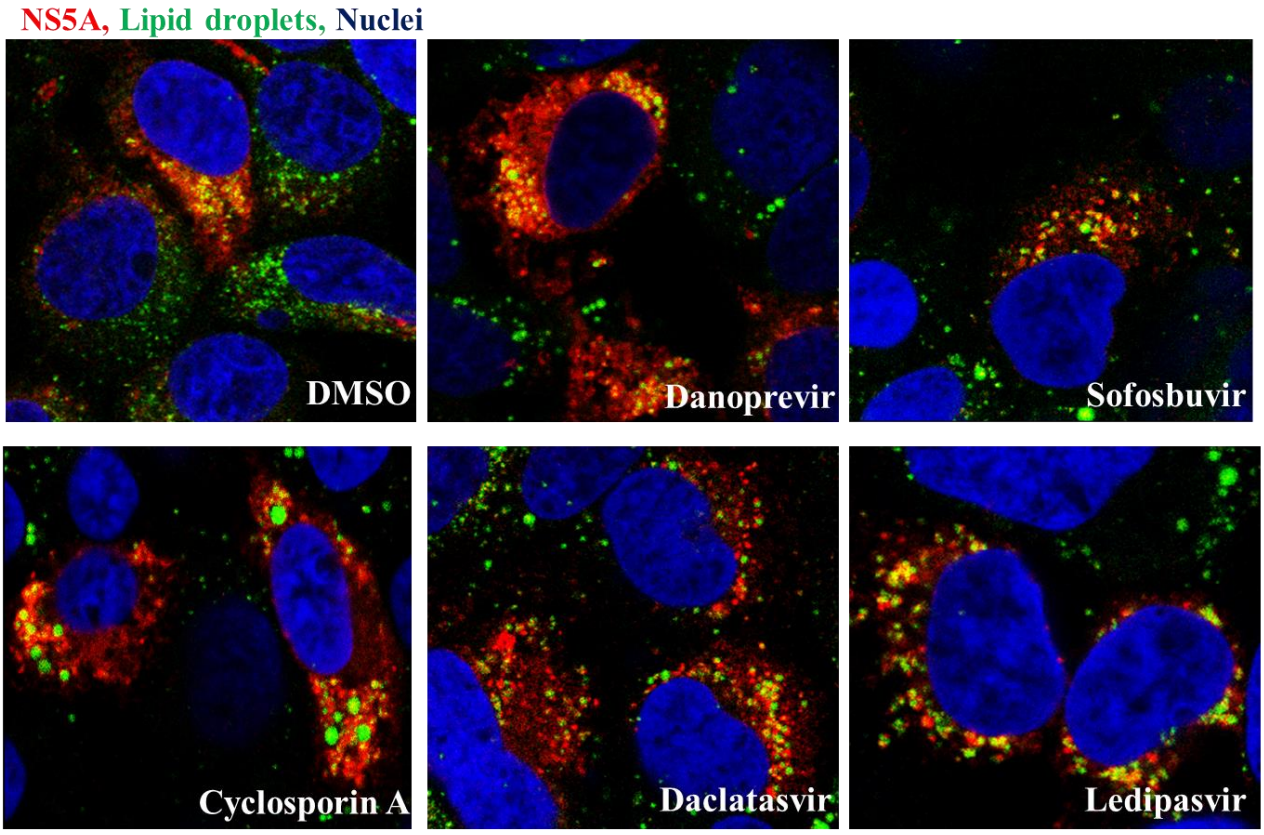
NS5A, Lipid droplets, Nuclei
DMSO
Danoprevir
Sofosbuvir
Cyclosporin A
Daclatasvir
Ledipasvir

Figure IV-11: NS5A-targeting drugs change the appearance of lipid droplets. Huh7.5.1 cells were infected with HCV (Jc1-378.1-NS5A-Ypet construct) for 72 hours before being treated with danoprevir, sofosbuvir, cyclosporin A, daclatasvir, ledipasvir, or DMSO as a control. The drugs were removed after 16 hours, and the cells were fixed in paraformaldehyde. The cells were stained for HCV NS5A protein and lipid droplets as outlined in Materials and Methods and imaged on a TCS Leica SP8 confocal microscope using a 63x oil objective lens. Representative images are shown.

A. DISCUSSION

Recently, several direct-acting antiviral agents (DAAs) with high potencies and specificity have been reported, and some approved for the treatment of HCV. Currently, there are promising DAAs against most of HCV's non-structural proteins, including drugs targeting the protease activity of NS3, the polymerase NS5B, and the multi-functional NS5A. Although there are reports on compounds that inhibit the helicase function of NS3, none of these compounds have made it into clinical trials or have been approved for treatment. None of the approved drug combinations include a helicase inhibitor. In order to more rapidly decrease HCV RNA in patients, and reduce the resurgence of infection or resistance, it is important to target several different viral targets simultaneously.

In the study detailed above we screened for and identified two novel compounds that inhibited the helicase activity of NS3 *in vitro*. The compounds also had inhibitory effects on HCV replication in cell-based assays. Preliminary hits from library screening are important tools in searching for and designing more potent compounds for clinical use. The compounds we identified can be used to initiate structure activity relationship (SAR) studies that can also be guided by structure-based drug design efforts towards the identification of more potent HCV helicase inhibitors. Additionally, these helicase inhibitors can be used as mechanistic tools in cell-based assays to better understand the timing and role of NS3's helicase activity during HCV replication.

As part of the innate immune system, the interferon response pathway is one of the cell's first lines of defense again a viral infection. Following the detection of viral products (proteins, nucleic acid) several proteins act as mediators and adaptors in a signaling pathway leading to the up-regulation of IFN transcription and translation and secretion of IFN out of the cell. Our results suggest Dcp2 is a component of this signaling pathway, acting in a positive feedback mechanism to induce IFN mRNA production. Further studies would be needed to elucidate which part of the pathway Dcp2 is involved in, and which of the other known facilitating proteins Dcp2 interacts

with, if any. Understanding what role Dcp2's de-capping functionality plays in IFN induction would also be important. Our results show Dcp2 as an indirect inhibitor of viral replication.

Of the several drugs recently discovered and approved for HCV treatment, NS5A-targeting drugs are the most potent but the least understood. Treatment with DCV and LDV leads to rapid decline in viral RNA and virus release. However, due to the multi-functional nature of NS5A, the exact mechanism of action of these drugs remains unclear. DCV has been reported to redistribute NS5A to assembly sites and also to disrupt the formation of the membranous web utilized for assembly of the virus replication complex. We sought to gain further insights into the mechanism of action of DCV and investigate whether LDV and CsA had similar (if any) effects on replication and/or assembly complexes. We found that both LDV and CsA redistributed NS5A to circular structures that we determined to be lipid droplets. However, the drugs differed in observed distribution patterns, suggesting differences in their mechanism of action. This could be due to differences in how NS5A binds DCV or LDV, and the effects of inhibitor binding has on the aggregation mechanism of NS5A, which in turn may result in differences in cellular distribution of these aggregates. Since NS5A binds viral RNA it may also be that the different inhibitors affect the RNA binding ability and mode of NS5A in different ways. In the case of CsA, this inhibitor will affect binding of the host factor cyclophilin A, which has been reported to affect multiple steps of the virus life-cycle. Our results suggest that the size and number of lipid droplets in a cell is an important factor in virus assembly and release. Interestingly, in addition to redistributing NS5A, LDV also disrupts the localization of viral dsRNA to lipid droplets with NS5A, a finding unique to LDV. The purpose for dsRNA's localization with core and NS5A at lipid droplets has not been determined, and LDV might prove to be a useful tool to investigate this.

Hence, our data also show that DAAs can be used as tools in understanding the composition and kinetics of viral complex formation and the effects of disturbing their balance. Using our type of analysis, further investigation might lead to new antivirals that have different or

even pleiotropic effects on HCV replication. In that respect, of particular interest would be compounds that disrupt the formation of critical viral complexes and upset the balance between sequential steps in the virus life cycle.

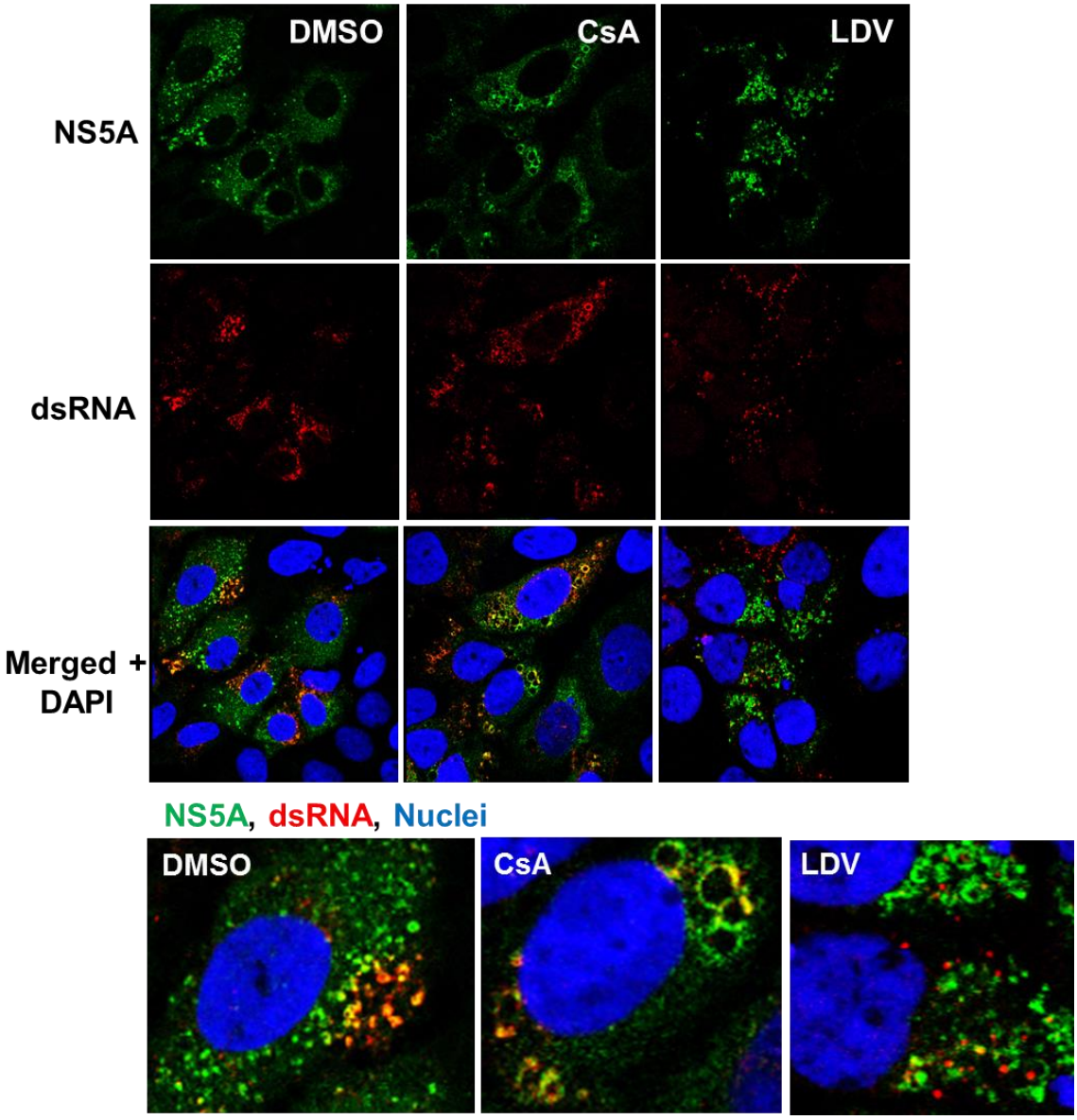
DMSO
CsA
LDV
NS5A
dsRNA
Merged +
DAPI
NS5A, dsRNA, Nuclei
DMSO
CsA
LDV

Figure IV-12: Ledipasvir treatment disrupts localization of HCV dsRNA with NS5A. Huh7.5.1 cells were infected with HCV (Jc1-378.1-NS5A-Ypet construct) for 72 hours before being treated with cyclosporin A, ledipasvir, or DMSO as a control. The drugs were removed after 16 hours, stained for dsRNA and nuclei as described in Materials and Methodsand imaged on a TCS Leica SP8 confocal microscope using a 63x oil objective lens. Representative images are shown.

V. SUMMARY

The studies described in this thesis focus on RNA viruses XMRV and HCV. We characterized the activity and kinetics of the XMRV reverse transcriptase and discovered key mechanistic differences between XMRV and HIV-1 RTs. Using steady and pre-steady state kinetics we demonstrated that XMRV RT is significantly less efficient in DNA synthesis and in unblocking chain-terminated primers. By surface plasmon resonance experiments, we observed that XMRV's decreased DNA binding ability was due to a remarkably higher rate of dissociating from DNA. XMRV RT has lower processivity when compared to HIV-1 RT, likely a result of XMRV RT's faster dissociation from bound DNA. Transient kinetics of mismatch incorporation revealed that XMRV RT has higher fidelity than HIV-1 RT.

In addition to characterizing XMRV RT, we determined whether agents known to inhibit MoMLV and HIV-1 RT would be effective against XMRV. To this end we identified RNA aptamers that potently inhibit XMRV, but interestingly, not HIV-1 RT. XMRV RT is highly susceptible to some nucleoside RT inhibitors, including Translocation Defective RT inhibitors, but not to nonnucleoside RT inhibitors that are potent against HIV-1 RT. We demonstrated that XMRV RT mutants K103R and Q190M, which are equivalent to HIV-1 mutants that are resistant to tenofovir (K65R) and AZT (Q151M), are also resistant to the respective drugs, suggesting that XMRV can acquire resistance to these compounds through the decreased incorporation mechanism reported in HIV-1.

Mov10 is an antiviral host factor that restricts replication of retroviruses, including HIV-1. Mov10 has also been reported to inhibit hepatitis C virus (HCV). However, the mechanism of this inhibition was yet to be studied. We investigated the

effect of Mov10 on HCV infection to determine which steps of the viral lifecycle are affected by overexpression of Mov10. We demonstrate that overexpression of Mov10 in human hepatoma cells restricts HCV RNA production from a sub-genomic replicon (genotype 1a) and fully infectious virus (genotype 2a). Inhibition of RNA replication in the infectious virus system leads to decreased virus production over time, as measured by HCV RNA levels in cell culture media by RT-pPCR, and the viral titer ($TCID_{50}$/ml) of released virus. In addition to decreasing virus production, overexpression of Mov10 in producer cells decreases the infectivity of the produced virus. In contrast, overexpression of a control P-body protein Dcp1a had no effect on HCV RNA production, virus production, or infectivity of progeny virus. By confocal imaging we show that in uninfected hepatoma cells endogenous Mov10 localizes to P-bodies were it co-localizes with Dcp1a. In HCV infected cells, endogenous Mov10 redistributes from P-bodies to circular structures around cytoplasmic lipid droplets. In these circular structures endogenous Mov10 partially co-localizes with HCV NS5A and the core protein. Finally, experiments with Mov10 active site mutants demonstrated that neither Mov10's putative helicase function nor localization to P-bodies was required for its antiviral activity.

In Chapter IV we studied the inhibition of HCV by (i) screening for novel small molecule inhibitors of the HCV helicase, (ii) discovering novel host restriction factors, and (iii) providing insights into the mechanism(s) of action of approved and clinically advanced direct-acting antiviral agents (DAAs). We screened for inhibitors of NS3's helicase domain (NS3h) and discovered two compounds that inhibited NS3h *in vitro*, and restricted HCV replication in cell-based assays. These preliminary hits can be used for future structure activity relationship studies g and structure assisted drug discovery

efforts to obtain more potent inhibitors. In addition, helicase inhibitors can be useful probes for addressing mechanistic questions regarding the specific roleof the HCV helicase in the virus life cycle.

Host proteins can act as restriction factors without directly inhibiting viruses. Instead, they could indirectly play a role in the IFN response pathway. We discovered one such factor Dcp2. Overexpression of Dcp2 restricts HCV replication by causing a profound increase in IFN transcription. This inhibition of HCV replication leads to a decrease in HCV production, but does not affect the infectivity of the virus produced.

Several DAAs have advanced in clinical trials and been approved for HCV treatment. NS5A-targeting drugs rapidly eliminate HCV RNA with unclear mechanism(s) of action. We show that treatment with the NS5A-targeting ledipasvir (LDV) or the CypA-targeting cyclosporine A (CsA) results in redistribution of NS5A into circular structures. This effect was similar to that of another NS5A inhibitor, daclatasvir (DCV). We determined these circular structures to be NS5A around lipid droplets, where it co-localized with the core protein. However, the three drugs had distinctly different effects on the size and number of circular structures and lipid droplets per cell. Additionally, LDV treatment disrupted the localization of HCV dsRNA to lipid droplets and its association with NS5A. We provide insights into the mechanism of action of DCV, CsA, and LDV and their effects on viral complexes: NS5A, core, and lipid droplets or NS5A and viral RNA.

This work provides insight into the replication processes of XMRV and HCV, strategies to restrict them, the mechanisms of action of drugs that inhibit them, and for HCV its interaction with host restriction factors.

Footnote:

The content of Tanyaradzwa P. Ndongwe's dissertation is based on one published manuscript, one manuscript under review, and two unpublished manuscripts in preparation. The contribution of co-authors appears after the description of each chapter.

Chapter II:

The work in Chapter II is based on a research paper that was published in the Nucleic Acids Research journal in 2011. TN performed the majority of the biochemical experiments and wrote the manuscript. AOA, EMR, YTO, and BM contributed some biochemical data. KF and AH performed cell based assays. ASW and DHB provided RNA aptamers for assays. HK and EM provided EFdA. KS helped with the initial conception of the project, training TN, and data analysis and interpretation. SGS contributed by overseeing all aspects of the project, data analysis and editing the manuscript.

Biochemical, inhibition and inhibitor resistance studies of xenotropic murine leukemia virus-related virus reverse transcriptase.
Ndongwe TP, Adedeji AO, Michailidis E, Ong YT, Hachiya A, Marchand B, Ryan EM, Rai DK, Kirby KA, Whatley AS, Burke DH, Johnson M, Ding S, Zheng YM, Liu SL, Kodama E, Delviks-Frankenberry KA, Pathak VK, Mitsuya H, Parniak MA, Singh K, Sarafianos SG.
Nucleic Acids Res. 2012 Jan;40(1):345-59.

Chapter III:

Chapter III is based on a submitted manuscript that is under review. TN performed the cell-based virology experiments. MPC performed some of the western blot analyses. TI and VKP provided reagents. RR assisted with data analysis and assay conception. SGS contributed by overseeing all aspects of the project, data analysis and editing the manuscript.

Effect of P-body component Mov10 on HCV virus production and infectivity.
Ndongwe, TP, Puray-Chavez, M, Izumi T, Pathak VK, Ralston R, Sarafianos SG. Journal of Virology, 2015. *Submitted*

Chapter IV:

Chapter IV is based on ongoing work. TN performed most of the cell-based and imaging assays and writing the manuscript. DL performed the inhibition data and contributed reagents. The other co-authors are contributing reagents, data analysis, and eventually editing the manuscript. SGS contributed by overseeing all aspects of the project, data analysis and editing the manuscript.

Other manuscripts (published or in preparation) in which TN is a co-author are not included in this thesis. A list of these manuscripts (published and in preparation) and the poster and oral presentations in national and international conferences follow:

LIST OF MANUSCRIPTS

1. **Ndongwe TP** *et al.* Biochemical, inhibition and inhibitor resistance studies of xenotropic murine leukemia virus-related virus reverse transcriptase. Nucleic Acids Res. 2012 Jan;40(1):345-59.

2. Kirby KA…**Ndongwe TP** *et al*. Structural and inhibition studies of the RNase H function of xenotropic murine leukemia virus-related virus reverse transcriptase. Antimicrob Agents Chemother. 2012 Apr;56(4):2048-61.

3. Liu D…**Ndongwe TP** *et al.* Fast HCV RNA elimination and NS5A redistribution by NS5A inhibitors studied by a multiplex assay approach. Antimicrob Agents Chemother. *Submitted.*

4. **Ndongwe TP** *et al*. Effect of P-body component Mov10 on HCV virus production and infectivity. Journal of Virology. *Submitted*.

5. **Ndongwe TP** *et al.* Role of Mov10 in stabilization of the HCV genome. *Research in progress*

6. Puray-Chavez M…**Ndongwe TP** *et al.* Effect of P-body component Mov10 on hepatitis B virus replication. *Research in progress.*

7. Liu D, **Ndongwe TP…***et al.* HCV NS5A-targeting compounds disrupt viral complexes, with distinctly different effects. *Research in progress.*

8. Casey MC…**Ndongwe TP** *et al.* Biochemical characterization of the Mov10 helicase. *Research in progress*

LIST OF PRESENTATIONS

2. **Ndongwe TP** *et al.* Biochemical, inhibition and inhibitor resistance studies of xenotropic murine leukemia virus-related virus reverse transcriptase. *ASM Conference on Viral Genome Replication, Banff, Alberta, Canada. February 2011.*
(Oral presentation)

3. **Ndongwe TP** *et al.* Biochemical, inhibition and inhibitor resistance studies of xenotropic murine leukemia virus-related virus reverse transcriptase. *ASM Conference on Viral Genome Replication, Banff, Alberta, Canada. February 2011*
(Poster presentation)

4. **Ndongwe TP** *et al.* P-body component Mov10 inhibits HCV virus production and infectivity. *International Conference on Antiviral Research, Raleigh, May 2014.*
(Poster presentation)

REFERENCES

1. A. Urisman *et al.*, Identification of a novel Gammaretrovirus in prostate tumors of patients homozygous for R462Q RNASEL variant. *PLoS pathogens* **2**, e25 (2006).
2. R. S. Arnold *et al.*, XMRV infection in patients with prostate cancer: novel serologic assay and correlation with PCR and FISH. *Urology* **75**, 755-761 (2010).
3. B. Dong *et al.*, An infectious retrovirus susceptible to an IFN antiviral pathway from human prostate tumors. *Proceedings of the National Academy of Sciences of the United States of America* **104**, 1655-1660 (2007).
4. G. Casey *et al.*, RNASEL Arg462Gln variant is implicated in up to 13% of prostate cancer cases. *Nature genetics* **32**, 581-583 (2002).
5. R. H. Silverman, Implications for RNase L in prostate cancer biology. *Biochemistry* **42**, 1805-1812 (2003).
6. R. H. Silverman, C. Nguyen, C. J. Weight, E. A. Klein, The human retrovirus XMRV in prostate cancer and chronic fatigue syndrome. *Nature reviews. Urology* **7**, 392-402 (2010).
7. R. Schlaberg, D. J. Choe, K. R. Brown, H. M. Thaker, I. R. Singh, XMRV is present in malignant prostatic epithelium and is associated with prostate cancer, especially high-grade tumors. *Proceedings of the National Academy of Sciences of the United States of America* **106**, 16351-16356 (2009).
8. E. C. Knouf *et al.*, Multiple integrated copies and high-level production of the human retrovirus XMRV (xenotropic murine leukemia virus-related virus) from 22Rv1 prostate carcinoma cells. *Journal of virology* **83**, 7353-7356 (2009).
9. N. Fischer *et al.*, Prevalence of human gammaretrovirus XMRV in sporadic prostate cancer. *Journal of clinical virology : the official publication of the Pan American Society for Clinical Virology* **43**, 277-283 (2008).
10. T. J. Henrich *et al.*, Xenotropic murine leukemia virus-related virus prevalence in patients with chronic fatigue syndrome or chronic immunomodulatory conditions. *J Infect Dis* **202**, 1478-1481 (2010).
11. O. Erlwein *et al.*, Failure to detect the novel retrovirus XMRV in chronic fatigue syndrome. *PloS one* **5**, e8519 (2010).
12. H. C. Groom *et al.*, Absence of xenotropic murine leukaemia virus-related virus in UK patients with chronic fatigue syndrome. *Retrovirology* **7**, 10 (2010).
13. W. M. Switzer *et al.*, Absence of evidence of xenotropic murine leukemia virus-related virus infection in persons with chronic fatigue syndrome and healthy controls in the United States. *Retrovirology* **7**, 57 (2010).
14. B. C. Satterfield *et al.*, Serologic and PCR testing of persons with chronic fatigue syndrome in the United States shows no association with xenotropic or polytropic murine leukemia virus-related viruses. *Retrovirology* **8**, 12 (2011).
15. V. C. Lombardi *et al.*, Detection of an infectious retrovirus, XMRV, in blood cells of patients with chronic fatigue syndrome. *Science* **326**, 585-589 (2009).

16. S. C. Lo *et al.*, Detection of MLV-related virus gene sequences in blood of patients with chronic fatigue syndrome and healthy blood donors. *Proceedings of the National Academy of Sciences of the United States of America* **107**, 15874-15879 (2010).
17. K. Knox *et al.*, No evidence of murine-like gammaretroviruses in CFS patients previously identified as XMRV-infected. *Science* **333**, 94-97 (2011).
18. K. Korn, H. Reil, A. Ensser, A. Knoll, No evidence of XMRV infection in immunocompromised patients and HIV-positive individuals from Germany. *Infection* **40**, 181-184 (2012).
19. J. Luczkowiak *et al.*, Lack of the detection of XMRV or polytropic MLV-related sequences in blood cells from HIV-1-infected patients in Spain. *Journal of acquired immune deficiency syndromes* **59**, 101-104 (2012).
20. B. Oakes, X. Qiu, S. Levine, J. Hackett, Jr., B. T. Huber, Failure to Detect XMRV-Specific Antibodies in the Plasma of CFS Patients Using Highly Sensitive Chemiluminescence Immunoassays. *Advances in virology* **2011**, 854540 (2011).
21. S. Rasa *et al.*, No evidence of XMRV provirus sequences in patients with myalgic encephalomyelitis/chronic fatigue syndrome and individuals with unspecified encephalopathy. *The new microbiologica* **37**, 17-24 (2014).
22. C. H. Shin *et al.*, Absence of XMRV retrovirus and other murine leukemia virus-related viruses in patients with chronic fatigue syndrome. *Journal of virology* **85**, 7195-7202 (2011).
23. G. Simmons *et al.*, Failure to confirm XMRV/MLVs in the blood of patients with chronic fatigue syndrome: a multi-laboratory study. *Science* **334**, 814-817 (2011).
24. I. Steffen *et al.*, No evidence for XMRV nucleic acids, infectious virus or anti-XMRV antibodies in Canadian patients with chronic fatigue syndrome. *PloS one* **6**, e27870 (2011).
25. S. Tang *et al.*, Absence of detectable XMRV and other MLV-related viruses in healthy blood donors in the United States. *PloS one* **6**, e27391 (2011).
26. G. Schauer, S. Leuba, N. Sluis-Cremer, Biophysical Insights into the Inhibitory Mechanism of Non-Nucleoside HIV-1 Reverse Transcriptase Inhibitors. *Biomolecules* **3**, 889-904 (2013).
27. K. Singh, N. Kaushik, J. Jin, M. Madhusudanan, M. J. Modak, Role of Q190 of MuLV RT in ddNTP resistance and fidelity of DNA synthesis: a molecular model of interactions with substrates. *Protein Eng* **13**, 635-643 (2000).
28. A. Telesnitsky, S. P. Goff, Two defective forms of reverse transcriptase can complement to restore retroviral infectivity. *EMBO J* **12**, 4433-4438 (1993).
29. M. M. Georgiadis *et al.*, Mechanistic implications from the structure of a catalytic fragment of Moloney murine leukemia virus reverse transcriptase. *Structure* **3**, 879-892 (1995).
30. D. Das, M. M. Georgiadis, The crystal structure of the monomeric reverse transcriptase from Moloney murine leukemia virus. *Structure* **12**, 819-829 (2004).
31. K. Chowdhury, N. Kaushik, V. N. Pandey, M. J. Modak, Elucidation of the role of Arg 110 of murine leukemia virus reverse transcriptase in the catalytic

mechanism: biochemical characterization of its mutant enzymes. *Biochemistry* **35**, 16610-16620 (1996).
32. N. Kaushik, K. Chowdhury, V. N. Pandey, M. J. Modak, Valine of the YVDD motif of moloney murine leukemia virus reverse transcriptase: role in the fidelity of DNA synthesis. *Biochemistry* **39**, 5155-5165 (2000).
33. A. Jacobo-Molina *et al.*, Crystal structure of human immunodeficiency virus type 1 reverse transcriptase complexed with double-stranded DNA at 3.0 A resolution shows bent DNA. *Proc Natl Acad Sci U S A* **90**, 6320-6324 (1993).
34. L. A. Kohlstaedt, J. Wang, J. M. Friedman, P. A. Rice, T. A. Steitz, Crystal structure at 3.5 A resolution of HIV-1 reverse transcriptase complexed with an inhibitor. *Science* **256**, 1783-1790 (1992).
35. S. G. Sarafianos *et al.*, Structure and function of HIV-1 reverse transcriptase: molecular mechanisms of polymerization and inhibition. *J Mol Biol* **385**, 693-713 (2009).
36. K. Singh, B. Marchand, K. A. Kirby, E. Michailidis, S. G. Sarafianos, Structural Aspects of Drug Resistance and Inhibition of HIV-1 Reverse Transcriptase. *Viruses* **2**, 606-638 PMCID: PMC2850067. (2010).
37. M. M. Schuckmann *et al.*, The N348I mutation at the connection subdomain of HIV-1 reverse transcriptase decreases binding to nevirapine. *J Biol Chem* **285**, 38700-38709 (2010).
38. A. Telesnitsky, S. P. Goff, RNase H domain mutations affect the interaction between Moloney murine leukemia virus reverse transcriptase and its primer-template. *Proc Natl Acad Sci U S A* **90**, 1276-1280 (1993).
39. T. Paprotka *et al.*, Recombinant origin of the retrovirus XMRV. *Science* **333**, 97-101 (2011).
40. K. Delviks-Frankenberry, O. Cingoz, J. M. Coffin, V. K. Pathak, Recombinant origin, contamination, and de-discovery of XMRV. *Current opinion in virology* **2**, 499-507 (2012).
41. K. Mohd Hanafiah, J. Groeger, A. D. Flaxman, S. T. Wiersma, Global epidemiology of hepatitis C virus infection: new estimates of age-specific antibody to HCV seroprevalence. *Hepatology* **57**, 1333-1342 (2013).
42. J. F. Perz, G. L. Armstrong, L. A. Farrington, Y. J. Hutin, B. P. Bell, The contributions of hepatitis B virus and hepatitis C virus infections to cirrhosis and primary liver cancer worldwide. *Journal of hepatology* **45**, 529-538 (2006).
43. R. Adam *et al.*, Evolution of liver transplantation in Europe: report of the European Liver Transplant Registry. *Liver transplantation : official publication of the American Association for the Study of Liver Diseases and the International Liver Transplantation Society* **9**, 1231-1243 (2003).
44. R. H. Wiesner, M. Sorrell, F. Villamil, P. International Liver Transplantation Society Expert, Report of the first International Liver Transplantation Society expert panel consensus conference on liver transplantation and hepatitis C. *Liver transplantation : official publication of the American Association for the Study of Liver Diseases and the International Liver Transplantation Society* **9**, S1-9 (2003).

45. Y. Sugawara, M. Makuuchi, Living donor liver transplantation for patients with hepatitis C virus cirrhosis: Tokyo experience. *Clinical gastroenterology and hepatology : the official clinical practice journal of the American Gastroenterological Association* **3**, S122-124 (2005).
46. Q. L. Choo *et al.*, Isolation of a cDNA clone derived from a blood-borne non-A, non-B viral hepatitis genome. *Science* **244**, 359-362 (1989).
47. M. Houghton, The long and winding road leading to the identification of the hepatitis C virus. *Journal of hepatology* **51**, 939-948 (2009).
48. V. Lohmann *et al.*, Replication of subgenomic hepatitis C virus RNAs in a hepatoma cell line. *Science* **285**, 110-113 (1999).
49. T. Kato *et al.*, Sequence analysis of hepatitis C virus isolated from a fulminant hepatitis patient. *Journal of medical virology* **64**, 334-339 (2001).
50. T. Kato *et al.*, Efficient replication of the genotype 2a hepatitis C virus subgenomic replicon. *Gastroenterology* **125**, 1808-1817 (2003).
51. C. W. Kim, K. M. Chang, Hepatitis C virus: virology and life cycle. *Clinical and molecular hepatology* **19**, 17-25 (2013).
52. B. D. Lindenbach, C. M. Rice, The ins and outs of hepatitis C virus entry and assembly. *Nature reviews. Microbiology* **11**, 688-700 (2013).
53. T. von Hahn, C. M. Rice, Hepatitis C virus entry. *The Journal of biological chemistry* **283**, 3689-3693 (2008).
54. T. K. Scheel, C. M. Rice, Understanding the hepatitis C virus life cycle paves the way for highly effective therapies. *Nature medicine* **19**, 837-849 (2013).
55. D. Egger *et al.*, Expression of hepatitis C virus proteins induces distinct membrane alterations including a candidate viral replication complex. *Journal of virology* **76**, 5974-5984 (2002).
56. R. Gosert *et al.*, Identification of the hepatitis C virus RNA replication complex in Huh-7 cells harboring subgenomic replicons. *Journal of virology* **77**, 5487-5492 (2003).
57. L. Gao, H. Aizaki, J. W. He, M. M. Lai, Interactions between viral nonstructural proteins and host protein hVAP-33 mediate the formation of hepatitis C virus RNA replication complex on lipid raft. *Journal of virology* **78**, 3480-3488 (2004).
58. I. Romero-Brey *et al.*, Three-dimensional architecture and biogenesis of membrane structures associated with hepatitis C virus replication. *PLoS pathogens* **8**, e1003056 (2012).
59. P. Ferraris, E. Blanchard, P. Roingeard, Ultrastructural and biochemical analyses of hepatitis C virus-associated host cell membranes. *The Journal of general virology* **91**, 2230-2237 (2010).
60. V. Madan, D. Paul, V. Lohmann, R. Bartenschlager, Inhibition of HCV replication by cyclophilin antagonists is linked to replication fitness and occurs by inhibition of membranous web formation. *Gastroenterology* **146**, 1361-1372 e1361-1369 (2014).
61. Z. Liu, F. Yang, J. M. Robotham, H. Tang, Critical role of cyclophilin A and its prolyl-peptidyl isomerase activity in the structure and function of the hepatitis C virus replication complex. *Journal of virology* **83**, 6554-6565 (2009).

62. D. Moradpour, F. Penin, C. M. Rice, Replication of hepatitis C virus. *Nature reviews. Microbiology* **5**, 453-463 (2007).
63. M. Lagos-Quintana *et al.*, Identification of tissue-specific microRNAs from mouse. *Current biology : CB* **12**, 735-739 (2002).
64. J. Chang *et al.*, miR-122, a mammalian liver-specific microRNA, is processed from hcr mRNA and may downregulate the high affinity cationic amino acid transporter CAT-1. *RNA biology* **1**, 106-113 (2004).
65. C. L. Jopling, S. Schutz, P. Sarnow, Position-dependent function for a tandem microRNA miR-122-binding site located in the hepatitis C virus RNA genome. *Cell host & microbe* **4**, 77-85 (2008).
66. G. Randall *et al.*, Cellular cofactors affecting hepatitis C virus infection and replication. *Proceedings of the National Academy of Sciences of the United States of America* **104**, 12884-12889 (2007).
67. P. S. Pang *et al.*, Structural map of a microRNA-122: hepatitis C virus complex. *Journal of virology* **86**, 1250-1254 (2012).
68. J. A. Wilson, C. Zhang, A. Huys, C. D. Richardson, Human Ago2 is required for efficient microRNA 122 regulation of hepatitis C virus RNA accumulation and translation. *Journal of virology* **85**, 2342-2350 (2011).
69. K. D. Conrad *et al.*, MicroRNA-122 dependent binding of Ago2 protein to hepatitis C virus RNA is associated with enhanced RNA stability and translation stimulation. *PloS one* **8**, e56272 (2013).
70. T. Shimakami *et al.*, Stabilization of hepatitis C virus RNA by an Ago2-miR-122 complex. *Proceedings of the National Academy of Sciences of the United States of America* **109**, 941-946 (2012).
71. T. Shimakami *et al.*, Base pairing between hepatitis C virus RNA and microRNA 122 3' of its seed sequence is essential for genome stabilization and production of infectious virus. *Journal of virology* **86**, 7372-7383 (2012).
72. J. Chang *et al.*, Liver-specific microRNA miR-122 enhances the replication of hepatitis C virus in nonhepatic cells. *Journal of virology* **82**, 8215-8223 (2008).
73. J. A. Wilson, A. Huys, miR-122 promotion of the hepatitis C virus life cycle: sound in the silence. *Wiley interdisciplinary reviews. RNA* **4**, 665-676 (2013).
74. E. S. Machlin, P. Sarnow, S. M. Sagan, Masking the 5' terminal nucleotides of the hepatitis C virus genome by an unconventional microRNA-target RNA complex. *Proceedings of the National Academy of Sciences of the United States of America* **108**, 3193-3198 (2011).
75. J. Elmen *et al.*, LNA-mediated microRNA silencing in non-human primates. *Nature* **452**, 896-899 (2008).
76. M. Dimitrova, I. Imbert, M. P. Kieny, C. Schuster, Protein-protein interactions between hepatitis C virus nonstructural proteins. *Journal of virology* **77**, 5401-5414 (2003).
77. Y. Huang, K. Staschke, R. De Francesco, S. L. Tan, Phosphorylation of hepatitis C virus NS5A nonstructural protein: a new paradigm for phosphorylation-dependent viral RNA replication? *Virology* **364**, 1-9 (2007).
78. A. Macdonald, M. Harris, Hepatitis C virus NS5A: tales of a promiscuous protein. *The Journal of general virology* **85**, 2485-2502 (2004).

79. E. M. Quezada, C. M. Kane, The Hepatitis C Virus NS5A Stimulates NS5B During In Vitro RNA Synthesis in a Template Specific Manner. *The open biochemistry journal* **3**, 39-48 (2009).
80. T. Shimakami *et al.*, Effect of interaction between hepatitis C virus NS5A and NS5B on hepatitis C virus RNA replication with the hepatitis C virus replicon. *Journal of virology* **78**, 2738-2748 (2004).
81. Y. Shirota *et al.*, Hepatitis C virus (HCV) NS5A binds RNA-dependent RNA polymerase (RdRP) NS5B and modulates RNA-dependent RNA polymerase activity. *The Journal of biological chemistry* **277**, 11149-11155 (2002).
82. Y. Ohsaki *et al.*, Biogenesis of cytoplasmic lipid droplets: from the lipid ester globule in the membrane to the visible structure. *Biochimica et biophysica acta* **1791**, 399-407 (2009).
83. D. J. Orlicky, J. Monks, A. L. Stefanski, J. L. McManaman, Dynamics and molecular determinants of cytoplasmic lipid droplet clustering and dispersion. *PloS one* **8**, e66837 (2013).
84. D. Moradpour, C. Englert, T. Wakita, J. R. Wands, Characterization of cell lines allowing tightly regulated expression of hepatitis C virus core protein. *Virology* **222**, 51-63 (1996).
85. S. Boulant, C. Vanbelle, C. Ebel, F. Penin, J. P. Lavergne, Hepatitis C virus core protein is a dimeric alpha-helical protein exhibiting membrane protein features. *Journal of virology* **79**, 11353-11365 (2005).
86. G. Barba *et al.*, Hepatitis C virus core protein shows a cytoplasmic localization and associates to cellular lipid storage droplets. *Proceedings of the National Academy of Sciences of the United States of America* **94**, 1200-1205 (1997).
87. E. Herker *et al.*, Efficient hepatitis C virus particle formation requires diacylglycerol acyltransferase-1. *Nature medicine* **16**, 1295-1298 (2010).
88. N. Appel *et al.*, Essential role of domain III of nonstructural protein 5A for hepatitis C virus infectious particle assembly. *PLoS pathogens* **4**, e1000035 (2008).
89. T. Masaki *et al.*, Interaction of hepatitis C virus nonstructural protein 5A with core protein is critical for the production of infectious virus particles. *Journal of virology* **82**, 7964-7976 (2008).
90. Y. Miyanari *et al.*, The lipid droplet is an important organelle for hepatitis C virus production. *Nature cell biology* **9**, 1089-1097 (2007).
91. R. A. Love, O. Brodsky, M. J. Hickey, P. A. Wells, C. N. Cronin, Crystal structure of a novel dimeric form of NS5A domain I protein from hepatitis C virus. *Journal of virology* **83**, 4395-4403 (2009).
92. T. L. Tellinghuisen, J. Marcotrigiano, C. M. Rice, Structure of the zinc-binding domain of an essential component of the hepatitis C virus replicase. *Nature* **435**, 374-379 (2005).
93. W. Cun, J. Jiang, G. Luo, The C-terminal alpha-helix domain of apolipoprotein E is required for interaction with nonstructural protein 5A and assembly of hepatitis C virus. *Journal of virology* **84**, 11532-11541 (2010).
94. J. Gentzsch *et al.*, hepatitis c Virus p7 is critical for capsid assembly and envelopment. *PLoS pathogens* **9**, e1003355 (2013).

95. V. Jirasko *et al.*, Structural and functional studies of nonstructural protein 2 of the hepatitis C virus reveal its key role as organizer of virion assembly. *PLoS pathogens* **6**, e1001233 (2010).
96. C. I. Popescu *et al.*, NS2 protein of hepatitis C virus interacts with structural and non-structural proteins towards virus assembly. *PLoS pathogens* **7**, e1001278 (2011).
97. Y. Ariumi *et al.*, The ESCRT system is required for hepatitis C virus production. *PloS one* **6**, e14517 (2011).
98. L. Corless, C. M. Crump, S. D. Griffin, M. Harris, Vps4 and the ESCRT-III complex are required for the release of infectious hepatitis C virus particles. *The Journal of general virology* **91**, 362-372 (2010).
99. K. Tamai *et al.*, Regulation of hepatitis C virus secretion by the Hrs-dependent exosomal pathway. *Virology* **422**, 377-385 (2012).
100. H. E. Drummer, A. Maerz, P. Poumbourios, Cell surface expression of functional hepatitis C virus E1 and E2 glycoproteins. *FEBS letters* **546**, 385-390 (2003).
101. J. Hundt, Z. Li, Q. Liu, Post-translational modifications of hepatitis C viral proteins and their biological significance. *World journal of gastroenterology : WJG* **19**, 8929-8939 (2013).
102. G. F. Gibbons, D. Wiggins, A. M. Brown, A. M. Hebbachi, Synthesis and function of hepatic very-low-density lipoprotein. *Biochemical Society transactions* **32**, 59-64 (2004).
103. S. L. B. Strader D.B., A brief history of the treatment of viral hepatitis C. *Clinics in liver disease* **1**, 6-11 (2012).
104. N. Shah, T. Pierce, K. V. Kowdley, Review of direct-acting antiviral agents for the treatment of chronic hepatitis C. *Expert opinion on investigational drugs* **22**, 1107-1121 (2013).
105. J. M. Pawlotsky *et al.*, Interferon resistance of hepatitis C virus genotype 1b: relationship to nonstructural 5A gene quasispecies mutations. *Journal of virology* **72**, 2795-2805 (1998).
106. D. A. Herbst, K. R. Reddy, NS5A inhibitor, daclatasvir, for the treatment of chronic hepatitis C virus infection. *Expert opinion on investigational drugs* **22**, 1337-1346 (2013).
107. R. Kumari, M. H. Nguyen, Fixed-dose combination of sofosbuvir and ledipasvir for the treatment of chronic hepatitis C genotype 1. *Expert opinion on pharmacotherapy*, 1-10 (2015).
108. Y. Waheed, Ledipasvir and sofosbuvir: Interferon free therapy for hepatitis C virus genotype 1 infection. *World journal of virology* **4**, 33-35 (2015).
109. S. Ottosen *et al.*, In vitro antiviral activity and preclinical and clinical resistance profile of miravirsen, a novel anti-hepatitis C virus therapeutic targeting the human factor miR-122. *Antimicrobial agents and chemotherapy* **59**, 599-608 (2015).
110. M. H. van der Ree *et al.*, Long-term safety and efficacy of microRNA-targeted therapy in chronic hepatitis C patients. *Antiviral research* **111**, 53-59 (2014).
111. P. Wang, J. Heitman, The cyclophilins. *Genome biology* **6**, 226 (2005).

112. A. Kaul *et al.*, Essential role of cyclophilin A for hepatitis C virus replication and virus production and possible link to polyprotein cleavage kinetics. *PLoS pathogens* **5**, e1000546 (2009).
113. G. Fischer, P. Gallay, S. Hopkins, Cyclophilin inhibitors for the treatment of HCV infection. *Current opinion in investigational drugs* **11**, 911-918 (2010).
114. F. E. Membreno, J. C. Espinales, E. J. Lawitz, Cyclophilin inhibitors for hepatitis C therapy. *Clinics in liver disease* **17**, 129-139 (2013).
115. O. Belda, P. Targett-Adams, Small molecule inhibitors of the hepatitis C virus-encoded NS5A protein. *Virus research* **170**, 1-14 (2012).
116. P. Targett-Adams *et al.*, Small molecules targeting hepatitis C virus-encoded NS5A cause subcellular redistribution of their target: insights into compound modes of action. *Journal of virology* **85**, 6353-6368 (2011).
117. C. Berger *et al.*, Daclatasvir-like inhibitors of NS5A block early biogenesis of hepatitis C virus-induced membranous replication factories, independent of RNA replication. *Gastroenterology* **147**, 1094-1105 e1025 (2014).
118. Y. M. Loo, M. Gale, Jr., Immune signaling by RIG-I-like receptors. *Immunity* **34**, 680-692 (2011).
119. K. Moriishi, Y. Matsuura, Host factors involved in the replication of hepatitis C virus. *Reviews in medical virology* **17**, 343-354 (2007).
120. R. K. Jangra, M. Yi, S. M. Lemon, DDX6 (Rck/p54) is required for efficient hepatitis C virus replication but not for internal ribosome entry site-directed translation. *Journal of virology* **84**, 6810-6824 (2010).
121. A. P. Roberts, R. Doidge, A. W. Tarr, C. L. Jopling, The P body protein LSm1 contributes to stimulation of hepatitis C virus translation, but not replication, by microRNA-122. *Nucleic acids research*, (2013).
122. N. Scheller *et al.*, Translation and replication of hepatitis C virus genomic RNA depends on ancient cellular proteins that control mRNA fates. *Proceedings of the National Academy of Sciences of the United States of America* **106**, 13517-13522 (2009).
123. J. W. Schoggins, C. M. Rice, Interferon-stimulated genes and their antiviral effector functions. *Current opinion in virology* **1**, 519-525 (2011).
124. C. T. Pager, S. Schutz, T. M. Abraham, G. Luo, P. Sarnow, Modulation of hepatitis C virus RNA abundance and virus release by dispersion of processing bodies and enrichment of stress granules. *Virology* **435**, 472-484 (2013).
125. G. Perez-Vilaro, N. Scheller, V. Saludes, J. Diez, Hepatitis C virus infection alters P-body composition but is independent of P-body granules. *Journal of virology* **86**, 8740-8749 (2012).
126. Y. Ariumi *et al.*, Hepatitis C virus hijacks P-body and stress granule components around lipid droplets. *Journal of virology* **85**, 6882-6892 (2011).
127. G. Perez-Vilaro *et al.*, Hepatitis C virus infection inhibits P-body granule formation in human livers. *Journal of hepatology*, (2014).
128. A. P. Roberts, R. Doidge, A. W. Tarr, C. L. Jopling, The P body protein LSm1 contributes to stimulation of hepatitis C virus translation, but not replication, by microRNA-122. *Nucleic acids research* **42**, 1257-1269 (2014).

129. Y. Itsui *et al.*, Expressional screening of interferon-stimulated genes for antiviral activity against hepatitis C virus replication. *Journal of viral hepatitis* **13**, 690-700 (2006).
130. D. Jiang *et al.*, Identification of three interferon-inducible cellular enzymes that inhibit the replication of hepatitis C virus. *Journal of virology* **82**, 1665-1678 (2008).
131. J. W. Schoggins *et al.*, A diverse range of gene products are effectors of the type I interferon antiviral response. *Nature* **472**, 481-485 (2011).
132. M. Poenisch *et al.*, Identification of HNRNPK as Regulator of Hepatitis C Virus Particle Production. *PLoS pathogens* **11**, e1004573 (2015).
133. G. Meister *et al.*, Identification of novel argonaute-associated proteins. *Current biology : CB* **15**, 2149-2155 (2005).
134. R. Burdick *et al.*, P body-associated protein Mov10 inhibits HIV-1 replication at multiple stages. *Journal of virology* **84**, 10241-10253 (2010).
135. S. Gallois-Montbrun *et al.*, Antiviral protein APOBEC3G localizes to ribonucleoprotein complexes found in P bodies and stress granules. *Journal of virology* **81**, 2165-2178 (2007).
136. M. E. Fairman-Williams, U. P. Guenther, E. Jankowsky, SF1 and SF2 helicases: family matters. *Current opinion in structural biology* **20**, 313-324 (2010).
137. A. Abudu *et al.*, Identification of molecular determinants from Moloney leukemia virus 10 homolog (MOV10) protein for virion packaging and anti-HIV-1 activity. *The Journal of biological chemistry* **287**, 1220-1228 (2012).
138. V. Furtak *et al.*, Perturbation of the P-body component Mov10 inhibits HIV-1 infectivity. *PloS one* **5**, e9081 (2010).
139. T. Izumi *et al.*, Mov10 and APOBEC3G Localization to Processing Bodies is not Required for Virion Incorporation and Antiviral Activity. *Journal of virology*, (2013).
140. C. Lu, Z. Luo, S. Jager, N. J. Krogan, B. M. Peterlin, Moloney leukemia virus type 10 inhibits reverse transcription and retrotransposition of intracisternal a particles. *Journal of virology* **86**, 10517-10523 (2012).
141. J. D. Bauman *et al.*, Crystal engineering of HIV-1 reverse transcriptase for structure-based drug design. *Nucleic Acids Res* **36**, 5083-5092 (2008).
142. E. Michailidis *et al.*, Mechanism of inhibition of HIV-1 reverse transcriptase by 4'-Ethynyl-2-fluoro-2'-deoxyadenosine triphosphate, a translocation-defective reverse transcriptase inhibitor. *J Biol Chem* **284**, 35681-35691 (2009).
143. P. R. Meyer, S. E. Matsuura, A. G. So, W. A. Scott, Unblocking of chain-terminated primer by HIV-1 reverse transcriptase through a nucleotide-dependent mechanism. *Proc Natl Acad Sci U S A* **95**, 13471-13476 (1998).
144. E. K. Halvas, E. S. Svarovskaia, V. K. Pathak, Development of an in vivo assay to identify structural determinants in murine leukemia virus reverse transcriptase important for fidelity. *J Virol* **74**, 312-319 (2000).
145. S. S. Patel, I. Wong, K. A. Johnson, Pre-steady-state kinetic analysis of processive DNA replication including complete characterization of an exonuclease-deficient mutant. *Biochemistry* **30**, 511-525 (1991).

146. S. G. Sarafianos, V. N. Pandey, N. Kaushik, M. J. Modak, Site-directed mutagenesis of arginine 72 of HIV-1 reverse transcriptase. Catalytic role and inhibitor sensitivity. *J Biol Chem* **270**, 19729-19735 (1995).
147. A. Hachiya *et al.*, K70Q adds high-level tenofovir resistance to "Q151M complex" HIV reverse transcriptase through the enhanced discrimination mechanism. *PLoS One* **6**, e16242 (2011).
148. S. G. Sarafianos *et al.*, Touching the heart of HIV-1 drug resistance: the fingers close down on the dNTP at the polymerase active site. *Chem Biol* **6**, R137-146 (1999).
149. P. L. Boyer, S. G. Sarafianos, P. K. Clark, E. Arnold, S. H. Hughes, Why do HIV-1 and HIV-2 use different pathways to develop AZT resistance? *PLoS Pathog* **2**, e10 (2006).
150. M. D. Powell *et al.*, Alanine-scanning mutations in the "primer grip" of p66 HIV-1 reverse transcriptase result in selective loss of RNA priming activity. *J Biol Chem* **272**, 13262-13269 (1997).
151. S. G. Sarafianos *et al.*, Lamivudine (3TC) resistance in HIV-1 reverse transcriptase involves steric hindrance with beta-branched amino acids. *Proc Natl Acad Sci U S A* **96**, 10027-10032 (1999).
152. C. A. Boucher *et al.*, High-level resistance to (-) enantiomeric 2'-deoxy-3'-thiacytidine in vitro is due to one amino acid substitution in the catalytic site of human immunodeficiency virus type 1 reverse transcriptase. *Antimicrob Agents Chemother* **37**, 2231-2234 (1993).
153. M. Tisdale, S. D. Kemp, N. R. Parry, B. A. Larder, Rapid in vitro selection of human immunodeficiency virus type 1 resistant to 3'-thiacytidine inhibitors due to a mutation in the YMDD region of reverse transcriptase. *Proc Natl Acad Sci U S A* **90**, 5653-5656 (1993).
154. L. Menendez-Arias, Molecular basis of human immunodeficiency virus drug resistance: an update. *Antiviral Res* **85**, 210-231.
155. S. G. Sarafianos, K. Das, S. H. Hughes, E. Arnold, Taking aim at a moving target: designing drugs to inhibit drug-resistant HIV-1 reverse transcriptases. *Curr Opin Struct Biol* **14**, 716-730 (2004).
156. L. Menendez-Arias, Molecular basis of human immunodeficiency virus drug resistance: an update. *Antiviral Res* **85**, 210-231 (2010).
157. L. Menendez-Arias, B. Berkhout, Retroviral reverse transcription. *Virus Res* **134**, 1-3 (2008).
158. S. Y. Rhee *et al.*, Human immunodeficiency virus reverse transcriptase and protease sequence database. *Nucleic Acids Res* **31**, 298-303 (2003).
159. Q. Shi, K. Singh, A. Srivastava, N. Kaushik, M. J. Modak, Lysine 152 of MuLV reverse transcriptase is required for the integrity of the active site. *Biochemistry* **41**, 14831-14842 (2002).
160. K. A. Johnson, Conformational coupling in DNA polymerase fidelity. *Annu Rev Biochem* **62**, 685-713 (1993).
161. L. F. Rezende, V. R. Prasad, Nucleoside-analog resistance mutations in HIV-1 reverse transcriptase and their influence on polymerase fidelity and viral mutation rates. *Int J Biochem Cell Biol* **36**, 1716-1734 (2004).

162. T. Paprotka *et al.*, Inhibition of xenotropic murine leukemia virus-related virus by APOBEC3 proteins and antiviral drugs. *J Virol* **84**, 5719-5729.
163. R. Sakuma, T. Sakuma, S. Ohmine, R. H. Silverman, Y. Ikeda, Xenotropic murine leukemia virus-related virus is susceptible to AZT. *Virology* **397**, 1-6 (2010).
164. I. R. Singh, J. E. Gorzynski, D. Drobysheva, L. Bassit, R. F. Schinazi, Raltegravir is a potent inhibitor of XMRV, a virus implicated in prostate cancer and chronic fatigue syndrome. *PloS one* **5**, e9948 (2010).
165. R. A. Smith, G. S. Gottlieb, A. D. Miller, Susceptibility of the human retrovirus XMRV to antiretroviral inhibitors. *Retrovirology* **7**, 70 (2010).
166. A. Kawamoto *et al.*, 2'-deoxy-4'-C-ethynyl-2-halo-adenosines active against drug-resistant human immunodeficiency virus type 1 variants. *The international journal of biochemistry & cell biology* **40**, 2410-2420 (2008).
167. E. I. Kodama *et al.*, 4'-Ethynyl nucleoside analogs: potent inhibitors of multidrug-resistant human immunodeficiency virus variants in vitro. *Antimicrob Agents Chemother* **45**, 1539-1546 (2001).
168. J. D. Kissel, D. M. Held, R. W. Hardy, D. H. Burke, Single-stranded DNA aptamer RT1t49 inhibits RT polymerase and RNase H functions of HIV type 1, HIV type 2, and SIVCPZ RTs. *AIDS Res Hum Retroviruses* **23**, 699-708 (2007).
169. H. Chen, L. Gold, Selection of high-affinity RNA ligands to reverse transcriptase: inhibition of cDNA synthesis and RNase H activity. *Biochemistry* **33**, 8746-8756 (1994).
170. P. J. Joshi, T. S. Fisher, V. R. Prasad, Anti-HIV inhibitors based on nucleic acids: emergence of aptamers as potent antivirals. *Curr Drug Targets Infect Disord* **3**, 383-400 (2003).
171. J. J. DeStefano, G. R. Nair, Novel aptamer inhibitors of human immunodeficiency virus reverse transcriptase. *Oligonucleotides* **18**, 133-144 (2008).
172. J. J. DeStefano, J. V. Cristofaro, Selection of primer-template sequences that bind human immunodeficiency virus reverse transcriptase with high affinity. *Nucleic Acids Res* **34**, 130-139 (2006).
173. D. Arion, N. Kaushik, S. McCormick, G. Borkow, M. A. Parniak, Phenotypic mechanism of HIV-1 resistance to 3'-azido-3'-deoxythymidine (AZT): increased polymerization processivity and enhanced sensitivity to pyrophosphate of the mutant viral reverse transcriptase. *Biochemistry* **37**, 15908-15917 (1998).
174. S. G. Sarafianos, S. H. Hughes, E. Arnold, Designing anti-AIDS drugs targeting the major mechanism of HIV-1 RT resistance to nucleoside analog drugs. *Int J Biochem Cell Biol* **36**, 1706-1715 (2004).
175. R. W. Shafer *et al.*, Combination therapy with zidovudine and didanosine selects for drug-resistant human immunodeficiency virus type 1 strains with unique patterns of pol gene mutations. *J Infect Dis* **169**, 722-729 (1994).
176. S. Tuske *et al.*, Structures of HIV-1 RT-DNA complexes before and after incorporation of the anti-AIDS drug tenofovir. *Nat Struct Mol Biol* **11**, 469-474 (2004).

177. T. Shirasaka *et al.*, Emergence of human immunodeficiency virus type 1 variants with resistance to multiple dideoxynucleosides in patients receiving therapy with dideoxynucleosides. *Proc Natl Acad Sci U S A* **92**, 2398-2402 (1995).
178. A. K. Iversen *et al.*, Multidrug-resistant human immunodeficiency virus type 1 strains resulting from combination antiretroviral therapy. *J Virol* **70**, 1086-1090 (1996).
179. M. A. Winters *et al.*, Human immunodeficiency virus type 1 reverse transcriptase genotype and drug susceptibility changes in infected individuals receiving dideoxyinosine monotherapy for 1 to 2 years. *Antimicrob Agents Chemother* **41**, 757-762 (1997).
180. Z. Gu *et al.*, Identification of a mutation at codon 65 in the IKKK motif of reverse transcriptase that encodes human immunodeficiency virus resistance to 2',3'-dideoxycytidine and 2',3'-dideoxy-3'-thiacytidine. *Antimicrob Agents Chemother* **38**, 275-281 (1994).
181. K. Knox *et al.*, No Evidence of Murine-Like Gammaretroviruses in CFS Patients Previously Identified as XMRV-Infected. *Science*, (2011).
182. S. Hue *et al.*, Disease-associated XMRV sequences are consistent with laboratory contamination. *Retrovirology* **7**, 111 (2010).
183. B. Oakes *et al.*, Contamination of human DNA samples with mouse DNA can lead to false detection of XMRV-like sequences. *Retrovirology* **7**, 109 (2010).
184. M. J. Robinson *et al.*, Mouse DNA contamination in human tissue tested for XMRV. *Retrovirology* **7**, 108 (2010).
185. E. Sato, R. A. Furuta, T. Miyazawa, An endogenous murine leukemia viral genome contaminant in a commercial RT-PCR kit is amplified using standard primers for XMRV. *Retrovirology* **7**, 110 (2010).
186. T. Paprotka *et al.*, Recombinant Origin of the Retrovirus XMRV. *Science*, (2011).
187. J. M. Coffin, J. P. Stoye, Virology. A new virus for old diseases? *Science* **326**, 530-531 (2009).
188. K. A. Kirby *et al.*, Structural and inhibition studies of the RNase H function of xenotropic murine leukemia virus-related virus reverse transcriptase. *Antimicrobial agents and chemotherapy* **56**, 2048-2061 (2012).
189. H. Huang, R. Chopra, G. L. Verdine, S. C. Harrison, Structure of a covalently trapped catalytic complex of HIV-1 reverse transcriptase: implications for drug resistance. *Science* **282**, 1669-1675 (1998).
190. S. G. Sarafianos *et al.*, Structures of HIV-1 reverse transcriptase with pre- and post-translocation AZTMP-terminated DNA. *EMBO J* **21**, 6614-6624 (2002).
191. S. G. Sarafianos *et al.*, Crystal structure of HIV-1 reverse transcriptase in complex with a polypurine tract RNA:DNA. *EMBO J* **20**, 1449-1461 (2001).
192. K. A. Kirby *et al.*, The sugar ring conformation of 4'-ethynyl-2-fluoro-2'-deoxyadenosine and its recognition by the polymerase active site of hiv reverse transcriptase. *Cell Mol Biol (Noisy-le-grand)* **57**, 40-46.
193. M. Gotte, D. Arion, M. A. Parniak, M. A. Wainberg, The M184V mutation in the reverse transcriptase of human immunodeficiency virus type 1 impairs rescue of chain-terminated DNA synthesis. *J Virol* **74**, 3579-3585 (2000).

194. M. A. Wainberg *et al.*, Enhanced fidelity of 3TC-selected mutant HIV-1 reverse transcriptase. *Science* **271**, 1282-1285 (1996).
195. V. N. Pandey *et al.*, Role of methionine 184 of human immunodeficiency virus type-1 reverse transcriptase in the polymerase function and fidelity of DNA synthesis. *Biochemistry* **35**, 2168-2179 (1996).
196. K. Das *et al.*, Structural basis for the role of the K65R mutation in HIV-1 reverse transcriptase polymerization, excision antagonism, and tenofovir resistance. *J Biol Chem* **284**, 35092-35100 (2009).
197. P. R. Meyer, S. E. Matsuura, A. M. Mian, A. G. So, W. A. Scott, A mechanism of AZT resistance: an increase in nucleotide-dependent primer unblocking by mutant HIV-1 reverse transcriptase. *Mol Cell* **4**, 35-43 (1999).
198. T. Ueno, T. Shirasaka, H. Mitsuya, Enzymatic characterization of human immunodeficiency virus type 1 reverse transcriptase resistant to multiple 2',3'-dideoxynucleoside 5'-triphosphates. *J Biol Chem* **270**, 23605-23611 (1995).
199. S. Marukian *et al.*, Cell culture-produced hepatitis C virus does not infect peripheral blood mononuclear cells. *Hepatology* **48**, 1843-1850 (2008).
200. B. D. Lindenbach *et al.*, Complete replication of hepatitis C virus in cell culture. *Science* **309**, 623-626 (2005).
201. P. D. Hsu, E. S. Lander, F. Zhang, Development and applications of CRISPR-Cas9 for genome engineering. *Cell* **157**, 1262-1278 (2014).
202. Y. Zhou *et al.*, High-throughput screening of a CRISPR/Cas9 library for functional genomics in human cells. *Nature* **509**, 487-491 (2014).
203. X. Wang *et al.*, Moloney leukemia virus 10 (MOV10) protein inhibits retrovirus replication. *The Journal of biological chemistry* **285**, 14346-14355 (2010).
204. J. L. Goodier, L. E. Cheung, H. H. Kazazian, Jr., MOV10 RNA helicase is a potent inhibitor of retrotransposition in cells. *PLoS genetics* **8**, e1002941 (2012).
205. K. J. Blight, J. A. McKeating, C. M. Rice, Highly permissive cell lines for subgenomic and genomic hepatitis C virus RNA replication. *Journal of virology* **76**, 13001-13014 (2002).
206. J. Niu, B. Zhang, H. Chen, Applications of TALENs and CRISPR/Cas9 in human cells and their potentials for gene therapy. *Molecular biotechnology* **56**, 681-688 (2014).
207. L. H. Gregersen *et al.*, MOV10 Is a 5' to 3' RNA helicase contributing to UPF1 mRNA target degradation by translocation along 3' UTRs. *Molecular cell* **54**, 573-585 (2014).
208. T. P. Chendrimada *et al.*, MicroRNA silencing through RISC recruitment of eIF6. *Nature* **447**, 823-828 (2007).
209. F. G. Wulczyn *et al.*, Post-transcriptional regulation of the let-7 microRNA during neural cell specification. *FASEB journal : official publication of the Federation of American Societies for Experimental Biology* **21**, 415-426 (2007).
210. C. Liu *et al.*, APOBEC3G inhibits microRNA-mediated repression of translation by interfering with the interaction between Argonaute-2 and MOV10. *The Journal of biological chemistry* **287**, 29373-29383 (2012).

211. M. Gu, C. M. Rice, Three conformational snapshots of the hepatitis C virus NS3 helicase reveal a ratchet translocation mechanism. *Proceedings of the National Academy of Sciences of the United States of America* **107**, 521-528 (2010).
212. A. O. Adedeji *et al.*, Evaluation of SSYA10-001 as a replication inhibitor of severe acute respiratory syndrome, mouse hepatitis, and Middle East respiratory syndrome coronaviruses. *Antimicrobial agents and chemotherapy* **58**, 4894-4898 (2014).
213. Z. S. Huang, C. C. Wang, H. N. Wu, HCV NS3 protein helicase domain assists RNA structure conversion. *FEBS letters* **584**, 2356-2362 (2010).
214. S. Chang, K. Kodys, G. Szabo, Impaired expression and function of toll-like receptor 7 in hepatitis C virus infection in human hepatoma cells. *Hepatology* **51**, 35-42 (2010).
215. J. Zhong *et al.*, Robust hepatitis C virus infection in vitro. *Proceedings of the National Academy of Sciences of the United States of America* **102**, 9294-9299 (2005).
216. M. Yi, R. A. Villanueva, D. L. Thomas, T. Wakita, S. M. Lemon, Production of infectious genotype 1a hepatitis C virus (Hutchinson strain) in cultured human hepatoma cells. *Proceedings of the National Academy of Sciences of the United States of America* **103**, 2310-2315 (2006).
217. A. Piodi, P. Chouteau, H. Lerat, C. Hezode, J. M. Pawlotsky, Morphological changes in intracellular lipid droplets induced by different hepatitis C virus genotype core sequences and relationship with steatosis. *Hepatology* **48**, 16-27 (2008).
218. R. K. Lyn, D. C. Kennedy, A. Stolow, A. Ridsdale, J. P. Pezacki, Dynamics of lipid droplets induced by the hepatitis C virus core protein. *Biochemical and biophysical research communications* **399**, 518-524 (2010).
219. L. J. Anderson, K. Lin, T. Compton, B. Wiedmann, Inhibition of cyclophilins alters lipid trafficking and blocks hepatitis C virus secretion. *Virology journal* **8**, 329 (2011).

VITA

Tanya Ndongwe was born on August 23rd, 1988 in Harare Zimbabwe. During her childhood her mother Patricia Mutama worked as a nurse, and her father David Ndongwe a teacher. Tanya did most of her schooling in Zimbabwe, up until high school at St. Augustine's Mission School in Penhalonga, Zimbabwe. At the age of 17 in 2005, she received an all-inclusive Presidential Scholarship to study at St. Augustine's University in Raleigh, North Carolina. She graduated with Bachelor of Science degree in Pre-medical Sciences in May 2009, before beginning her PhD in the Molecular Microbiology and Immunology department in June 2009.